INVESTIGATING MAMMALIAN MEIOSIS: THE ROLE OF MISMATCH REPAIR PROTEINS AND THEIR INTERACTORS

A Dissertation

Presented to the Faculty of the Graduate School

of Cornell University

In Partial Fulfillment of the Requirements for the Degree of

Doctor of Philosophy

by

Xianfei Sun

August 2012

INVESTIGATING MAMMALIAN MEIOSIS: THE ROLE OF MISMATCH REPAIR PROTEINS AND THEIR INTERACTORS

Xianfei Sun, Ph. D.

Cornell University 2012

Prophase I is the defining stage of meiosis when chromosomes must first pair with their homologous partner, then synapse, and undergo precisely controlled reciprocal recombination. Due to the complexity of the process, meiotic recombination requires highly ordered cooperation from various proteins, including the mismatch repair (MMR) protein family.

Mouse MLH3 belongs to the MutL homolog family that functions as effector molecules for MMR. Research has suggested that MLH3 has critical roles in both DNA mismatch repair and meiosis. In the research for this thesis, I investigated two unique structural features of mouse MLH3: the potential endonuclease domain $DQHA(X)_2E(X)_4E$, and the large mammalian-specific region within exon 2.

To investigate the function of the conserved endonuclease domain of MLH3, a transgenic mouse line containing a point mutation in this potential endonuclease domain was made. I hypothesized that, due to the conservation of this domain, disruption of this domain would lead to the abolishment of normal meiotic progression *in vivo*.

To explore the function of the exon 2 region of mouse MLH3, I performed yeast two-hybrid assay and identified nine possible interacting partners of this region. To further screen for key sub-motifs within this region, a microsatellite instability reporter assay was tested. It is hypothesized that the unique region in exon 2 is important for the function of mouse MLH3 in maintaining genome integrity, and confers mammalian-specific functions to MLH3 in higher eukaryotes.

Mouse CNTD1 is a newly identified cyclin-related protein. Its worm ortholog, COSA-1, functions in conjunction with the MMR pathway to process crossovers during meiosis. To explore the role of mouse CNTD1 in mammalian gametogenesis, I generated *Cntd1* gene targeted mice. Consistent with the findings in *C. elegans*, deletion of *Cntd1* in mice caused severe defects in meiotic CO formation, which leads to sterility in both males and females. No epididymal sperm were found in *Cntd1* mutant males, and mutant females underwent severe oocyte-depletion after puberty. These data indicate a pivotal role for CNTD1 in regulating meiotic COs, possibly by helping select the sites of late recombination nodules through promoting or stabilizing other Class I CO-promoting proteins on meiotic chromosomes.

BIOGRAPHICAL SKETCH

Xianfei Sun was born on April 12, 1982, in Shanghai, China, to Zhigang Sun and Qinfen Liu. She was the only child in the family and spent her childhood enjoying painting, dancing and sports. After graduating from Shanghai Jingye Middle School in 2000, she entered Fudan University, where she studied biological sciences in the Department of Life Sciences. Meanwhile, she also worked in several labs as research assistant, and got involved in research projects of various biological fields, including studying the effects of size class and group size structure on cannibalism in basin-raised larval salamanders (*Hynobius amjiensis*) under the direction of Dr. Cui-Chang Fu, carrying out the survey of the distribution of Chinese medicinal herbs in Tianmu Mountain area under the direction of Dr. Zhengdao Wei, and performing molecular cloning and characterization of a novel human protein phosphatase 2C under the direction of Dr. Yi Xie. Her interest in biological sciences was fostered through these projects, which also strengthened her faith in pursuing a scientific career after graduation. After her receiving bachelor degree in 2004, she attended the Interdisciplinary Graduate Program at the Department of Biological Sciences in Vanderbilt University for one year, and then moved to Ithaca, New York to attend graduate school at Cornell University and to pursue a Ph.D. in Molecular and Integrative Physiology, under the direction of Dr. Paula Cohen. In the Cohen lab, she was given the chance to investigate mammalian meiosis and used mouse as a model studying the regulation of meiotic recombination by mismatch repair proteins and their interactors. Upon completion of her dissertation in 2012, she plans continuing her research in the Cohen lab in a postdoctoral position.

For my parents, Zhigang Sun and Qinfen Liu, and my husband Xu Wang for all their love and support.

ACKNOWLEDGMENTS

First and foremost I would like to thank my advisor, Dr. Paula Cohen, for her guidance, support, and admirable patience over the years. I felt very fortunate for having such a great mentor who was always there encouraging me and offering me suggestions whenever I needed it the most. With a cheerful and passionate personality, she created a free and friendly environment in the lab, which was perfect for scientific work, and made sure that everybody would have the opportunity to perform up to their full potential. Without her, I can never finish my Ph. D. study. I also would like to thank my other advisory committee members, Dr. Mariana Wolfner, Dr. Joanne Fortune and Dr. Robert Weiss for their help and guidance along the way, especially during my difficult phases of my Ph. D. projects.

I thank all the past and current members of the Cohen lab: Dr. Kim Holloway, Peter Borst, Dr. Swapna Mohan, Andrew Modzelewski, Kadeine Campbell, Dr. Jack Jayaram, Dr. Anton Svetlanov, Dr. Meisha Morelli, Dr. Rui Kan, Dr. Rebecca Holmes, Robert Christensen, Dr. Claudia Sutton for being both great colleagues and wonderful friends over the seven years.

I also have to thank our collaborators and the experts from Cornell Life Science Core Facilities for providing help, materials, advice and discussions indispensable to all my projects including the work presented in my thesis: Dr. Winfred Edelmann and Dr. Harry Hou from Albert Einstein College of Medicine for helping me generate *Mlh*^{DN} mice; Dr. Anne M. Villeneuve from Stanford University for providing invaluable suggestions for *Cntd1* project; Robert Munroe and Dr. Ke-Yu Deng for generating *Cntd1* transgenic mice; Lavanya Sayam for helping me perform

flow cytometry; Christian Abratte for making lentivirus and sharing his experience on MEF transfection; Dr. Longying (Lynn) Dong for giving me training on cryosectioning; Dr. Chengtao Her from Washington State University for offering their miscrosatellite instability reporter plasmids; Dr. Johanna van Oers and Dr. Uwe Werling from Albert Einstein College of Medicine for providing cell lines and antibodies; Dr. Xuemei Wu from Oregon Health and Science University for collecting fetal ovaries from rhesus monkeys.

Last, but not least, I want to thank my family and friends, especially my parents Zhigang Sun and Qinfen Liu, and my husband Xu Wang. Thank you for always listening to me and trusting me. I could never have come this far without your love and support.

TABLE OF CONTENTS

LIST OF FIGURES

LIST OF TABLES

CHAPTER 1

Introduction to mammalian meiosis

Given the importance of meiosis to gametogenesis in all sexually reproducing organisms, a profound understanding of meiosis is crucial. It has been suggested that, compared with other eukaryotic organisms, the complexity of meiotic regulation increases in mammals, probably because of the larger genome size and/or more complicated cellular environment (Cohen et al. 2006). While errors during the first meiotic division occur at a rate of 1:10,000 in budding yeast, it is found that the error rate is at 1–2% in mice and human males, and jumps to 20% in women (Hassold and Hunt 2001). Moreover, beginning with genetically programmed double strand breaks (DSBs), which are processed and repaired during meiotic progression, meiosis is also a great model for studying DSB repair mechanisms. Thus, in-depth study of meiotic genes and their interactions during mammalian meiosis is pivotal for a better understanding of meiotic mechanism and regulation. Ultimately, these studies will provide valuable information for human reproduction problems, such as infertility and birth defects.

1. Meiosis and prophase I

Meiosis is a specialized cell division used by sexually reproducing organisms. During this process, diploid precursor cells give rise to haploid gametes through one round of genome replication and two rounds of cell division, which divide the process of meiosis into two stages, meiosis I and II. Each stage includes four substages: prophase, metaphase, anaphase and telophase (See Figure 1-1). During meiosis I, pairs of homologous chromosomes (which each

Figure 1-1. Meiosis in mammals and its sexual dimorphism.

This figure depicts meiotic progression in mammals. Note that the development of male and female germ cells differs remarkably. In females, oocytes enter prophase I of meiosis during embryonic development, and then get arrested at diakinesis (dictyate arrest) by birth. The resumption of meiosis happens in puberty, when cohorts of follicles are recruited for ovulation during each menstrual cycle and their oocytes finish the first division of meiosis by extruding the first polar body. The second meiotic division and polar body extrusion do not happen until the oocyte is fertilized by a sperm. In males, germ cells enter meiosis after birth. In human, a group of male germ cells are recruited to enter meiosis at puberty and produce mature sperm. Meiotic entry then proceeds in waves throughout the lifetime of the animal. This figure is adapted from "*Genetics of mammalian meiosis: regulation, dynamics and impact on fertility*" (Handel and Schimenti 2010).

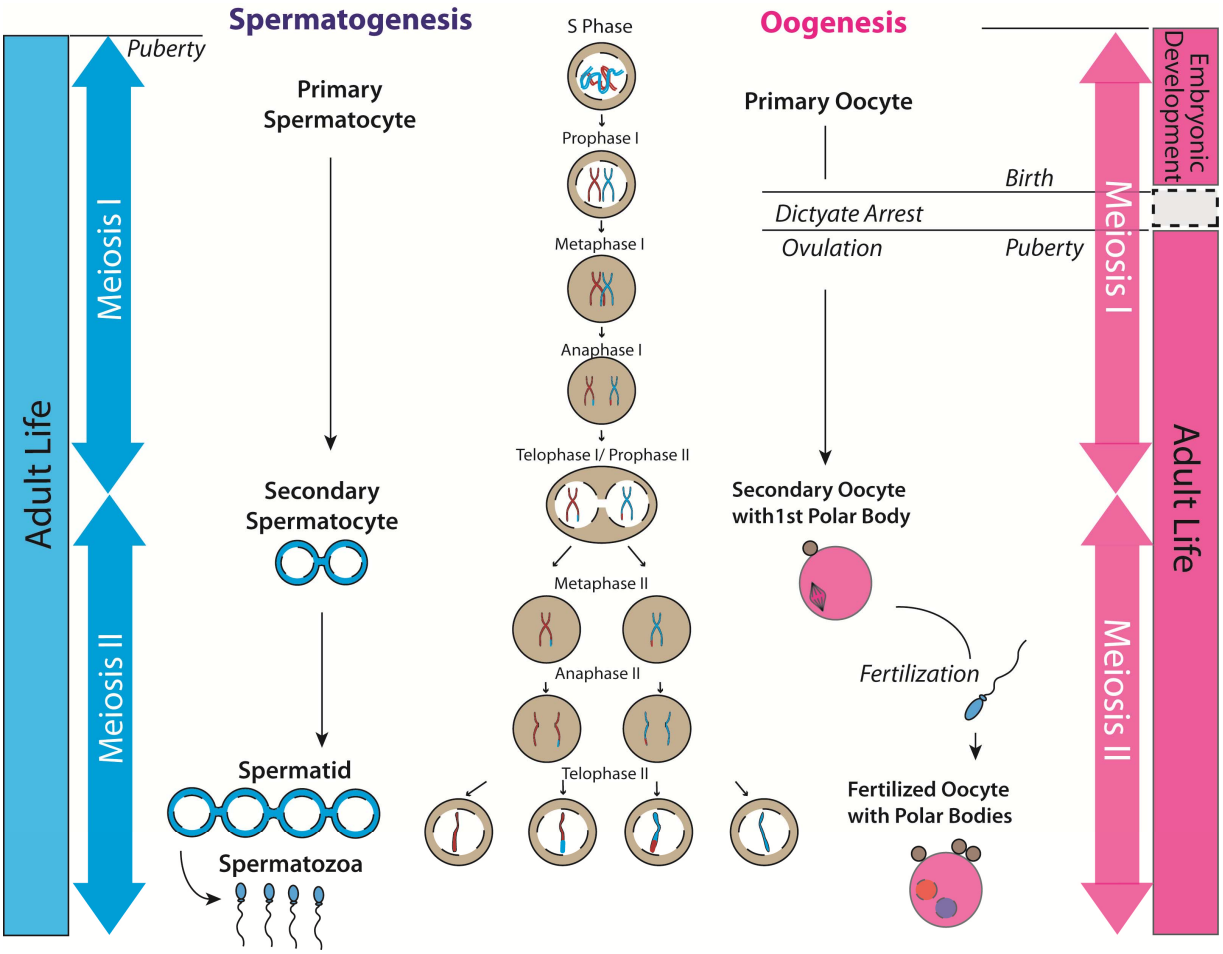
Spermatogenesis
Puberty
Adult Life
Meiosis I
Meiosis II
Primary Spermatocyte
Secondary Spermatocyte
Spermatid
Spermatozoa
S Phase
Prophase I
Metaphase I
Anaphase I
Telophase I/ Prophase II
Metaphase II
Anaphase II
Telophase II
Oogenesis
Primary Oocyte
Birth
Dictyate Arrest
Ovulation
Puberty
Secondary Oocyte with1st Polar Body
Fertilization
Fertilized Oocyte with Polar Bodies
Embryonic Development
Meiosis I
Meiosis II
Adult Life

consist of replicated pairs of sister chromatids) become physically tethered together and then segregate equationally at the first meiotic division. During meiosis II, the sister chromatids separate in a reductional division that is highly reminiscent of mitosis. Thus, a successful meiotic event ensures that each gamete will have exactly one copy of each chromosome from each parent so that the integrity of the genome will be preserved through subsequent generations.

Meiosis is a common feature of all sexually reproducing organisms. The importance of this process cannot be emphasized enough. In mammals, the meiotic products, which are the gametes, are the very first "stem cells" that the whole multicellular organism will develop from. Failure of meiotic chromosome segregation often leads to aneuploidy, which is the leading cause of pregnancy loss in humans and account for about one-third of the miscarriages. In the well-known Down's syndrome, also known as trisomy 21, errors occurring during maternal or paternal meiosis contribute to 99.5% of the resulting trisomy (Hassold and Hunt 2001).

To accomplish this demanding task and ensure proper segregation of meiotic chromosomes, meiosis employs two unique sequential processes before the first meiotic division: 1) pairing and synapsis of homologous chromosomes; 2) precisely controlled reciprocal crossover between homologs, which results in the association of homologs at the site where reciprocal recombination happens. Although these two events can occur independently in some species, such as *Schizosaccharomyces pombe*, whose chromosomes recombine without synapsis, and *Bombyx mori* females, whose chromosomes synapse without homologous recombination (Champion and Hawley 2002), both events are necessary for successful meiotic process in most organisms, from yeast to humans.

Prophase I is the first and also the longest stage during meiosis. It is the time when these two defining events happen. The importance of prophase I is underscored by the observation that

errors occurring in first meiotic division account for more than 60% of trisomies found in humans (Hassold and Hunt 2001; Hunt and Hassold 2008).

2. Homologous chromosome pairing and synaptonemal complex formation

During prophase I, the physical pairing between homologous chromosomes occurs through the proteinaceous structure known as synaptonemal complex (SC). SC is a protein scaffold connecting paired chromosome together during most of meiosis I. A typical SC is composed of three elements: two lateral elements, which are on the side of SC and form an axis along the entire length of each individual homologous chromosome (consisting of two sister chromatids), and one central region between the lateral elements, which is composed of the central elements and transverse filaments (Moses 1969). The central region connects lateral elements, and the assembly of the central region marks the synapsis, or physical tethering, of homologous chromosomes. When the homologous chromosomes are not fully synapsed, the lateral element is called the axial element (Page and Hawley 2004). In mammals, SYCP3 and SYCP2 are major structural constituents of the lateral elements (Dobson et al. 1994; Lammers et al. 1994; Offenberg et al. 1998; Schalk et al. 1998). As for the central region, the transverse filament is mainly composed of SYCP1 (Schmekel et al. 1996), a coiled-coil domain protein, and the central elements contain SYCE1, SYCE2, TEX12, FKBP6 and newly identified SYCE3 (Crackower et al. 2003; Hamer et al. 2006; Bolcun-Filas et al. 2007; Bolcun-Filas et al. 2009; Schramm et al. 2011). SYCP1 serves as a framework for the central region and interacts with other central element proteins, such as SYCE1 and SYCE2 (Costa et al. 2005; Bolcun-Filas et al. 2007). SYCE1, SYCE2 and SYCE3 interact with each other whereas TEX12 forms a complex with

SYCE2 (Hamer et al. 2006). While the structure of SC is highly conserved in many species, from budding yeast to humans, the proteins that make up the SC vary among species. As mentioned above, in mammals, the lateral element of the SC is mainly composed of SYCP2 and SYCP3, and the transverse filament mostly consists of SYCP1. Budding yeast, *C. elegans* and *Arabidopsis* also have lateral element and transverse filament, but the protein composition of these structures is very different. In yeast, the major components of the yeast lateral element are *RED1* and *HOP1*, and the main protein of the transverse filament is *ZIP1*. *C. elegans* utilizes HIM-3 for lateral element, and SYP-1 and SYP-2 for transverse filament, whereas *Arabidopsis* uses SYN1 for lateral element, and ZYP1 for transverse filament (Bai et al. 1999; Zetka et al. 1999; Woltering et al. 2000; Hawley 2002; Page and Hawley 2004; Loidl 2006).

In terms of the structure and status of synaptonemal complex, prophase I can be divided into five substages: leptonema (adjective: leptotene), zygonema (adjective: zygotene), pachynema (adjective: pachytene), diplonema (adjective: diplotene) and diakinesis (See Figure 1- 2). In leptonema, the replicated chromosomes are long and loose structures consisting of sister chromatids held together by a ring-like cohesion complex. In mammals, meiosis specific cohesin proteins include Structural Maintenance of Chromosomes 1β (SMC1β), REC8 and STAG3 (Suja and Barbero 2009). While most cohesin complexes dissemble by the end of anaphase I, cohesions around centromere region are maintained until the metaphase–anaphase transition of meiosis II. Meanwhile, the lateral element of the SC starts to form as short tracks along the axes of homologus chromosomes at this stage. During zygonema, the lateral elements form along chromosomes, which are shortened and paired. The central element of the SC element starts to

Figure 1-2. Prophase I substages and synaptonemal complex.

A cartoon summary of the events during the first four substages of prophase I (leptonema, zygonema, pachynema, and diplonema), with synaptonemal complex (SC) (SYCP1; green, SYCP3; light orange, SYCP2; light blue) and other related structures (Cohesins; yellow circle, early meiotic nodule; beige oval, late meiotic nodule; dark orange oval). Homologous chromosomes of different parental origins (paternal; dark blue, maternal; pink) are depicted as double looping lines around SC core. The progression of SC assembly and synapsis are shown for each substage. This figure is adapted from "*Predicting gene networks in human oocyte meiosis*" (Cohen and Holloway 2010).

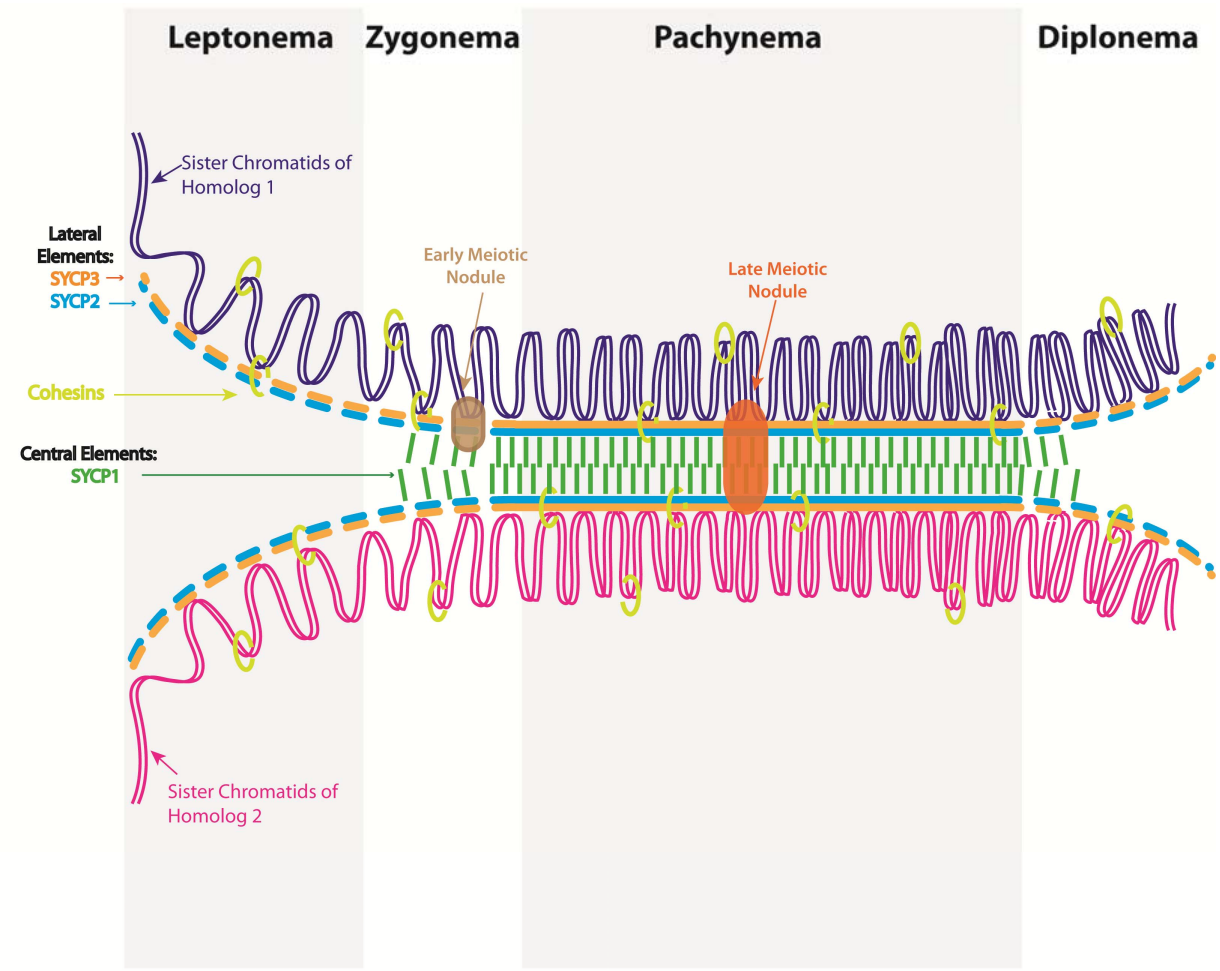
Leptonema
Zygonema
Pachynema
Diplonema
Sister Chromatids of Homolog 1
Lateral Elements:
SYCP3
SYCP2
Early Meiotic Nodule
Late Meiotic Nodule
Cohesins
Central Elements:
SYCP1
Sister Chromatids of Homolog 2

accumulate between homologs and “zips” the chromosome pairs together. At pachynema, the chromosomes are fully condensed and SC formation between homologs is complete. Pachynema is the longest stage of prophase I. According to changes in the length of the SC, pachynema can be further subdivided into early, middle and late pachynema. Then the cell enters diplonema when the SC starts to degrade and chromosome pairs begin to disassociate from each other. By the time the cell has progressed to diakinesis, the SC has completely broken down and the chromosomes remain attached only at sites of chiasmata where crossing over, or reciprocal recombination, has occurred.

3. Differences in the timeline of prophase I progression between males and females

Interestingly, the onset and progression of prophase I show significant sexually dimorphism in mammals (Figure 1-1). In female mice, oocytes initiate prophase I entry soon after the oogonia populate the fetal ovaries at embryonic day 10.5 ~12.5 (Borum 1961). Then the oocytes progress into leptonema from embryonic day 13.5 (Evans et al. 1982). At around the time of birth, the oocytes start to enter diakinesis, and become arrested at a prolonged quiescent state known as dictyate (Borum 1961). By the fifth day after birth, all oocytes are arrested in dictyate, remaining dormant until puberty, when only a few will be selected to resume meiosis at each estrous cycle. Even for these selected oocytes, they will not complete meiosis but get arrested again in metaphase II unless they can be fertilized by sperm after ovulation. By contrast, male germ cells enter meiosis after birth. In mice, the first wave of spermatogenesis begins at day 8 post partum (pp) when a group of spermatogonia are recruited to enter meiosis (Goetz et al. 1984). At around day 22pp, most spermatocytes complete the first meiotic process and turn into round spermatids.

Mature spermatozoa can be observed from day 27pp onward (Cohen et al. 2006).Then waves of spermatogenesis are repeated continuously throughout the lifetime of the animal. Importantly, the first waves of meiosis occur prior to the onset of puberty and, as such, can be considered to be androgen independent.

One explanation for this interesting sexual difference is based on the interaction between retinoic acid (RA) and a gene called Stimulated by retinoic acid8 (*Stra8*) (Bowles et al. 2006; Anderson et al. 2008). In female mice, RA secreted by mesonephroi induces the expression of *Stra8* at embryonic day 10.5 ~12.5, which cause the initiation of prophase I. Meanwhile, in males, the fetal testes are also exposed to RA from the mesonephroi. But *Stra8* is not expressed because of a retinoid-degrading enzyme, CYP26B1, which is expressed in male-specific Sertoli cells at that stage (MacLean et al. 2007). So prophase I in male testis will not begin until CYP26B1 is removed. However, this view has been recently challenged by the observation that disruption of RA synthesis and signaling in fetal mesonephros and gonads did not prevent the expression of *Stra8* in fetal ovaries and entry into prophase I was observed (Kumar et al. 2011). Additionally, inhibition of CYP26B1 in fetal testis of these RA defective mutants led to *Stra8* expression (Kumar et al. 2011), which implies that either *Cyp26b1* prevents the onset of meiosis by suppressing a target other than RA that regulates the expression of *Stra8* or the synthesis of RA was not completely abolished in the mutants.

4. Meiotic recombination is essential for establishing the chiasmata that characterize meiosis I

In parallel with chromosome pairing and synapsis, homologous recombination happens between

chromosomes at the DNA level. Homologous recombination is the defining event of meiosis. First of all, this event is pivotal for proper segregation of meiotic chromosomes, and ensures the normal progression of meiotic event. Chiasmata are χ (Chi)-shaped structures consisting of crossovers and inter-sister connection. They form by the end of prophase I through reciprocal recombination events that tether the homologs together when inter-homolog cohesins are dissolved (Nasmyth 2001), which prevents missegregation of homologous chromosomes at the end of meiosis I. Secondly, reciprocal crossovers also contribute to the exchange of genetic information between paternal and maternal alleles, which allows the offspring to inherit a hybrid chromosome composed of genetic information from both parents. Evolutionarily, the increase in genetic diversity will eventually raise viability in one population.

Recombination events can lead to either crossover (CO) or non-crossover (NCO) products depending on whether the flanking chromosome arms are exchanged (CO) or not (NCO). Meiotic CO is defined as reciprocal exchange of genetic material between parental chromosomes. Tracking of the crossover sites on the meiotic chromosome cores can be realized by electron microscopy and immunogold staining. The electron-dense meiotic nodules (MN) are visible during prophase I. Different from the abundant early nodules (EN), which appear during late leptonema to mid-pachynema, the number and distribution of the late nodules (LN), which are associated with pachytene SCs, correlate well with those of meiotic crossover sites (Carpenter 1975; Moens 1978; Zickler and Kleckner 1999).

Actually, the number and distribution of meiotic crossovers through the genome is stringently controlled. In mammals, the crossover control is a dynamic balance between obligate crossover and crossover interference (de Boer et al. 2006; Jones and Franklin 2006). Obligate crossover ensures that there is at least one crossover site per pair of chromosomes so that each homologous

pair will be held together until the end of meiosis I. It has been demonstrated that, although the foci numbers of early recombination proteins, such as RAD51 and DMC1, vary among mouse spermatocytes, the foci numbers of the crossover marker MLH1 display little variation, which is called homeostatic control of recombination (Cole et al. 2012). Crossover interference refers to the observation that the presence of one crossover reduces the chances of another crossover occurring nearby (de Boer et al. 2006). The effect of interference decreases when the distance from the recombination spot increases, which makes crossovers widely spaced among the genome. The location of crossover along the chromosomes is also not random. Some regions are preferred as crossover sites, which are called hot spots, while in others, called cold spots, the frequency of crossover is low. It is believed that hot spots are located at sites with more frequent double strand breaks and influenced by chromatin structure (Fukuda et al. 2008; Mets and Meyer 2009). Additionally, crossovers are always located away from the centromere, and most of the time, away from telomere end. Deviations from this rule could lead to homolog missegregation and aneuploidy (Lamb et al. 2005) .

Compared with single-celled eukaryotes, the study of meiotic recombination in mammals is more difficult due to the complexity of the multicelluar, endocrine organism itself, lengthy breeding period and also a more closed system for monitoring meiotic progression. By contrast, meiotic recombination is extensively studied in yeast, where multiple meiotic mutants can be generated rapidly and recombination products can be examined via tetrad analysis. Therefore, in the following discussion, the studies done in yeast are often the basis of our understanding of mammalian meiotic recombination.

4.1 Initiation of meiotic recombination

In mammals, as in most other organisms utilizing meiosis, meiotic recombination process begins as a genetically programmed double strand break (DSB) catalyzed by the type II topoisomerase-like DNA transesterase SPO11 during leptonema (Keeney 2001). In budding yeast, it has been found that many other proteins also participate in DSB formation. These proteins include *MER2*, *MRE11*, *RAD50*, *XRS2*, *REC114*, *MEI4*, *SKI8*, *REC102* and *REC104* (Maleki et al. 2007; Murakami and Keeney 2008). It is believed that, as in yeast, there may exist more proteins regulating meiotic DSB formation in mammals. Indeed, four of these yeast meiotic recombination proteins, *RAD50*, *MRE11*, *MEI4 and REC114*, have orthologues in mouse. Among them, RAD50 and MRE11 are found to function in mammalian mitotic, but not meiotic, DSB formation (Handel and Schimenti 2010), while MEI4 and REC114 are implicated to have important roles during meiosis (Kumar et al. 2010). Recent research indicates that mouse *Mei4* and *Rec114* are expressed in testis and embryonic ovary of mouse. In meiocytes, discrete MEI4 foci were found on the lateral elements of the synaptonemal complex at leptonema and zygonema. The number of MEI4 foci peak during leptonema and decrease after that. *Mei4* knockout mice show greatly reduced DSB formation and defects in synapsis, which imply the function of MEI4 as a structural component of the mammalian DSB machinery (Kumar et al. 2010). Additionally, one forward genetic mutation screening in mice identified another new gene *Mei1* required for DSB formation in vertebrate. Orthologues of *Mei1* are only present in the genomes of mammals, chickens, and zebrafish, but not yeast, worms, or flies (Libby et al. 2003).

The repair of SPO11-induced DSB is a multi-step process spanning from zygonema to the end of

pachynema. The process includes sensing of these breaks, recruitment of related proteins, forming and then processing of recombination intermediates.

The first step of DSB repair is the 5' to 3' end resection of the single strands of DNA at the breaks. In yeast, key proteins involved in this reaction include exonuclease-1 (*EXO1*) and bifunctional endo/exonuclease *MRE11* (Mimitou and Symington 2008; Zhu et al. 2008; Nicolette et al. 2010; Garcia et al. 2011). The involvement of EXO1 in mouse meiosis is uncertain, since *Exo1* mutant mice show later meiotic arrest than would be predicted by such an early requirement (Wei et al. 2003). *Mre11* inactivation prevents mouse embryonic stem cells from proliferating, and leads to embryonic lethality in gene targeted mice (Xiao and Weaver 1997; Buis et al. 2008). Although there is no direct evidence from mouse meiocytes, the experiments using mouse embryonic fibroblast cells indicates that the nuclease activity of MRE11 may function in generating single-stranded DNA and hence initiating homologous recombination in mammals (Buis et al. 2008).

After the 5' to 3' resection, the newly formed 3' protruding overhangs are then bound by single-strand exchange proteins, such as recA-related protein RAD51 and DMC1 (Pittman et al. 1998; Thacker 2005), forming nucleoprotein filaments, and invade the opposite homologous chromosomes, which lead to the formation of a displacement loop (also referred as D-loop or single-end invasion, SEI (Hunter and Kleckner 2001)).

It is believed that these initial interhomolog contacts may facilitate correct choice of the recombination partner (homology search) and the initiation of synapsis. The mechanism of recombination partner choice is well-studied in yeast. The inter-homolog exchange has been found to be promoted by "barriers to sister chromatid repair" (SCBR). In yeast, key regulators of the homolog bias include two SC axial element phosphoproteins, *RED1* and *HOP1*, and one

meiosis-specific kinase *MEK1* (Niu et al. 2005; Carballo et al. 2008). However, the study of recombination partner choice is more challenging in mammals since it is difficult to track inter-sister recombination products. Potential mammalian orthologues of *HOP1* had been identified. They are HORMA domain containing 1(HORMAD1) and HORMAD2 (Wojtasz et al. 2009; Fukuda et al. 2010). Like yeast *HOP1*, these two proteins also localize to chromosome axes in meiosis. However, further study is needed to prove their function in recombination partner choice.

As mentioned previously, *RAD51* and *DMC1* are identified in yeast as single strand invasion proteins and catalyze the formation of D-loop. They are also regarded as cellular markers of the sites where the repair by homologous recombination has begun. In mammals, the number of recombination events per meiosis can be estimated by counting RAD51/DMC1 foci. In mice and humans, more than 200 recombination events can be estimated per meiosis according to RAD51/DMC1 foci on chromosome cores with variations depending on species and sex (Ashley et al. 1995; Moens et al. 1997) and the vast majority are resolved by NCO.

There are several recombination pathways downstream of D-loop formation. Different pathways result in different recombination outcomes (See Figure 1- 3). The major ones include the well-studied interference-dependent Class I CO pathway, the interference-independent Class II CO pathway and the non-crossover (NCO) pathway (also known as synthesis dependent strand annealing (SDSA) pathway). The molecular details regarding SDSA remain unclear in mammals, but the temporally distinct appearance of NCO relative to CO implies that such a pathway exists and is distinguishable from the two CO pathways (Allers and Lichten 2001). Our understanding of the NCO pathway, therefore, is confined to extrapolation from the yeast literature.

Figure 1-3. Mammalian meiotic recombination pathways.

This diagram depicts hypothesized events during meiotic recombination. Recombination is initiated by the formation of DSB in leptonema. The repair of DSB is a multi-step process beginning with the formation of D-loop structure in zygonema. After D-loop formation, there are four hypothesized pathways to DSB repair: Class I CO (DSBR) pathway, Class II CO pathway, SDSA pathway, and anti-recombination pathway. These pathways lead to either CO or NCO between homologs. Homologous chromosomes are shown as horizontal blue and pink lines. The proteins hypothesized to be responsible for each step are listed on the right in bold. This figure is adapted from "*Crossover promotion and prevention*" (Lorenz and Whitby 2006).

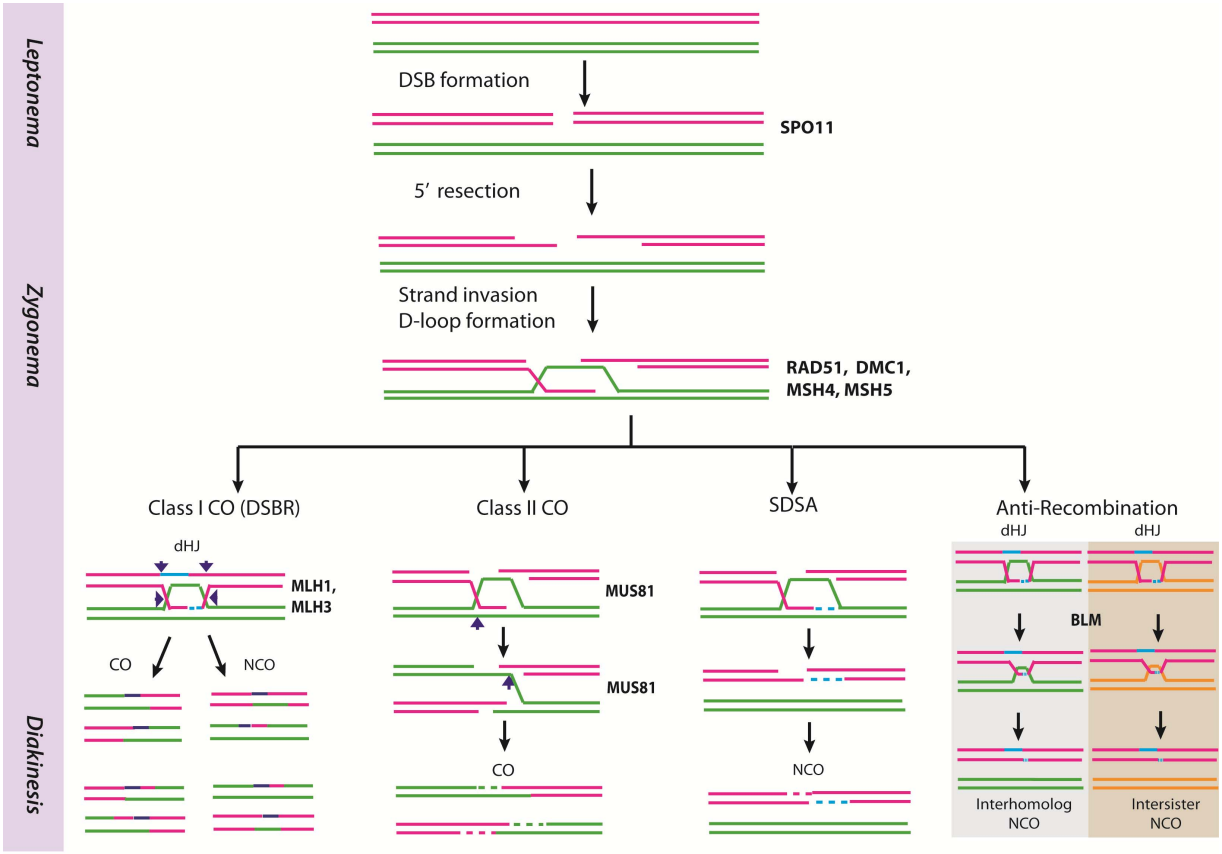
Leptonema
Zygonema
Diakinesis
DSB formation
SPO11
5′ resection
Strand invasion
D-loop formation
RAD51, DMC1,
MSH4, MSH5
Class I CO (DSBR)
Class II CO
SDSA
Anti-Recombination
dHJ
MLH1,
MLH3
CO
NCO
MUS81
MUS81
CO
NCO
dHJ
dHJ
BLM
Interhomolog
NCO
Intersister
NCO

Of the two CO pathways, it is clear that they are utilized to different extents in different organisms. For example, in *C. elegans*, almost all COs are generated from the Class I CO pathway (Zalevsky et al. 1999), whereas fission yeast heavily depends on the Class II CO pathway (Boddy et al. 2001). Both mouse and budding yeast use Class I and Class II CO pathways, and prefer Class I pathway for CO generation (Woods et al. 1999; de los Santos et al. 2003; Borner et al. 2004; Guillon et al. 2005). Mouse mutants defective in key proteins during Class I CO proteins have reduced COs to 10% of wild-type level, while equivalent mutants in budding yeast still have ~20% COs left compared with wild-type (Edelmann et al. 1999; Argueso et al. 2004; Borner et al. 2004). More details about these two CO pathways will be provided in the discussion below.

4.2 Meiotic recombination pathways

4.2.1 The Class I CO pathway and the role of the DNA mismatch repair family

The Class I CO pathway is the most extensively studied pathway, and is also known as double strand break repair (DSBR) pathway or ZMM (for yeast protein Zip1/ Zip2/ Zip3, Msh4/Msh5 and Mer3) pathway (Borner et al. 2004). This pathway follows the canonical Szostak model (Szostak et al. 1983). In this model, after DSB formation and resection of the 5' ends, 3' overhangs are generated and invade the opposite homologous chromosomes forming D- loop (or SEI), a three-strand structure formed between the invading single-stranded and homologous double-stranded DNA. The D-loop is then extended through DNA synthesis and pairs with the other end of the break, which is known as second end capture. Further DNA extension and ligation lead to the formation of a meiotic intermediate, known as the double Holliday junction (dHJ). Then dHJ is resolved through reciprocal exchange of DNA segments from each

homologous chromosome by the action of a nuclear HJ resolvase, which is still poorly characterized. Depending on the way dHJ is cleaved, resolution of the intermediate can result in CO or NCO events.

Presumably, the chances to generate CO or NCO after dHJ resolution should be equal since the structure of dHJ is essentially symmetrical. However, the dHJ resolution is often biased towards CO formation with the majority of meiotic CO events arising from DSBR pathway, as seen in both yeast and mammals (Borner et al. 2004; Guillon et al. 2005), and it now appears that NCO events arise at a temporally distinct time point, somewhat earlier in prophase I, at least in yeast (Allers and Lichten 2001; Borner et al. 2004). In yeast, the establishing of biased dHJ resolution depends on the so-called ZMM proteins, including *ZIP1*, *ZIP2*, *ZIP3*, *MSH4*, *MSH5* and *MER3*. Strains carrying mutations in any of these genes have a reduction of COs, whereas NCOs are not affected (Borner et al. 2004). It is believed that ZMM proteins are responsible for stabilizing SEI during leptonema to zygonema at sites of future CO and maturing SEI into dHJ in yeast (Agarwal and Roeder 2000; Henderson and Keeney 2004; Lynn et al. 2007), partly by protecting the nascent CO intermediates from dissolution by RecQ-helicase *SGS1* (Jessop et al. 2006).

ZMM proteins are a group of functionally collaborating proteins. They can be divided into three functional subgroups. *ZIP1* is the functional and structural orthologue of mammalian SYCP1 (Page and Hawley 2004), and it establishes the association between homologous chromosomes as one component of SC central element. *ZIP2* and *ZIP3* are thought to mediate protein-protein interaction and have been implicated in ubiquitinylation and SUMOylation (Perry et al. 2005). Although there is evidence suggesting *ZIP3* is a SUMO E3 ligase that regulates SC proteins on meiotic chromosome cores and is necessary for SC formation in yeast (Cheng et al. 2006), no direct evidence has been found supporting the role of *ZIP3* in meiotic recombination. *MER3* is a

DNA helicase that unwinds double-stranded DNA from 3' to 5'. It is thought that *MER3* stabilizes the nascent recombination intermediate by promoting second end capture of a double strand break (Mazina et al. 2004).

The other two ZMM proteins, Msh4 and Msh5, are two homologs of bacterial MutS protein belonging to the mismatch repair (MMR) protein family. The MMR protein family is a group of highly conserved proteins. As its name implies, when first characterized in bacteria, the MMR protein family is identified for its function in correcting mismatches during S phase and maintaining the stability of the genome. Defects in this system often result in a mutator phenotype. In the canonical *E. coli* MMR system, there are three members: MutS, MutL and MutH, all of which act as homodimers. In a typical prokaryotic mismatch repair event, MutS protein plays as an ATPase and recognizes the mismatch site. MutL is the coordinator, which is recruited to the mismatch site and couples the detection of mismatch by MutS to downstream MutH. MutH is a methylation-sensitive endonuclease, which cuts the unmethylated newly synthesized strand. Depending on the side of the nick induced by MutH, one of the four exonucleases will be recruited to remove the mismatch- containing nicked strand in either 3' to 5' (ExoI, ExoX or ExoVII) or 5' to 3' direction (RecJ or ExoVII). Following excision, DNA is resynthesized by DNA polymerase III and then ligated by an unknown ligase (Kunkel and Erie 2005).

The MMR system is highly conserved through evolution, although the system is more complex in eukaryotes and more mismatch repair proteins are involved. In mammals, there are five MutS homologs, MSH2 through MSH6, and four MutL homologs, MLH1, PMS1, MLH3 and PMS2. No convincing MutH homologs have been found in eukaryotes. The MutS homologs form three heterodimer complexes: MSH2-MSH6 (MutSα), MSH2-MSH3 (MutSβ), and MSH4-MSH5

(MutSγ), while the MutL homologs also form three heterodimer complexes: MLH1- PMS2 (MutLα) and MLH1- PMS1 (MutLβ), MLH1- MLH3 (MutLγ).

In mouse somatic cells, it has been demonstrated that the heterodimers mentioned above all have their own speciality. MutSα participates in correction of base substitution and small insertion-deletion mismatches, while MutSβ is partially redundant with MutSα and specifically repairs insertion-deletion mismatches (Acharya et al. 1996; Genschel et al. 1998; Macpherson et al. 1998). MutLα is the major MutL heterodimer involved in various mismatch repair processes, and may interact with both MutSα and MutSβ (Kolas and Cohen 2004; Kunkel and Erie 2005). The important function of these MMR complexes in maintaining genomic integrity is underscored by the fact that the majority of human non-polyposis colorectal cancer (HNPCC) is associated with mutations in MSH2 (the major MutS homolog) and MLH1(the principle MutL homolog) (Pedroni et al. 2001).

Besides the important function in detecting and repairing DNA mismatches, MMR protein family is also found to play a critical role in eukaryotic meiosis. It has been demonstrated that MSH4 and MSH5, which form MutSγ, have no mitotic mismatch repair activity in either vegetative or meiotic cells (Svetlanov and Cohen 2004). Instead, this heterodimer functions exclusively during meiotic crossover. Deleting either *MSH4* or *MSH5* in yeast results in decreased spore viability and a significant reduction in crossovers (Ross-Macdonald and Roeder 1994; Hollingsworth et al. 1995; Pochart et al. 1997). The homologs of *MSH4* and *MSH5* have also been found in a number of other organisms, including *C. elegans*, mice and humans, which shows their conservation through evolution and underscores the importance of these two proteins during meiosis (Paquis-Flucklinger et al. 1997; Winand et al. 1998; Bocker et al. 1999; Edelmann et al. 1999; Kneitz et al. 2000). Deleting either *Msh4* or *Msh5* from mice leads to

infertility in both males and females. Mutants from both sexes show meiotic arrest at zygonema and a high degree of mispairing, self-synapsis and nonhomologous pairing, followed by apoptosis prior to pachynema (Edelmann et al. 1999; Kneitz et al. 2000; Cohen et al. 2006). Consistent with their meiosis-specific function, *Msh4* or *Msh5* mutant mice show no increase in the risk of tumorigenesis compared with wild-type mice (de Vries et al. 1999; Edelmann et al. 1999; Kneitz et al. 2000). Cytologically, in mouse and also in human, both proteins can be observed as distinct immunofluorescent foci along the paired chromosomes starting from zygonema (100~200 foci per cell), continuing into early to mid-pachynema (50~100 foci per cell), when MSH4 colocalizes with another protein MLH1, which marks the sites of crossovers (Kneitz et al. 2000; Santucci-Darmanin et al. 2000) and disappearing in late pachynema (Moens et al. 2002; Kolas et al. 2005; Lenzi et al. 2005). The distribution of MSH4 foci along the chromosome shows a low level of interference since MSH4 foci are more evenly distributed compared to a totally random distribution (de Boer et al. 2006). However, different from the restricted number of MLH1 foci on each chromosome at pachynema, MSH4 foci along zygotene chromosomes significantly outnumber the prospective COs, indicating that MSH4/ MSH5 may also be responsible for the formation of NCO in mammals.

After the preloading of MSH4-MSH5 onto the meiotic chromosome, they are joined by MutLγ (MLH1- MLH3 heterodimer), which is the other MMR complex with pivotal role in meiosis. MLH1 and MLH3 function after ZMM proteins, possibly during resolution of dHJs, and are critical for meiotic cell progression through the Class I CO pathway (Hunter and Borts 1997; Wang et al. 1999). In yeast, the *mlh1* mutant strains show a elevated rate of spontaneous mutations while the deletion of Mlh3 only causes subtle defects in suppression of frameshift repair (Flores-Rozas and Kolodner 1998; Harfe and Jinks-Robertson 2000). Meanwhile, both

mutants show decreased spore viability and reduced frequencies of crossing over caused by homolog nondisjunction (Hunter and Borts 1997; Wang et al. 1999). Furthermore, the meiotic phenotype of *msh4 mlh1* double mutant strain is similar to *msh4* single mutant strain, which indicates that Mlh1/Mlh3 act after Msh4/Msh5 in the same meiotic recombination pathway (Hunter and Borts 1997).

Both Mlh1 and Mlh3 genes are evolutionally conserved across species and their homologs can be found in both humans and mice. Research in the mouse has confirmed the involvement of *Mlh1* and *Mlh3* during mammalian meiotic recombination pathways. There is evidence suggesting that MLH3 and MLH1 are recruited sequentially to a subset of MSH4-MSH5 foci (Santucci-Darmanin et al. 2000; Santucci-Darmanin et al. 2002; Kolas et al. 2005). Both protein foci can be found on meiotic chromosome cores during pachynema and colocalize at electron-dense recombination nodules during the pachytene stage (Baker et al. 1996; Lipkin et al. 2002; Marcon and Moens 2003; Kolas et al. 2005).

It is noteworthy that MLH1 foci are now a widely accepted marker for meiotic crossovers in mammals since the number (~ 22-31 foci per nuclei) and distribution of these foci correlate well with the number and distribution of chiasmata on diakinesis/ metaphase I chromosomes in both mice and humans (Baker et al. 1996; Barlow and Hulten 1998; Anderson et al. 1999; Tease et al. 2002). Consequently, both *Mlh1* and *Mlh3* knockout mice show impaired chiasmata formation by the end of prophase I, which causes infertility in both males and females (Baker et al. 1996; Edelmann et al. 1996; Lipkin et al. 2002; Kan et al. 2008). While massive cell death is found in luminal spermatocytes of mutant males, follicular development and ovulation are normal in females but the oocytes cannot bypass two-cell stage after fertilization (Edelmann et al. 1996; Lipkin et al. 2002; Kan et al. 2008).

While the localization of MLH1 and MLH3 has become proxy for chiasmata distribution in many organisms, it is clear that not all COs are MLH1/ MLH3 dependent. In yeast meiosis, Mlh1/Mlh3 is required for 30%-50% of all crossovers (Hunter and Borts 1997). The contribution of MLH1/MLH3 to meiotic COs is larger in mice. They are necessary for the formation of 90% of all COs but not for NCO formation (Guillon et al. 2005; Svetlanov et al. 2008).

4.2.2 Class II Crossover pathway

The residual crossovers detected in yeast *mlh1* or *mlh3* mutants, together with the numerical discrepancy between numbers of MLH1/MLH3 foci at pachynema and chiasmata at diakinesis in the mouse, imply that there exists another recombination pathway that can lead to crossovers. Indeed, based on the studies in yeast, it has been shown that there is another CO pathway in eukaryotes, known as Class II CO pathway. In contrast to the Class I CO pathway, the Class II CO pathway is non-interfering and depends on the activity of Mus81. Mus81 is an evolutionarily conserved endonuclease that shares homology with the XPF/Rad1 protein family. It usually acts as a heterodimer with another protein, which is called Mms4 in budding yeast, *S. cerevisiae*, and Eme1 in fission yeast, *S. pombe* (Boddy et al. 2001; Kaliraman et al. 2001). The human partner protein of MUS81 is known as MMS4 or EME1 (Ciccia et al. 2003; Ogrunc and Sancar 2003).

While budding yeast and mammals only use this pathway to generate a minor portion of COs (Holloway et al. 2008), fission yeast uses this Mus81-dependent pathway as its major CO pathway during meiosis (Boddy et al. 2001). The deletion of *mus81* from fission yeast dramatically reduces the number of viable meiotic progeny and the frequency of COs in the surviving progeny (Boddy et al. 2001; Osman et al. 2003).

The actual mechanism of Mus81 action is still under debate. It was originally proposed that

Mus81 generated COs by resolving HJs, which was based on the discovery that partially purified Mus81 could cleave intact HJs *in vitro* (Hollingsworth and Brill 2004). However, recent research in fission yeast shows that Mus81 is required for the resolution of the single HJs, which are the meiotic recombination intermediates in this organism and formed preferentially between sister chromatids (Cromie et al. 2006). On the other hand, studies in budding yeast suggest that the major function of Mus81 during budding yeast meiosis is to resolve aberrant recombination intermediates prior to HJ formation (de los Santos et al. 2003; Borner et al. 2004; Jessop and Lichten 2008; Oh et al. 2008).

Although *Mus81* deficient mice are not entirely sterile (McPherson et al. 2004; Dendouga et al. 2005; Holloway et al. 2008), a more detailed study of the meiotic phenotype shows that the knockout of *Mus81* leads to significant meiotic defects, including reduced sperm number and increased apoptotic cells in seminiferous tubules (Holloway et al. 2008). MLH1-MLH3 foci are found to be accumulated on pachytene chromosomes of these mutants, suggesting an intact Class I CO pathway in these mutant mice. Chiasmata numbers are found to be normal in spermatocytes from these *Mus81*$^{-/-}$ animals, indicating that MUS81 may play important roles in mammalian CO regulation and may generate a small subset of COs through a MLH1- MLH3- independent pathway (Holloway et al. 2008). Importantly, the significant increase in MLH1 and MLH3 accumulation at pachynema in these *Mus81* mutant mice suggests that the loss of MUS81-dependent recombination events results in a compensatory increase in MLH1/MLH3. This results in an overall maintenance of final chiasmata counts, indicating that the class I pathway can be utilized in the absence of the class II pathway, but not *vice versa*.

Besides the CO pathways mentioned above, research in budding yeast also suggests a third

pathway which generates COs without Msh4–Msh5 and Mus81-Mms4 (Argueso et al. 2004). While yeast double mutants defective for genes from both pathways show an additive decrease in COs compared with single mutants, residual COs can still be found in these mutants. Similar evidence has also been observed in mice. In *Mus81*$^{-/-}$ *Mlh3*$^{-/-}$ double null mice, the number of COs is significantly reduced compared with wild-type or single null mice, but residual COs can still be observed in diakinesis spermatocytes of the double null mouse (Holloway et al. 2008).

4.2.3 Synthesis dependent strand annealing (SDSA) pathway

In the original Szostak model, the DSBR pathway is responsible for both COs and NCOs depending on which strands are cleaved during dHJ resolution (Szostak et al. 1983). However, this paradigm has been challenged by recent studies, which show that COs and NCOs are generated through temporally distinct recombination pathways (Allers and Lichten 2001; Guillon et al. 2005). Although the formation of both COs and NCOs involves early steps, such as Spo11-induced DSB and resection of 5' end, it has been found that CO and NCOs have separate heteroduplex intermediates and certain yeast mutants have reduced numbers of COs with unaffected levels of NCOs (Allers and Lichten 2001). Instead of the classic DSBR pathway, the synthesis-dependent strand annealing (SDSA) pathway has been suggested to be responsible for generating most NCOs in budding yeast. In this pathway, strand invasion occurs on only one side of the DSB. The newly synthesized DNA strand is displaced from the template and anneals with the other DSB end, resulting a non-crossover event (Paques and Haber 1999).

A separate pathway for producing NCOs has also been suggested in mammals. In mouse meiosis, the formation of NCO products has a similar kinetics as CO products during mid- to late-pachynema. Additionally, NCO and CO products show different sizes of conversion tracts

(500bp for CO products and 300bp for NCO products), which implies that NCO and CO are generated through different pathways through different recombination intermediates in mice (Guillon et al. 2005; Baudat and de Massy 2007).

4.2.4 RecQ helicases and anti-recombination pathway

The RecQ helicases are one of the most highly conserved groups of helicases, named after the prototypical family member found in *E. coli*. As a special type of helicases, which can unwind complex DNA structures, such as dHJ and D-loop, RecQ helicases have been implicated in maintaining genome integrity across different species (Gangloff et al. 1994; Hanada et al. 1997; Lindor et al. 2000; Hickson 2003; Hanada and Hickson 2007). Sgs1 is the RecQ orthologue in budding yeast, and its mammalian orthologue is BLM. It has been found that both proteins can act during meiotic recombination to eliminate CO intermediates (Karow et al. 2000; Hanada and Hickson 2007; Jessop and Lichten 2008). *In vitro* studies show that, during meiotic recombination, BLM can displace the invading strand of D-loop, while both BLM and Sgs1 are able to promote branch migration of *bona fide* dHJs generated by the RecA protein (Hickson 2003; Bachrati et al. 2006). Furthermore, together with topoisomerase III and Rmi1 family proteins, BLM and Sgs1 can lead to of dHJ dissolution and produce NCO products (Mankouri and Hickson 2007).

Further studies done in budding yeast show that Sgs1 is required for normal metabolism of joint molecule recombination intermediates (Oh et al. 2008). It is reported that Sgs1 is antagonized by ZMM synapsis-promoting proteins at designated CO sites and contributes to the prevention of the accumulation of multi-chromatid joint molecules although its activity is not required for the formation of NCOs (Jessop et al. 2006; Jessop and Lichten 2008; Oh et al. 2008).

The impact of *Blm* in mammalian meiosis has been estimated by several studies using gene targeted mice as a model (Chester et al. 1998; Luo et al. 2000; Holloway et al. 2010). In *Blm* conditional knockout mice, the classic DSBR pathway seems functional in *Blm* deficient spermatocytes, given that the RAD51, MSH4 and MLH1 localization profile is normal. However, the knockout of *Blm* from spermatocytes leads to the formation of complex multichromatid structures and increased mispairing and asynapsis during prophase I (Holloway et al. 2010), indicating defects in meiotic pairing and synapsis. Meanwhile, the absence of *Blm* also causes an increase in chiasmata numbers at diakinesis (Holloway et al. 2010), which is consistent with the phenotype seen in *sgs1* yeast mutant and suggests the role of *Blm* in regulating meiotic recombination through non-DSBR pathway (Oh et al. 2007).

4.3 Cross-regulation between recombination pathways

It is notable that these various recombination pathways are not completely independent. Research evidence from both yeast and mammals suggests that meiotic recombination is a dynamic process, and crosstalk may exist between different recombination pathways. In budding yeast, it is suggested that yeast *MLH2* (*Pms1* in mouse), one MutL homolog protein, can transverse a subset of recombination intermediates into Class I CO pathway by preventing *MUS81* from binding with the substrate (Abdullah et al. 2004). In mice, the deletion of *Mus81* does not cause any changes in chiasmata, but leads to an increase in MLH1-MLH3 foci on pachytene chromosomes, implying possible crosstalk between two major CO recombination pathways (Holloway et al. 2008). Indeed, it has been demonstrated that BLM interacts with the key players in both Class I and Class II CO pathways, implying that BLM may be one of the

regulators between these two CO pathways. In one *in vitro* study, the C-terminus of BLM is found to interact with MLH1 (Langland et al. 2001). Another *in vivo* study in human somatic cell shows that BLM physically interacts and colocalizes with MUS81, stimulating MUS81 endonuclease activity through facilitating the binding of MUS81 to its DNA substrates (Zhang et al. 2005). More recently, the gene *Slx4* (or *Btbd12)* was also implicated as a possible mediator of crosstalk between the Class I and Class II pathways in the mouse (Holloway et al. 2011).

5. Investigating the role of Class I pathway components in establishing the bulk of CO events in the mouse

As discussed above, one important question to be answered in mammalian meiosis is how meiotic intermediates are processed so that COs and NCOs are generated through different recombination pathways. However, our understanding about this process is far from complete, even for the better-studied Class I recombination pathway, which is the major CO pathway responsible for about 90% of COs in mammals. While some critical pieces of this Class I pathway jigsaw have been identified, such as MSH4, MSH5, MLH1 and MLH3, and the loading sequence of these proteins has been determined (MSH4-MSH5 heterodimer loads first, and then comes MLH3 and MLH1 sequentially to a subset of these foci), it is still not clear how the ultimate CO sites are selected from the pool of MSH4-MSH5 sites, and how MutLγ, especially MLH3, or some unknown players facilitate the selection.

Mouse MLH3 is the most recently identified MutL homolog with unique structural features. First, mouse MLH3 contains a highly conserved metal binding motif, and the potential endonuclease activity of this domain has been implicated in the study of human MutL homolog PMS2

(Kadyrov et al. 2006). Second, mouse MLH3 also features a large region in exon 2 which is highly conserved in mammals, and which results in a mammalian MLH3 protein that is doubled in size compared with its yeast counterpart. However, no known functional protein motif has been predicted for this region. This is an intriguing observation given the high similarity among yeast and mammalian MMR proteins.

Mouse CNTD1 is a newly identified cyclin-related protein, whose critical function in eukaryotic meiosis has been implicated in the study of its *C. elegans* orthologue COSA-1. Studies in *C.elegans cosa-1* mutant has shown that mutations in this gene lead to frequent missegregaton of sex chromosomes and a high incidence of non-viable embryos (Yokoo et al. 2012). It was found that homolog pairing, synapsis and double strand break formation were normal in these mutants during meiosis, while interhomolog crossovers were defective without COSA-1.

In this dissertation, I study mammalian meiosis using mice as a model. I hypothesize that both regions of mouse MLH3 are indispensable for normal function of this protein, and mouse CNTD1 has critical function during meiotic recombination in mammals. Three specific aims will be addressed in the following chapters: 1) to investigate the role of mouse MLH3 endonuclease domain during meiosis, 2) to explore the function of mouse *Mlh3* exon 2 region, and 3) to exam the role of *Cntd1* during mouse meiosis.

6. References

Abdullah MF, Hoffmann ER, Cotton VE, Borts RH. 2004. A role for the MutL homologue MLH2 in controlling heteroduplex formation and in regulating between two different crossover pathways in budding yeast. *Cytogenet Genome Res* **107**(3-4): 180-190.

Acharya S, Wilson T, Gradia S, Kane MF, Guerrette S, Marsischky GT, Kolodner R, Fishel R. 1996. hMSH2 forms specific mispair-binding complexes with hMSH3 and hMSH6. *Proc Natl Acad Sci U S A* **93**(24): 13629-13634.

Agarwal S, Roeder GS. 2000. Zip3 provides a link between recombination enzymes and synaptonemal complex proteins. *Cell* **102**(2): 245-255.

Allers T, Lichten M. 2001. Differential timing and control of noncrossover and crossover recombination during meiosis. *Cell* **106**(1): 47-57.

Anderson EL, Baltus AE, Roepers-Gajadien HL, Hassold TJ, de Rooij DG, van Pelt AM, Page DC. 2008. Stra8 and its inducer, retinoic acid, regulate meiotic initiation in both spermatogenesis and oogenesis in mice. *Proc Natl Acad Sci U S A* **105**(39): 14976-14980.

Anderson LK, Reeves A, Webb LM, Ashley T. 1999. Distribution of crossing over on mouse synaptonemal complexes using immunofluorescent localization of MLH1 protein. *Genetics* **151**(4): 1569-1579.

Argueso JL, Wanat J, Gemici Z, Alani E. 2004. Competing crossover pathways act during meiosis in Saccharomyces cerevisiae. *Genetics* **168**(4): 1805-1816.

Ashley T, Plug AW, Xu J, Solari AJ, Reddy G, Golub EI, Ward DC. 1995. Dynamic changes in Rad51 distribution on chromatin during meiosis in male and female vertebrates. *Chromosoma* **104**(1): 19-28.

Bachrati CZ, Borts RH, Hickson ID. 2006. Mobile D-loops are a preferred substrate for the Bloom's syndrome helicase. *Nucleic Acids Res* **34**(8): 2269-2279.

Bai X, Peirson BN, Dong F, Xue C, Makaroff CA. 1999. Isolation and characterization of SYN1, a RAD21-like gene essential for meiosis in Arabidopsis. *Plant Cell* **11**(3): 417-430.

Baker SM, Plug AW, Prolla TA, Bronner CE, Harris AC, Yao X, Christie DM, Monell C, Arnheim N, Bradley A et al. 1996. Involvement of mouse Mlh1 in DNA mismatch repair and meiotic crossing over. *Nature Genetics* **13**(3): 336-342.

Barlow AL, Hulten MA. 1998. Crossing over analysis at pachytene in man. *Eur J Hum Genet* **6**(4): 350-358.

Baudat F, de Massy B. 2007. Regulating double-stranded DNA break repair towards crossover or non-crossover during mammalian meiosis. *Chromosome Res* **15**(5): 565-577.

Bocker T, Barusevicius A, Snowden T, Rasio D, Guerrette S, Robbins D, Schmidt C, Burczak J, Croce CM, Copeland T et al. 1999. hMSH5: a human MutS homologue that forms a novel heterodimer with hMSH4 and is expressed during spermatogenesis. *Cancer Res* **59**(4): 816-822.

Boddy MN, Gaillard PH, McDonald WH, Shanahan P, Yates JR, 3rd, Russell P. 2001. Mus81-Eme1 are essential components of a Holliday junction resolvase. *Cell* **107**(4): 537-548.

Bolcun-Filas E, Costa Y, Speed R, Taggart M, Benavente R, De Rooij DG, Cooke HJ. 2007. SYCE2 is required for synaptonemal complex assembly, double strand break repair, and homologous recombination. *J Cell Biol* **176**(6): 741-747.

Bolcun-Filas E, Speed R, Taggart M, Grey C, de Massy B, Benavente R, Cooke HJ. 2009. Mutation of the mouse Syce1 gene disrupts synapsis and suggests a link between synaptonemal complex structural components and DNA repair. *PLoS Genet* **5**(2):

e1000393.

Borner GV, Kleckner N, Hunter N. 2004. Crossover/noncrossover differentiation, synaptonemal complex formation, and regulatory surveillance at the leptotene/zygotene transition of meiosis. *Cell* **117**(1): 29-45.

Borum K. 1961. Oogenesis in the mouse. *Exp Cell Res* **24**: 495-507.

Bowles J, Knight D, Smith C, Wilhelm D, Richman J, Mamiya S, Yashiro K, Chawengsaksophak K, Wilson MJ, Rossant J et al. 2006. Retinoid signaling determines germ cell fate in mice. *Science* **312**(5773): 596-600.

Buis J, Wu Y, Deng Y, Leddon J, Westfield G, Eckersdorff M, Sekiguchi JM, Chang S, Ferguson DO. 2008. Mre11 nuclease activity has essential roles in DNA repair and genomic stability distinct from ATM activation. *Cell* **135**(1): 85-96.

Carballo JA, Johnson AL, Sedgwick SG, Cha RS. 2008. Phosphorylation of the axial element protein Hop1 by Mec1/Tel1 ensures meiotic interhomolog recombination. *Cell* **132**(5): 758-770.

Carpenter AT. 1975. Electron microscopy of meiosis in Drosophila melanogaster females: II. The recombination nodule--a recombination-associated structure at pachytene? *Proc Natl Acad Sci U S A* **72**(8): 3186-3189.

Champion MD, Hawley RS. 2002. Playing for half the deck: the molecular biology of meiosis. *Nat Cell Biol* **4 Suppl**: s50-56.

Cheng CH, Lo YH, Liang SS, Ti SC, Lin FM, Yeh CH, Huang HY, Wang TF. 2006. SUMO modifications control assembly of synaptonemal complex and polycomplex in meiosis of Saccharomyces cerevisiae. *Genes Dev* **20**(15): 2067-2081.

Chester N, Kuo F, Kozak C, O'Hara CD, Leder P. 1998. Stage-specific apoptosis, developmental

delay, and embryonic lethality in mice homozygous for a targeted disruption in the murine Bloom's syndrome gene. *Genes Dev* **12**(21): 3382-3393.

Ciccia A, Constantinou A, West SC. 2003. Identification and characterization of the human mus81-eme1 endonuclease. *J Biol Chem* **278**(27): 25172-25178.

Cohen PE, Holloway JK. 2010. Predicting gene networks in human oocyte meiosis. *Biol Reprod* **82**(3): 469-472.

Cohen PE, Pollack SE, Pollard JW. 2006. Genetic analysis of chromosome pairing, recombination, and cell cycle control during first meiotic prophase in mammals. *Endocr Rev* **27**(4): 398-426.

Cole F, Kauppi L, Lange J, Roig I, Wang R, Keeney S, Jasin M. 2012. Homeostatic control of recombination is implemented progressively in mouse meiosis. *Nat Cell Biol* **14**(4): 424-430.

Costa Y, Speed R, Ollinger R, Alsheimer M, Semple CA, Gautier P, Maratou K, Novak I, Hoog C, Benavente R et al. 2005. Two novel proteins recruited by synaptonemal complex protein 1 (SYCP1) are at the centre of meiosis. *Journal of Cell Science* **118**(Pt 12): 2755-2762.

Crackower MA, Kolas NK, Noguchi J, Sarao R, Kikuchi K, Kaneko H, Kobayashi E, Kawai Y, Kozieradzki I, Landers R et al. 2003. Essential role of Fkbp6 in male fertility and homologous chromosome pairing in meiosis. *Science* **300**(5623): 1291-1295.

Cromie GA, Hyppa RW, Taylor AF, Zakharyevich K, Hunter N, Smith GR. 2006. Single Holliday junctions are intermediates of meiotic recombination. *Cell* **127**(6): 1167-1178.

de Boer E, Stam P, Dietrich AJ, Pastink A, Heyting C. 2006. Two levels of interference in mouse meiotic recombination. *Proc Natl Acad Sci U S A* **103**(25): 9607-9612.

de los Santos T, Hunter N, Lee C, Larkin B, Loidl J, Hollingsworth NM. 2003. The Mus81/Mms4 endonuclease acts independently of double-Holliday junction resolution to promote a distinct subset of crossovers during meiosis in budding yeast. *Genetics* **164**(1): 81-94.

de Vries SS, Baart EB, Dekker M, Siezen A, de Rooij DG, de Boer P, te Riele H. 1999. Mouse MutS-like protein Msh5 is required for proper chromosome synapsis in male and female meiosis. *Genes Dev* **13**(5): 523-531.

Dendouga N, Gao H, Moechars D, Janicot M, Vialard J, McGowan CH. 2005. Disruption of murine Mus81 increases genomic instability and DNA damage sensitivity but does not promote tumorigenesis. *Mol Cell Biol* **25**(17): 7569-7579.

Dobson MJ, Pearlman RE, Karaiskakis A, Spyropoulos B, Moens PB. 1994. Synaptonemal complex proteins: occurrence, epitope mapping and chromosome disjunction. *J Cell Sci* **107 (Pt 10)**: 2749-2760.

Edelmann W, Cohen PE, Kane M, Lau K, Morrow B, Bennett S, Umar A, Kunkel T, Cattoretti G, Chaganti R et al. 1996. Meiotic pachytene arrest in MLH1-deficient mice. *Cell* **85**(7): 1125-1134.

Edelmann W, Cohen PE, Kneitz B, Winand N, Lia M, Heyer J, Kolodner R, Pollard JW, Kucherlapati R. 1999. Mammalian MutS homologue 5 is required for chromosome pairing in meiosis. *Nat Genet* **21**(1): 123-127.

Evans CW, Robb DI, Tuckett F, Chanlloner S. 1982. Regulation of meiosis in the foetal mouse gonad. *J Embryol exp Morph* **68**: 59-67.

Flores-Rozas H, Kolodner RD. 1998. The Saccharomyces cerevisiae MLH3 gene functions in MSH3-dependent suppression of frameshift mutations. *Proc Natl Acad Sci U S A* **95**(21):

12404-12409.

Fukuda T, Daniel K, Wojtasz L, Toth A, Hoog C. 2010. A novel mammalian HORMA domain-containing protein, HORMAD1, preferentially associates with unsynapsed meiotic chromosomes. *Exp Cell Res* **316**(2): 158-171.

Fukuda T, Kugou K, Sasanuma H, Shibata T, Ohta K. 2008. Targeted induction of meiotic double-strand breaks reveals chromosomal domain-dependent regulation of Spo11 and interactions among potential sites of meiotic recombination. *Nucleic Acids Res* **36**(3): 984-997.

Gangloff S, McDonald JP, Bendixen C, Arthur L, Rothstein R. 1994. The yeast type I topoisomerase Top3 interacts with Sgs1, a DNA helicase homolog: a potential eukaryotic reverse gyrase. *Mol Cell Biol* **14**(12): 8391-8398.

Garcia V, Phelps SE, Gray S, Neale MJ. 2011. Bidirectional resection of DNA double-strand breaks by Mre11 and Exo1. *Nature* **479**(7372): 241-244.

Genschel J, Littman SJ, Drummond JT, Modrich P. 1998. Isolation of MutSbeta from human cells and comparison of the mismatch repair specificities of MutSbeta and MutSalpha. *J Biol Chem* **273**(31): 19895-19901.

Goetz P, Chandley AC, Speed RM. 1984. Morphological and temporal sequence of meiotic prophase development at puberty in the male mouse. *J Cell Sci* **65**: 249-263.

Guillon H, Baudat F, Grey C, Liskay RM, de Massy B. 2005. Crossover and noncrossover pathways in mouse meiosis. *Mol Cell* **20**(4): 563-573.

Hamer G, Gell K, Kouznetsova A, Novak I, Benavente R, Hoog C. 2006. Characterization of a novel meiosis-specific protein within the central element of the synaptonemal complex. *J Cell Sci* **119**(Pt 19): 4025-4032.

Hanada K, Hickson ID. 2007. Molecular genetics of RecQ helicase disorders. *Cell Mol Life Sci* **64**(17): 2306-2322.

Hanada K, Ukita T, Kohno Y, Saito K, Kato J, Ikeda H. 1997. RecQ DNA helicase is a suppressor of illegitimate recombination in Escherichia coli. *Proc Natl Acad Sci U S A* **94**(8): 3860-3865.

Handel MA, Schimenti JC. 2010. Genetics of mammalian meiosis: regulation, dynamics and impact on fertility. *Nat Rev Genet* **11**(2): 124-136.

Harfe BD, Jinks-Robertson S. 2000. DNA mismatch repair and genetic instability. *Annu Rev Genet* **34**: 359-399.

Hassold T, Hunt P. 2001. To err (meiotically) is human: the genesis of human aneuploidy. *Nat Rev Genet* **2**(4): 280-291.

Hawley RS. 2002. Meiosis: how male flies do meiosis. *Curr Biol* **12**(19): R660-662.

Henderson KA, Keeney S. 2004. Tying synaptonemal complex initiation to the formation and programmed repair of DNA double-strand breaks. *Proc Natl Acad Sci U S A* **101**(13): 4519-4524.

Hickson ID. 2003. RecQ helicases: caretakers of the genome. *Nat Rev Cancer* **3**(3): 169-178.

Hollingsworth NM, Brill SJ. 2004. The Mus81 solution to resolution: generating meiotic crossovers without Holliday junctions. *Genes Dev* **18**(2): 117-125.

Hollingsworth NM, Ponte L, Halsey C. 1995. MSH5, a novel MutS homolog, facilitates meiotic reciprocal recombination between homologs in Saccharomyces cerevisiae but not mismatch repair. *Genes Dev* **9**(14): 1728-1739.

Holloway JK, Booth J, Edelmann W, McGowan CH, Cohen PE. 2008. MUS81 generates a subset of MLH1-MLH3-independent crossovers in mammalian meiosis. *PLoS Genet* **4**(9):

e1000186.

Holloway JK, Mohan S, Balmus G, Sun X, Modzelewski A, Borst PL, Freire R, Weiss RS, Cohen PE. 2011. Mammalian BTBD12 (SLX4) protects against genomic instability during mammalian spermatogenesis. *PLoS Genet* **7**(6): e1002094.

Holloway JK, Morelli MA, Borst PL, Cohen PE. 2010. Mammalian BLM helicase is critical for integrating multiple pathways of meiotic recombination. *J Cell Biol* **188**(6): 779-789.

Hunt PA, Hassold TJ. 2008. Human female meiosis: what makes a good egg go bad? *Trends Genet* **24**(2): 86-93.

Hunter N, Borts RH. 1997. Mlh1 is unique among mismatch repair proteins in its ability to promote crossing-over during meiosis. *Genes Dev* **11**(12): 1573-1582.

Hunter N, Kleckner N. 2001. The single-end invasion: an asymmetric intermediate at the double-strand break to double-holliday junction transition of meiotic recombination. *Cell* **106**(1): 59-70.

Jessop L, Lichten M. 2008. Mus81/Mms4 endonuclease and Sgs1 helicase collaborate to ensure proper recombination intermediate metabolism during meiosis. *Mol Cell* **31**(3): 313-323.

Jessop L, Rockmill B, Roeder GS, Lichten M. 2006. Meiotic chromosome synapsis-promoting proteins antagonize the anti-crossover activity of sgs1. *PLoS Genet* **2**(9): e155.

Jones GH, Franklin FC. 2006. Meiotic crossing-over: obligation and interference. *Cell* **126**(2): 246-248.

Kadyrov FA, Dzantiev L, Constantin N, Modrich P. 2006. Endonucleolytic function of MutLalpha in human mismatch repair. *Cell* **126**(2): 297-308.

Kaliraman V, Mullen JR, Fricke WM, Bastin-Shanower SA, Brill SJ. 2001. Functional overlap between Sgs1-Top3 and the Mms4-Mus81 endonuclease. *Genes Dev* **15**(20): 2730-2740.

Kan R, Sun X, Kolas NK, Avdievich E, Kneitz B, Edelmann W, Cohen PE. 2008. Comparative analysis of meiotic progression in female mice bearing mutations in genes of the DNA mismatch repair pathway. *Biol Reprod* **78**(3): 462-471.

Karow JK, Constantinou A, Li JL, West SC, Hickson ID. 2000. The Bloom's syndrome gene product promotes branch migration of holliday junctions. *Proc Natl Acad Sci U S A* **97**(12): 6504-6508.

Keeney S. 2001. Mechanism and control of meiotic recombination initiation. *Curr Top Dev Biol* **52**: 1-53.

Kneitz B, Cohen PE, Avdievich E, Zhu L, Kane MF, Hou H, Jr., Kolodner RD, Kucherlapati R, Pollard JW, Edelmann W. 2000. MutS homolog 4 localization to meiotic chromosomes is required for chromosome pairing during meiosis in male and female mice. *Genes Dev* **14**(9): 1085-1097.

Kolas NK, Cohen PE. 2004. Novel and diverse functions of the DNA mismatch repair family in mammalian meiosis and recombination. *Cytogenet Genome Res* **107**(3-4): 216-231.

Kolas NK, Svetlanov A, Lenzi ML, Macaluso FP, Lipkin SM, Liskay RM, Greally J, Edelmann W, Cohen PE. 2005. Localization of MMR proteins on meiotic chromosomes in mice indicates distinct functions during prophase I. *J Cell Biol* **171**(3): 447-458.

Kumar R, Bourbon HM, de Massy B. 2010. Functional conservation of Mei4 for meiotic DNA double-strand break formation from yeasts to mice. *Genes Dev* **24**(12): 1266-1280.

Kumar S, Chatzi C, Brade T, Cunningham TJ, Zhao X, Duester G. 2011. Sex-specific timing of meiotic initiation is regulated by Cyp26b1 independent of retinoic acid signalling. *Nat Commun* **2**: 151.

Kunkel TA, Erie DA. 2005. DNA mismatch repair. *Annu Rev Biochem* **74**: 681-710.

Lamb NE, Yu K, Shaffer J, Feingold E, Sherman SL. 2005. Association between maternal age and meiotic recombination for trisomy 21. *Am J Hum Genet* **76**(1): 91-99.

Lammers JH, Offenberg HH, van Aalderen M, Vink AC, Dietrich AJ, Heyting C. 1994. The gene encoding a major component of the lateral elements of synaptonemal complexes of the rat is related to X-linked lymphocyte-regulated genes. *Mol Cell Biol* **14**(2): 1137-1146.

Langland G, Kordich J, Creaney J, Goss KH, Lillard-Wetherell K, Bebenek K, Kunkel TA, Groden J. 2001. The Bloom's syndrome protein (BLM) interacts with MLH1 but is not required for DNA mismatch repair. *J Biol Chem* **276**(32): 30031-30035.

Lenzi ML, Smith J, Snowden T, Kim M, Fishel R, Poulos BK, Cohen PE. 2005. Extreme heterogeneity in the molecular events leading to the establishment of chiasmata during meiosis i in human oocytes. *Am J Hum Genet* **76**(1): 112-127.

Libby BJ, Reinholdt LG, Schimenti JC. 2003. Positional cloning and characterization of Mei1, a vertebrate-specific gene required for normal meiotic chromosome synapsis in mice. *Proc Natl Acad Sci U S A* **100**(26): 15706-15711.

Lindor NM, Furuichi Y, Kitao S, Shimamoto A, Arndt C, Jalal S. 2000. Rothmund-Thomson syndrome due to RECQ4 helicase mutations: report and clinical and molecular comparisons with Bloom syndrome and Werner syndrome. *Am J Med Genet* **90**(3): 223-228.

Lipkin SM, Moens PB, Wang V, Lenzi M, Shanmugarajah D, Gilgeous A, Thomas J, Cheng J, Touchman JW, Green ED et al. 2002. Meiotic arrest and aneuploidy in MLH3-deficient mice. *Nat Genet* **31**(4): 385-390.

Loidl J. 2006. S. pombe linear elements: the modest cousins of synaptonemal complexes. *Chromosoma* **115**(3): 260-271.

Lorenz A, Whitby MC. 2006. Crossover promotion and prevention. *Biochem Soc Trans* **34**(Pt 4): 537-541.

Luo G, Santoro IM, McDaniel LD, Nishijima I, Mills M, Youssoufian H, Vogel H, Schultz RA, Bradley A. 2000. Cancer predisposition caused by elevated mitotic recombination in Bloom mice. *Nat Genet* **26**(4): 424-429.

Lynn A, Soucek R, Borner GV. 2007. ZMM proteins during meiosis: crossover artists at work. *Chromosome Res* **15**(5): 591-605.

MacLean G, Li H, Metzger D, Chambon P, Petkovich M. 2007. Apoptotic extinction of germ cells in testes of Cyp26b1 knockout mice. *Endocrinology* **148**(10): 4560-4567.

Macpherson P, Humbert O, Karran P. 1998. Frameshift mismatch recognition by the human MutS alpha complex. *Mutat Res* **408**(1): 55-66.

Maleki S, Neale MJ, Arora C, Henderson KA, Keeney S. 2007. Interactions between Mei4, Rec114, and other proteins required for meiotic DNA double-strand break formation in Saccharomyces cerevisiae. *Chromosoma* **116**(5): 471-486.

Mankouri HW, Hickson ID. 2007. The RecQ helicase-topoisomerase III-Rmi1 complex: a DNA structure-specific 'dissolvasome'? *Trends Biochem Sci* **32**(12): 538-546.

Marcon E, Moens P. 2003. MLH1p and MLH3p localize to precociously induced chiasmata of okadaic-acid-treated mouse spermatocytes. *Genetics* **165**(4): 2283-2287.

Mazina OM, Mazin AV, Nakagawa T, Kolodner RD, Kowalczykowski SC. 2004. Saccharomyces cerevisiae Mer3 helicase stimulates 3'-5' heteroduplex extension by Rad51; implications for crossover control in meiotic recombination. *Cell* **117**(1): 47-56.

McPherson JP, Lemmers B, Chahwan R, Pamidi A, Migon E, Matysiak-Zablocki E, Moynahan ME, Essers J, Hanada K, Poonepalli A et al. 2004. Involvement of mammalian Mus81 in

genome integrity and tumor suppression. *Science* **304**(5678): 1822-1826.

Mets DG, Meyer BJ. 2009. Condensins regulate meiotic DNA break distribution, thus crossover frequency, by controlling chromosome structure. *Cell* **139**(1): 73-86.

Mimitou EP, Symington LS. 2008. Sae2, Exo1 and Sgs1 collaborate in DNA double-strand break processing. *Nature* **455**(7214): 770-774.

Moens PB. 1978. Ultrastructural studies of chiasma distribution. *Annual Reviews of Genetics* **12**: 433-450.

Moens PB, Chen DJ, Shen Z, Kolas NK, Tarsounas M, Heng HH, Spyropoulos B. 1997. Rad51 immunocytology in rat and mouse spermatocytes and oocytes. *Chromosoma* **106**(4): 207-215.

Moens PB, Kolas NK, Tarsounas M, Marcon E, Cohen PE, Spyropoulos B. 2002. The time course and chromosomal localization of recombination-related proteins at meiosis in the mouse are compatible with models that can resolve the early DNA-DNA interactions without reciprocal recombination. *J Cell Sci* **115**(Pt 8): 1611-1622.

Moses MJ. 1969. Structure and function of the synaptonemal complex. *Genetics* **61**(1): Suppl:41-51.

Murakami H, Keeney S. 2008. Regulating the formation of DNA double-strand breaks in meiosis. *Genes Dev* **22**(3): 286-292.

Nasmyth K. 2001. Disseminating the genome: joining, resolving, and separating sister chromatids during mitosis and meiosis. *Annu Rev Genet* **35**: 673-745.

Nicolette ML, Lee K, Guo Z, Rani M, Chow JM, Lee SE, Paull TT. 2010. Mre11-Rad50-Xrs2 and Sae2 promote 5' strand resection of DNA double-strand breaks. *Nat Struct Mol Biol* **17**(12): 1478-1485.

Niu H, Wan L, Baumgartner B, Schaefer D, Loidl J, Hollingsworth NM. 2005. Partner choice during meiosis is regulated by Hop1-promoted dimerization of Mek1. *Mol Biol Cell* **16**(12): 5804-5818.

Offenberg HH, Schalk JA, Meuwissen RL, van Aalderen M, Kester HA, Dietrich AJ, Heyting C. 1998. SCP2: a major protein component of the axial elements of synaptonemal complexes of the rat. *Nucleic Acids Res* **26**(11): 2572-2579.

Ogrunc M, Sancar A. 2003. Identification and characterization of human MUS81-MMS4 structure-specific endonuclease. *J Biol Chem* **278**(24): 21715-21720.

Oh SD, Lao JP, Hwang PY, Taylor AF, Smith GR, Hunter N. 2007. BLM ortholog, Sgs1, prevents aberrant crossing-over by suppressing formation of multichromatid joint molecules. *Cell* **130**(2): 259-272.

Oh SD, Lao JP, Taylor AF, Smith GR, Hunter N. 2008. RecQ helicase, Sgs1, and XPF family endonuclease, Mus81-Mms4, resolve aberrant joint molecules during meiotic recombination. *Mol Cell* **31**(3): 324-336.

Osman F, Dixon J, Doe CL, Whitby MC. 2003. Generating crossovers by resolution of nicked Holliday junctions: a role for Mus81-Eme1 in meiosis. *Mol Cell* **12**(3): 761-774.

Page SL, Hawley RS. 2004. The genetics and molecular biology of the synaptonemal complex. *Annu Rev Cell Dev Biol* **20**: 525-558.

Paques F, Haber JE. 1999. Multiple pathways of recombination induced by double-strand breaks in Saccharomyces cerevisiae. *Microbiol Mol Biol Rev* **63**(2): 349-404.

Paquis-Flucklinger V, Santucci-Darmanin S, Paul R, Saunieres A, Turc-Carel C, Desnuelle C. 1997. Cloning and expression analysis of a meiosis-specific MutS homolog: the human MSH4 gene. *Genomics* **44**(2): 188-194.

Pedroni M, Sala E, Scarselli A, Borghi F, Menigatti M, Benatti P, Percesepe A, Rossi G, Foroni M, Losi L et al. 2001. Microsatellite instability and mismatch-repair protein expression in hereditary and sporadic colorectal carcinogenesis. *Cancer Res* **61**(3): 896-899.

Perry J, Kleckner N, Borner GV. 2005. Bioinformatic analyses implicate the collaborating meiotic crossover/chiasma proteins Zip2, Zip3, and Spo22/Zip4 in ubiquitin labeling. *Proc Natl Acad Sci U S A* **102**(49): 17594-17599.

Pittman DL, Cobb J, Schimenti KJ, Wilson LA, Cooper DM, Brignull E, Handel MA, Schimenti JC. 1998. Meiotic prophase arrest with failure of chromosome synapsis in mice deficient for Dmc1, a germline-specific RecA homolog. *Mol Cell* **1**(5): 697-705.

Pochart P, Woltering D, Hollingsworth NM. 1997. Conserved properties between functionally distinct MutS homologs in yeast. *J Biol Chem* **272**(48): 30345-30349.

Ross-Macdonald P, Roeder GS. 1994. Mutation of a meiosis-specific MutS homolog decreases crossing over but not mismatch correction. *Cell* **79**(6): 1069-1080.

Santucci-Darmanin S, Neyton S, Lespinasse F, Saunieres A, Gaudray P, Paquis-Flucklinger V. 2002. The DNA mismatch-repair MLH3 protein interacts with MSH4 in meiotic cells, supporting a role for this MutL homolog in mammalian meiotic recombination. *Hum Mol Genet* **11**(15): 1697-1706.

Santucci-Darmanin S, Walpita D, Lespinasse F, Desnuelle C, Ashley T, Paquis-Flucklinger V. 2000. MSH4 acts in conjunction with MLH1 during mammalian meiosis. *Faseb J* **14**(11): 1539-1547.

Schalk JA, Dietrich AJ, Vink AC, Offenberg HH, van Aalderen M, Heyting C. 1998. Localization of SCP2 and SCP3 protein molecules within synaptonemal complexes of the rat. *Chromosoma* **107**(8): 540-548.

Schmekel K, Meuwissen RL, Dietrich AJ, Vink AC, van Marle J, van Veen H, Heyting C. 1996. Organization of SCP1 protein molecules within synaptonemal complexes of the rat. *Exp Cell Res* **226**(1): 20-30.

Schramm S, Fraune J, Naumann R, Hernandez-Hernandez A, Hoog C, Cooke HJ, Alsheimer M, Benavente R. 2011. A novel mouse synaptonemal complex protein is essential for loading of central element proteins, recombination, and fertility. *PLoS Genet* **7**(5): e1002088.

Suja JA, Barbero JL. 2009. Cohesin complexes and sister chromatid cohesion in mammalian meiosis. *Genome Dyn* **5**: 94-116.

Svetlanov A, Baudat F, Cohen PE, de Massy B. 2008. Distinct Functions of MLH3 at Recombination Hot Spots in the Mouse. *Genetics* **178**(4): 1937-1945.

Svetlanov A, Cohen PE. 2004. Mismatch repair proteins, meiosis, and mice: understanding the complexities of mammalian meiosis. *Exp Cell Res* **296**(1): 71-79.

Szostak JW, Orr-Weaver TL, Rothstein RJ, Stahl FW. 1983. The double-strand-break repair model for recombination. *Cell* **33**(1): 25-35.

Tease C, Hartshorne GM, Hulten MA. 2002. Patterns of meiotic recombination in human fetal oocytes. *Am J Hum Genet* **70**(6): 1469-1479.

Thacker J. 2005. The RAD51 gene family, genetic instability and cancer. *Cancer Lett* **219**(2): 125-135.

Wang TF, Kleckner N, Hunter N. 1999. Functional specificity of MutL homologs in yeast: evidence for three Mlh1-based heterocomplexes with distinct roles during meiosis in recombination and mismatch correction. *Proc Natl Acad Sci U S A* **96**(24): 13914-13919.

Wei K, Clark AB, Wong E, Kane MF, Mazur DJ, Parris T, Kolas NK, Russell R, Hou H, Jr., Kneitz B et al. 2003. Inactivation of Exonuclease 1 in mice results in DNA mismatch

repair defects, increased cancer susceptibility, and male and female sterility. *Genes Dev* **17**(5): 603-614.

Winand NJ, Panzer JA, Kolodner RD. 1998. Cloning and characterization of the human and Caenorhabditis elegans homologs of the Saccharomyces cerevisiae MSH5 gene. *Genomics* **53**(1): 69-80.

Wojtasz L, Daniel K, Roig I, Bolcun-Filas E, Xu H, Boonsanay V, Eckmann CR, Cooke HJ, Jasin M, Keeney S et al. 2009. Mouse HORMAD1 and HORMAD2, two conserved meiotic chromosomal proteins, are depleted from synapsed chromosome axes with the help of TRIP13 AAA-ATPase. *PLoS Genet* **5**(10): e1000702.

Woltering D, Baumgartner B, Bagchi S, Larkin B, Loidl J, de los Santos T, Hollingsworth NM. 2000. Meiotic segregation, synapsis, and recombination checkpoint functions require physical interaction between the chromosomal proteins Red1p and Hop1p. *Mol Cell Biol* **20**(18): 6646-6658.

Woods LM, Hodges CA, Baart E, Baker SM, Liskay RM, Hunt PA. 1999. Chromosomal influence on meiotic spindle assembly: abnormal meiosis I in female Mlh1 mutant mice. *Journal of Cell Biology* **145**(7): 1395-1406.

Xiao Y, Weaver DT. 1997. Conditional gene targeted deletion by Cre recombinase demonstrates the requirement for the double-strand break repair Mre11 protein in murine embryonic stem cells. *Nucleic Acids Res* **25**(15): 2985-2991.

Yokoo R, Zawadzki KA, Nabeshima K, Drake M, Arur S, Villeneuve AM. 2012. COSA-1 Reveals Robust Homeostasis and Separable Licensing and Reinforcement Steps Governing Meiotic Crossovers. *Cell* **149**(1): 75-87.

Zalevsky J, MacQueen AJ, Duffy JB, Kemphues KJ, Villeneuve AM. 1999. Crossing over during

Caenorhabditis elegans meiosis requires a conserved MutS-based pathway that is partially dispensable in budding yeast. *Genetics* **153**(3): 1271-1283.

Zetka MC, Kawasaki I, Strome S, Muller F. 1999. Synapsis and chiasma formation in Caenorhabditis elegans require HIM-3, a meiotic chromosome core component that functions in chromosome segregation. *Genes Dev* **13**(17): 2258-2270.

Zhang R, Sengupta S, Yang Q, Linke SP, Yanaihara N, Bradsher J, Blais V, McGowan CH, Harris CC. 2005. BLM helicase facilitates Mus81 endonuclease activity in human cells. *Cancer Res* **65**(7): 2526-2531.

Zhu Z, Chung WH, Shim EY, Lee SE, Ira G. 2008. Sgs1 helicase and two nucleases Dna2 and Exo1 resect DNA double-strand break ends. *Cell* **134**(6): 981-994.

Zickler D, Kleckner N. 1999. Meiotic chromosomes: integrating structure and function. *Annu Rev Genet* **33**: 603-754.

CHAPTER 2

The function of putative mouse MLH3 endonuclease domain during mammalian meiosis

1. Abstract

Mammalian MutL homolog 3 (MLH3) is a member of the DNA mismatch repair (MMR) family and is the most recently characterized eukaryotic MutL homolog protein. Previous studies have suggested essential functions for MLH3 during meiotic recombination. The deletion of *Mlh3* in mice results in defects in meiotic recombination and infertility in both sexes. MLH3 is believed to function during Class I crossover pathway and promote the resolution of double Holliday junctions, given that MLH3 can interact with both MLH1 and MSH4, both of which are key players of this crossover pathway. However, to date, our knowledge about how MLH3 participates in meiotic recombination and contributes to the resolution of double Holliday junction is still very limited. The current study investigates a well-conserved putative endonuclease domain of MLH3, which is localized within the predicted MutL C-terminal dimerization domain. The importance of this domain in both mismatch repair and meiosis has been underscored by research done in budding yeast. I hypothesize that, with this well-conserved domain, mouse MLH3 may function as endonuclease *in vivo*, recruiting downstream factors and promoting resolution of meiotic recombination intermediates. I took advantage of previous data showing that point mutations in the endonuclease domain of PMS2, a closely related MutL homolog, completely abrogated the mismatch repair function of PMS2, and generated a targeting vector containing an analogous point mutation in mouse MLH3 potential endonuclease domain.

This construct is based on PL253 as the backbone and contains two homologous arms, one of which carries the point mutation, and one neomycin reporter cassette. After linearization, the construct was electroporated in to ES cells, which were cultured and then selected by drug resistance and Southern blotting. The successful integration of the point mutation was confirmed by PCR and DNA sequencing. Then the correctly targeted ES cell clones were injected into blastocysts and transplanted into pseudopregnant mothers. The chimeric mice bearing the point mutation in their genome were generated. To get preliminary data on how the point mutation would affect the function of MLH3 in meiosis, I performed immunofluorescent staining on meiotic chromosomes from $Mlh3^{DN\ neo/-}$ oocytes containing one copy of the *Mlh3* null allele and one copy of the point mutant allele. The results indicate that pairing, synapsis and the formation of early recombination nodules are normal in the mutant oocytes, but the Class I CO pathway is impaired, illustrated by the significant decreased MLH1/MLH3 foci. It is hoped that further examination of the meiotic phenotype of the mutant transgenic mice will allow more insights into the role of MLH3 during mammalian meiosis.

2. Introduction

As discussed in Chapter 1, meiotic recombination during prophase I begins with endogenous DNA double strand breaks (DSBs), which triggers a series of cellular events similar to a DNA-damage response, including DSB detecting and processing of recombination intermediates. Due to the complexity of meiotic recombination, the list of the proteins involved in this process is overwhelming (Cohen et al. 2006; Handel and Schimenti 2010), and includes the proteins from mismatch repair family. The mismatch repair (MMR) system was first defined in bacteria (Jiricny et al. 1988; Yamaguchi et al. 1998; Hall and Matson 1999). As its name implies, this system was initially identified for its capacity in correcting base substitution mismatches and insertion-deletion mismatches during S phase. Defects in this system result in the accumulation of DNA replication errors, and the mutants exhibit mutator phenotype (Horst et al. 1999; Kunkel and Erie 2005).

The paradigmatic *E. coli* MMR system is composed of three members: MutS, MutL, and MutH, all of which function as homodimers. MMR activity begins with the detection of a substrate by a homodimer of MutS protein. MutS protein is an ATPase, in charge of the recognition of mismatch. MutL is the coordinator, which is recruited to the mismatch site and couples the detection of mismatch by MutS to downstream MutH. MutH is a methylation-sensitive endonuclease, which cuts the unmethylated newly synthesized strand. Depending on the side of the nick induced by MutH, one of the four exonucleases will be recruited to remove the mismatch-containing nicked strand in either 3’ to 5’ (ExoI , ExoX or ExoVII) or 5’ to 3’ direction (RecJ or ExoVII) (Feschenko et al. 2003). Following excision, DNA is resynthesized by DNA polymerase III and then ligated by an unknown ligase (Buermeyer et al. 1999; Kolas

and Cohen 2004; Kunkel and Erie 2005).

Besides the ability to detect endogenous mismatches, the MMR system can also detect DNA damage generated by intracellular oxidative stress and by external chemical reagents, such as cisplatin and alkylating reagents (Kat et al. 1993; Aebi et al. 1996; Cenni et al. 1999). Furthermore, the MMR system is found to function in events unrelated to DNA mismatch repair or binding. For example, the anti-recombination activity of MMR proteins prevent DNA rearrangements within the genome and DNA exchange between different microbial species (Greig et al. 2003; Matic et al. 2003), and suppresses deleterious recombination between diverged (homologous) sequences, either present in the same genome or from different species (Chambers et al. 1996; Hunter et al. 1996). Additionally, some MMR proteins are found to participate in the regulation of meiosis. The absence of these MMR proteins can result in reduction in fertility in both yeast and mice (Harfe and Jinks-Robertson 2000).

Given the importance of the MMR system, it is not surprising to find that it is highly conserved. Homologs of the prokaryotic MutS and MutL are identified in eukaryotic organisms from fungi to humans. While the prokaryotic MMR proteins function as homodimers, eukaryotic MMR homologs act as heterodimers. In mammals, there are five MutS homologs, MSH2 through MSH6. These MutS homologs form three heterodimer complexes: MSH2-MSH6 (MutSα), MSH2-MSH3 (MutSβ), and MSH4-MSH5 (MutSγ). Each of these complexes has its own speciality (Figure 2-1). MutSα participates in correction of base substitutions and small insertion-deletion mismatches, while MutSβ is partially redundant with MutSα and specifically repairs insertion-deletion mismatches (Acharya et al. 1996; Genschel et al. 1998; Macpherson et al. 1998). Notably, MutSγ complex doesn't have mismatch repair activity, but has a very important function for meiotic recombination in many different species, including yeast

Figure 2-1. Mammalian mismatch repair complexes in somatic cells.

In contrast to the prokaryotic mismatch repair system, mammalian mismatch repair proteins act as heterodimers. MSH2-MSH6 (MutSα) participates in correction of base substitutions and small insertion-deletion mismatches, while MSH2-MSH3 (MutSβ) is partially redundant with MutS and specifically repairs insertion-deletion mismatches. MLH1-PMS2 (MutLα) is the major MutL heterodimer involved in various mismatch repair processes, and may interact with both MutSα and MutSβ. MLH1-MLH3 (MutLγ) is believed to participate in repairing a subset of insertion-deletion mismatches. The function of MutLβ complex is still not clear. This figure is adapted from "*Novel and diverse functions of the DNA mismatch repair family in mammalian meiosis and recombination*" (Kolas and Cohen 2004).

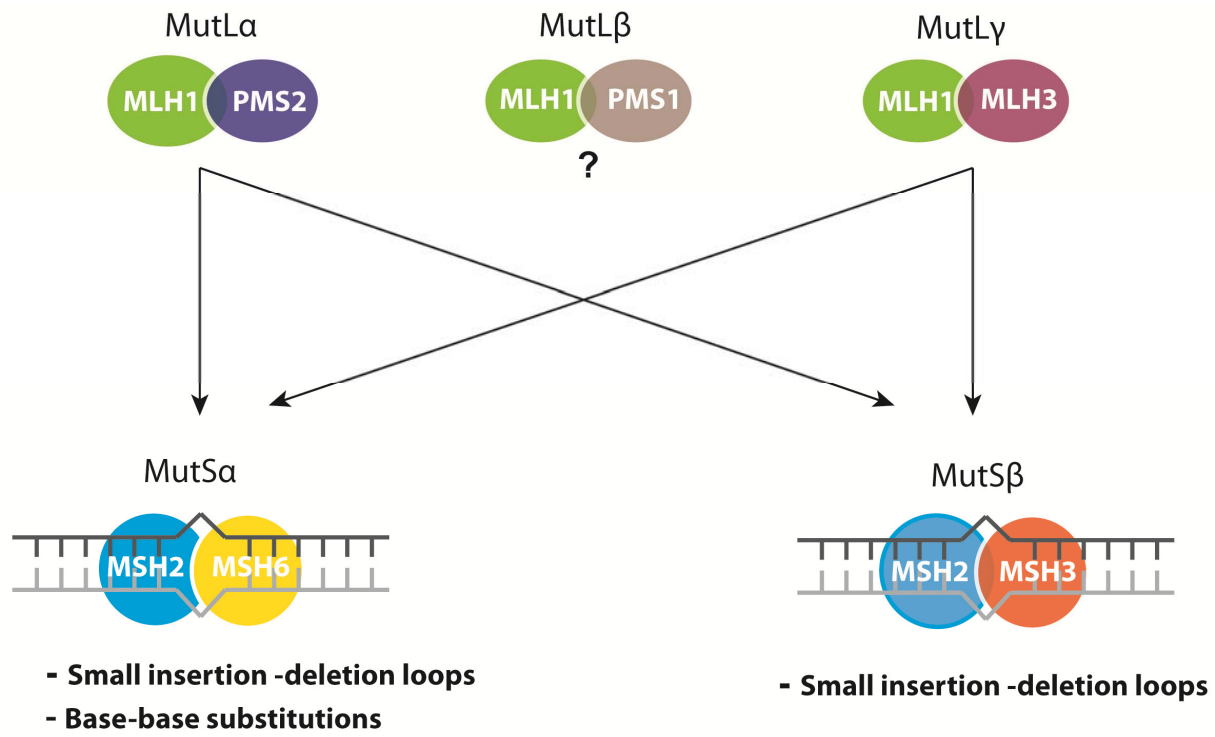

(Hollingsworth et al. 1995), nematodes (Winand et al. 1998; Zalevsky et al. 1999), mice and humans (de Vries et al. 1999; Edelmann et al. 1999; Kneitz et al. 2000; Lenzi et al. 2005). Similarly, MutL also has several homologs in mammals: MLH1, PMS1, MLH3 and PMS2. MLH1 is the principal MutL homolog and can form heterodimer with PMS2 (MutLα), or with PMS1 (MutLβ), or with MLH3 (MutLγ). Among these heterodimers, MutLα is the major MutL complex, which may interact with both MutSα and MutSβ, and be involved in various mismatch repair activities, while MutLγ is believed to participate in repairing a subset of insertion-deletion mismatches. Additionally, MutLγ is also involved in promoting meiotic recombination, mainly through Class I crossover (CO) pathway (Kolas and Cohen 2004; Kunkel and Erie 2005). So far there is no convincing evidence for eukaryotic MutH homologs. It is speculated that the ends of discontinuous Okazaki fragments of the lagging strand and the growing 3' ends of the leading strand may serve as strand discrimination signals during replication (Harfe and Jinks-Robertson 2000).

Mlh3 is the most recently characterized eukaryotic MutL homolog in mammals. Research evidences from yeast and mice have suggested its critical roles in both DNA mismatch repair and meiosis. Early studies done in yeast have shown that the *MLH3* forms a heterodimer with *MLH1*, and this heterodimer plays a role in the repair of insertion-deletion misrepairs (Flores-Rozas and Kolodner 1998). Yeast *mlh3* mutants show a mutator phenotype characterized by an increase in the rate of accumulation of frameshift mutations. Meanwhile, Mlh3 is also an indispensable player during meiotic recombination. Yeast *mlh3* mutant has shown defects in homolog disjunction, and crossing-over is reduced to approximately 70% of wild-type levels (Wang et al. 1999).

Mouse MLH3 was identified as an interacting partner of MLH1 (Lipkin et al. 2000). When *Mlh3*

is inactivated in mice, both male and female mice are sterile (Lipkin et al. 2002). Spermatocytes from *Mlh3* null males succumb to apoptosis at metaphase I. By contrast, while the *Mlh3*$^{-/-}$ female are sterile and oocytes show severely aberrant spindle configuration in metaphase I (Kan et al. 2008), some oocytes are able to reach two-cell stage after fertilization (Lipkin et al. 2002). Mouse meiotic chromosome spreads show that MLH3 and MLH1 are loaded onto the chromosome sequentially. MLH3 binds to the chromosome first during late zygonema to early pachynema, and MLH1 is recruited later in mid- pachytema and forms heterodimer with MLH3, which persist on the chromosome until late pachynema (Kolas et al. 2005). The MLH1-MLH3 foci during this stage are major cytological markers for meiotic COs, and required by 90-95% of all CO events (Svetlanov and Cohen 2004; Guillon et al. 2005). Interestingly, in *Mlh1* knockout animals, residual MLH3 foci are found to be associated with meiotic nodules and centromeres on meiotic chromosome in spermatocytes, while no MLH1 foci have been seen on meiotic chromosomes from *Mlh3* mutant males (Lipkin et al. 2002; Kolas et al. 2005). Combined with the fact that MLH3 foci appear earlier on pachytene chromosomes compared with MLH1, these observations may suggest a MLH1-independent function of MLH3 in processing recombination intermediates or other meiotic events.

Mouse *Mlh3* is located on chromosome 12 and its 12 exons encode a 1411-residue protein.

Of note, this protein contains a highly conserved 12-residue long 'DQHAAHERIRLE' domain, encoded by exon 6 (Figure 2-2 A). This domain is consistent with the metal-binding motif found in human PMS2, which has a DQHA$(X)_2$E$(X)_4$E pattern and was reported to have *in vitro* endonuclease activity (Kadyrov et al. 2006). The importance of this domain in the MutL proteins has also been underscored by research done in both yeast and mouse (Nishant et al. 2008; van Oers et al. 2010). The *Pms2* transgenic mice with a point mutation in the DQHA$(X)_2$E$(X)_4$E

domain demonstrate elevated genomic mutation rates and a strong cancer predisposition. But no meiotic phenotype is specified in these mice. On the other hand, studies in yeast show that, besides disruption of insertion/deletion repair, one or two point mutations in yeast *MLH3* DQHA$(X)_2$E$(X)_4$E motif can result in defects in spore viability and meiotic crossing over, similar to *mlh3* full-null (Nishant et al. 2008), which implies an important function of this domain during meiosis.

While this 12-residue domain is conserved in PMS2 and MLH3 homologs of various eukaryotic species and in MutL proteins from a number of bacterial species, it is absent from bacterial strains, such as *E. coli*, using d(GATC) methylation for strand discrimination during mismatch repair (Kadyrov et al. 2006), indicates an essential difference in excision initiation between *E. coli* MutS/L/H system and eukaryotic mismatch repair system. It can be speculated that, if this domain does function as an endonuclease *in vivo*, MutL homologs could act as prokaryotic MutH and help to resolve DNA intermediate, which helps explain the absence of MutH homolog in eukaryotic system, and indicates new roles of eukaryotic MutL proteins in mismatch repair and meiosis.

In order to further investigate the function of MLH3 and the *in vivo* role of its conserved 'DQHAAHERIRLE' domain during mammalian meiosis, a transgenic mouse line containing a point mutation in the potential endonuclease domain of MLH3 was made. I hypothesize that, with this well-conserved domain, mouse MLH3 may function as endonuclease, promoting resolution of meiotic recombination intermediates and also recruiting downstream factors, such as exonuclease. Disruption of this domain will lead to the abolishment of normal meiotic progression *in vivo*.

Figure 2-2. MLH3 potential endonuclease domain is highly conserved in multiple species. **(A)** The Mlh3 protein sequences from eleven different species (*Mus musculus, Homo sapiens, Pan troglodytes, Bos taurus, Canis lupus familiarias, Xenopus tropicalis, Danio rerio, Gallus gallus, Saccharomyces cerevisiae, Arabidopsis thaliana and Aspergillus fumigatus*) are aligned using ClustalX2. Part of the alignment results is shown. Protein sequences are obtained from GenBank. The potential endonuclease domain is indicated on the top, and the highly conserved the nucleotides are labeled as asterisks. **(B)** The localization of the three predicted functional domains and the potential endonuclease domain is shown. Note that the 12-residue long endonuclease domain is localized within one predicted dimerization domain. The targeted mutation site within the potential endonuclease domain is highlighted in red.

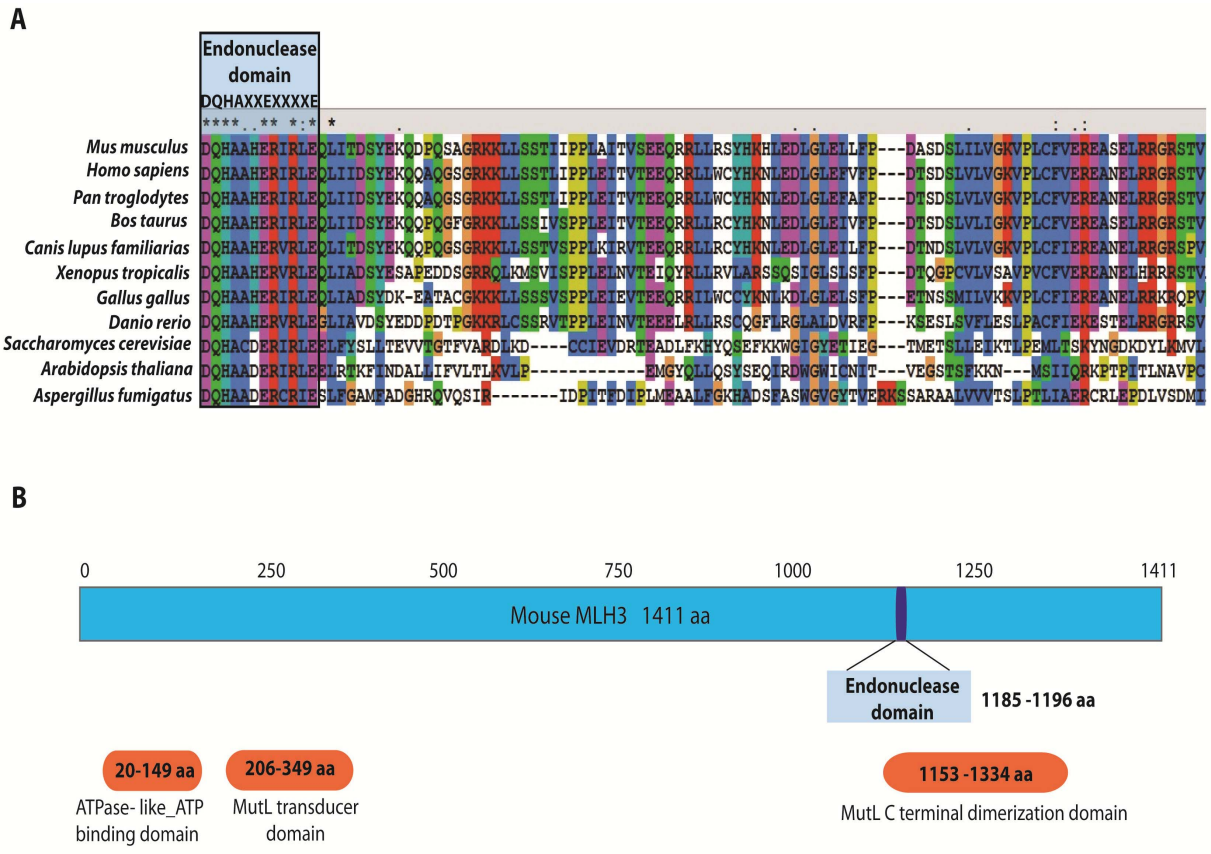

3. Materials and Methods

3.1 Construction of the Mlh3^{DN} targeting vector

The point mutation site in the potential endonuclease domain was chosen based on the previous studies on human PMS2 and yeast MLH3 (Kadyrov et al. 2006; Nishant et al. 2008). The mouse MLH3 point mutation is analogous to human PMS2 D699N mutation and yeast *MLH3* D523N mutation. Thus, I called the mutant allele *Mlh3^{DN}*. The *Mlh3^{DN}* targeting vector was prepared through homologous recombination to introduce a point mutation into the potential endonuclease domain and to insert a *loxP*-flanked neomycin resistance gene into intron 5-6 of *Mlh3*. This targeting vector uses PL253 as a backbone and contains 1) a 5' homologous arm containing 2.2 kb of the *Mlh3* genomic sequence, 2) the neomycin resistance (*neo*) gene flanked by two *loxP* sites, 3) a 3' homologous arm containing 6.7 kb of the *Mlh3* genomic sequence with one point mutation in the potential endonuclease region, which changes the first nucleotide of the potential domain from G to A, resulting in the change of corresponding amino acid from Asp (GAC) to Asn (AAC), and 4) the thymidine kinase gene (*tk*), which is outside of the homologous arms (See Figure 2-3). The *neo* cassette is a selectable marker for homologous integration of the targeting vector into genomic DNA of electroporated embryonic stem (ES) cells, and can be removed later by the Cre recombinase (See Figure 2-5). The *tk* cassette serves as a negative selection marker for ES cell selection. The protein product of *tk* gene phosphorylates nucleotide analogs, such as 1-(-2-deoxy-2-fluoro-1-beta-D-arabino-furanosyl)-5- iodouracil (FIAU), into toxic metabolites, which can be incorporated into the replicating DNA strands and terminate replication, and eventually select against the host cells (Chen and Bradley 2000). Since the *tk* cassette is cloned outside of the homologous arms, it should not be incorporated into the targeted genomic region, but will be inserted into the genome of the ES cells during random integrations,

Figure 2-3. *Mlh*^{DN} targeting construct.

The following elements were cloned between NotI and BamHI site of PL253 to obtain the targeting vector: a 5' homologous arm containing 2.2 kb of the *Mlh3* genomic sequence, the neomycin resistance (*neo*) gene cassette flanked by two *loxP* sites, a 3' homologous arm containing 6.7 kb of the *Mlh3* genomic sequence with one point mutation in the potential endonuclease domain, and the thymidine kinase gene (*tk*) cassette. The *neo* cassette can be removed later by Cre/*loxP* system. This plasmid was linearized by SalI before electroporation into ES cells.

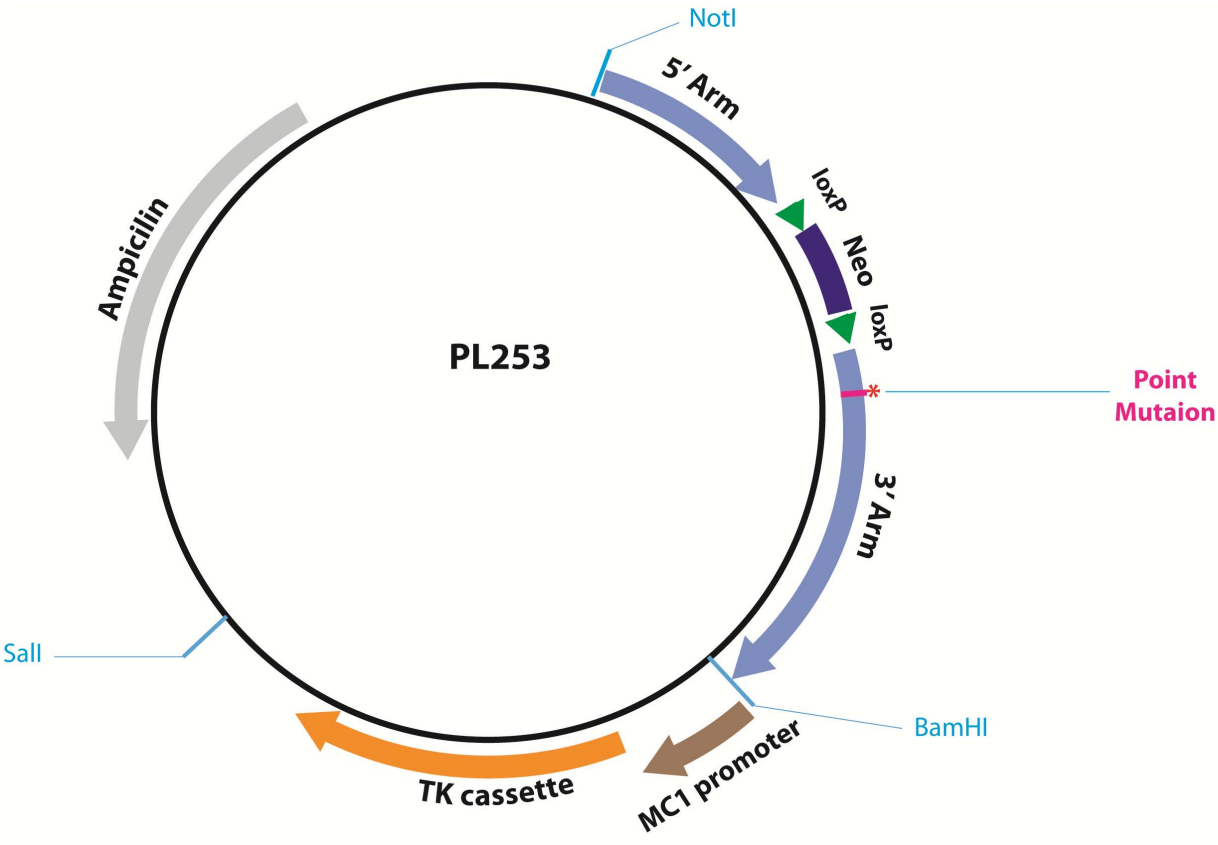
NotI
5′ Arm
loxP
Neo
loxP
Point
Mutaion
3′ Arm
BamHI
MC1 promoter
TK cassette
SalI
Ampicilin
PL253

Figure 2-4. Screening for targeted ES cell clones.

(A) The restriction maps of the *Mlh3* wild-type allele, targeting vector and the *Mlh3* allele after gene targeting are shown. Homologous recombination introduces *neo* cassette (~2 kb) into wild-type genomic sequence and produces $Mlh3^{DN}$ allele. The exons are shown as filled boxes. The location of Southern probes (5' probe and 3' probe) is indicated as shaded boxes. The targeted point mutation is highlighted in red. **(B)** Two rounds of Southern blot analysis were done for identification of targeted ES cells. Genomic DNA from individual ES cell clones was first digested with XmnI and hybridized with 5' external probe. The 7.4 kb band corresponds to the wild-type allele. An additional 9.4 kb band is seen when the allele is correctly targeted. The 3' external probe yields a 15 kb band in wild-type allele when the genomic DNA is digested with AvrII. The 17 kb band corresponds to targeted allele. In the 5' screening, 2 out of 3 clones shown contain the *neo* cassette insertion in one of their alleles. In the 3' screening, all three clones shown display targeted insertion in one of their alleles. **(C)** The clones positive for both 5' and 3' screening were sent for DNA sequencing to confirm the integration of the point mutation. In the targeted allele, the first nucleotide of the potential endonuclease domain changes from G to A, which leads to the change of corresponding amino acid from Asp (GAC) to Asn (AAC). In correctly targeted ES cell clones, the targeted point mutation site shows heterozygosity (50% G and 50% A, highlighted in light grey).

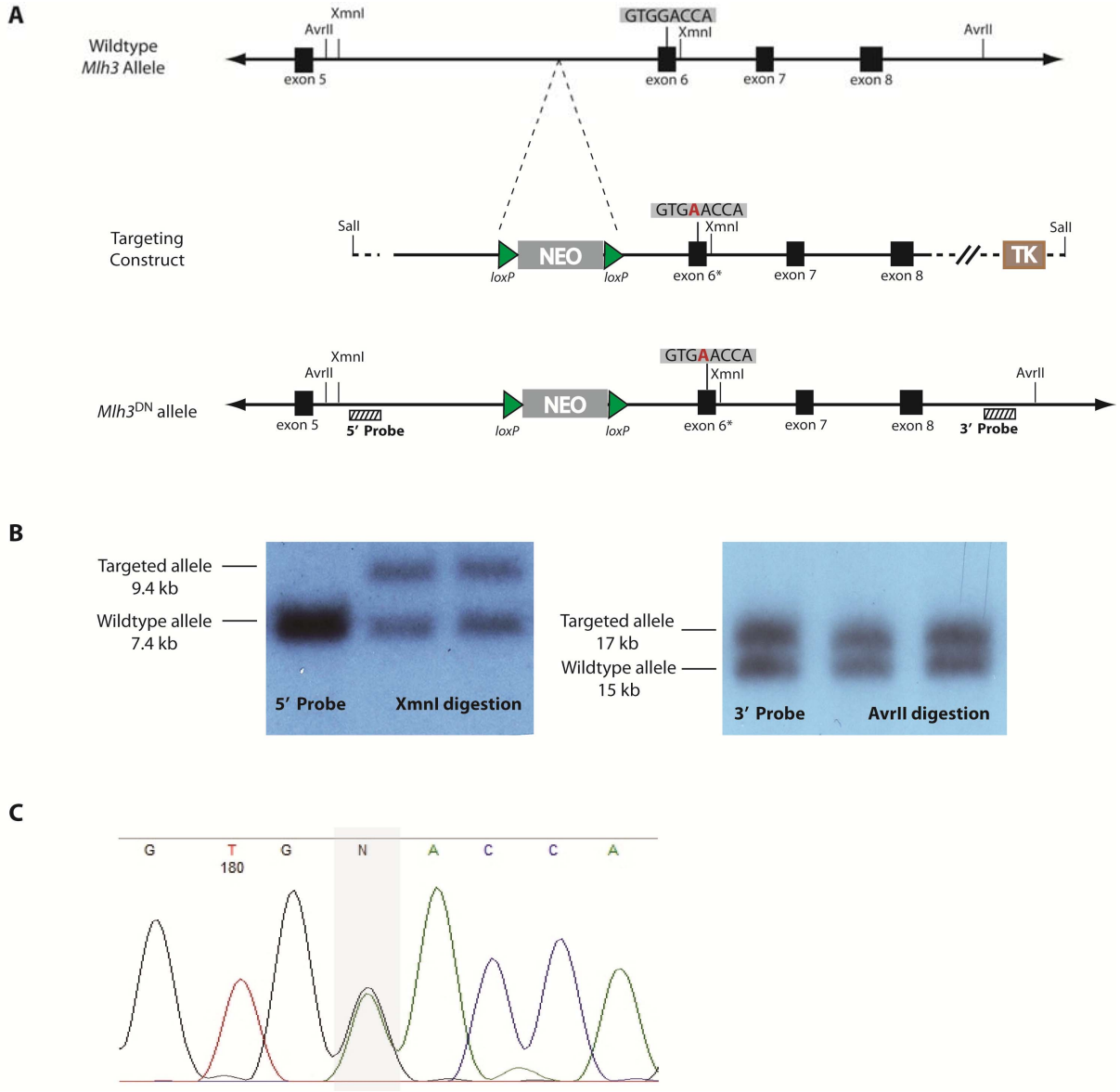
A
Wildtype
Mlh3 Allele
XmnI
AvrII
GTGGACCA
XmnI
AvrII
exon 5
exon 6
exon 7
exon 8
Targeting
Construct
SalI
GTGAACCA
XmnI
SalI
NEO
loxP
loxP
exon 6*
exon 7
exon 8
TK
Mlh3DN allele
XmnI
AvrII
GTGAACCA
XmnI
AvrII
exon 5
5′ Probe
NEO
loxP
loxP
exon 6*
exon 7
exon 8
3′ Probe
B
Targeted allele
9.4 kb
Wildtype allele
7.4 kb
5′ Probe
XmnI digestion
Targeted allele
17 kb
Wildtype allele
15 kb
3′ Probe
AvrII digestion
C
G
T
180
G
N
A
C
C
A

which helps negatively select these cells.

3.2 Electroporation and selection of embryonic stem cells

The *Mlh3*^{DN} targeting construct was linearized by SalI and electroporated into E14.1 male feeder-independent embryonic stem (ES) cells. Electroporation was performed at 3 microF/ 0.8 kV using Bio-Rad Gene Pulser II in a 0.4 cm electroporation cuvette. Electroporated ES cells were left at room temperature for 20 minutes for recovery and then plated onto gelatinized 100 mm tissue culture plates with culture media not containing G418 or FIAU. The next day, the ES cells were transferred to media containing 125 ug/ml G418 and 37.2 ng/ml FIAU for selection.

One week after electroporation, individual ES cell colonies were picked from the 100 mm plates and moved to 48-well plates for further expansion. When the wells were confluent, each well was split into two fractions, one of which was frozen down at -80^{o}C as a stock. The other was lysed with proteinase K and ethanol-precipitated to obtain genomic DNA for Southern blot analysis. Two Southern probes were used for verification of correct targeting of ES cells (See figure 2-4). One is a 5' probe external to the targeting vector (amplified with 5'Probe_2FXmnI 5'-GAT AAT GCT TAA TTT TTT GAC C -3' and 5'Probe_2RXmnI 5'-AGA GCA GCC ATG GTT TCT G-3'). When digested with XmnI, the wild-type allele shows a 7.4 kb band, while the targeted allele shows a 9.4 kb band. Positive colonies selected from the 5' screening were confirmed by a second 3' external probe (amplified with Mlh3_3Probe Upper 5'-TTA GGC GTG GTT GAG TCT GTG T-3' and Mlh3_3ProbrLower 5'-AGA CAT CAA ACT GGA CCA CAA A -3'). In the 3' screening, genomic DNA from ES cell clones was digested with AvrII, which resulted in a 15 kb band for wild-type allele and a 17 kb band for targeted allele. The colonies showing positive results for both 5' and 3' screening were further checked for the point mutation

site using PCR (amplified with Mlh3DN_genotype702_F 5'-AAG CCA AGT CTG CAT GAG TA -3' and Mlh3DN_genotype702_R TAA ATG TGC CAC TGA CTA AAT -3'). The PCR products were purified and sent to sequencing. The successfully targeted colonies showed heterozygosity at the point mutation site (See Figure 2-4 C).

3.3 Blastocyst injection and generation of chimeric animals

The successfully targeted ES cell clones were injected into C57/BL6 blastocysts and transplanted into pseudopregnant recipient mothers. Knock-in chimeric animals were identified by coat color. Coat color chimerism is an indication of ES cell incorporation into the inner cell mass (ICM) of the blastocyst following microinjection. The higher percentage of ES cell derived coat color, which is agouti in this case, the better chance that the incorporated ES cells were able to generate germ cells.

3.4 Identification of germline chimeric animals

The chimeric animals (F_0) were then mated with wild-type mice (See Figure 2-5), and the progeny carrying the targeted mutation was the F1 generation. These mice were termed *Mlh3*$^{DN\ neo/+}$ to indicate the point mutation and the inserted *neo* cassette in one of the *Mlh3* alleles. *Mlh3*$^{DN\ neo/+}$ mice were first identified by agouti coat color and then the region flanking the point mutation is amplified by PCR (using primers: Mlh3^{DN}_genotype702_F 5'-AAG CCA AGT CTG CAT GAG TA -3' and Mlh3^{DN}_genotype702_R TAA ATG TGC CAC TGA CTA AAT -3'). The PCR product was either sent to DNA sequencing or digested by restriction enzyme digestion to confirm the point mutation (See Figure 2-6). For the restriction enzyme digestion, the PCR product was digested with Sau96I at 37^{o}C for 2~3 hours, which yielded two bands in wild-type

Figure 2-5. Breeding strategy for *Mlh3*^{DN} transgenic animals.

Correctly targeted E14.1 ES cell clones were injected into blastocysts, which were transferred into the uterus of pseudopregnant C57/B6 females. Chimeras with mixed coat color (agouti and black) were obtained (F0 generation). Then these chimeras were mated with wild-type C57/B6 male or females (F_0 X wt). Those pups, which were generated from F_0 X Wt mating cages and carried the point mutation and *neo* insertion, were called F1 generation. F1 mice will be crossed with *Spo11-Cre* mice to remove the neo cassette, which results in F2 generation. F2 mice will be intercrossed to get transgenic animals carrying the point mutations in both *Mlh3* alleles (F3).

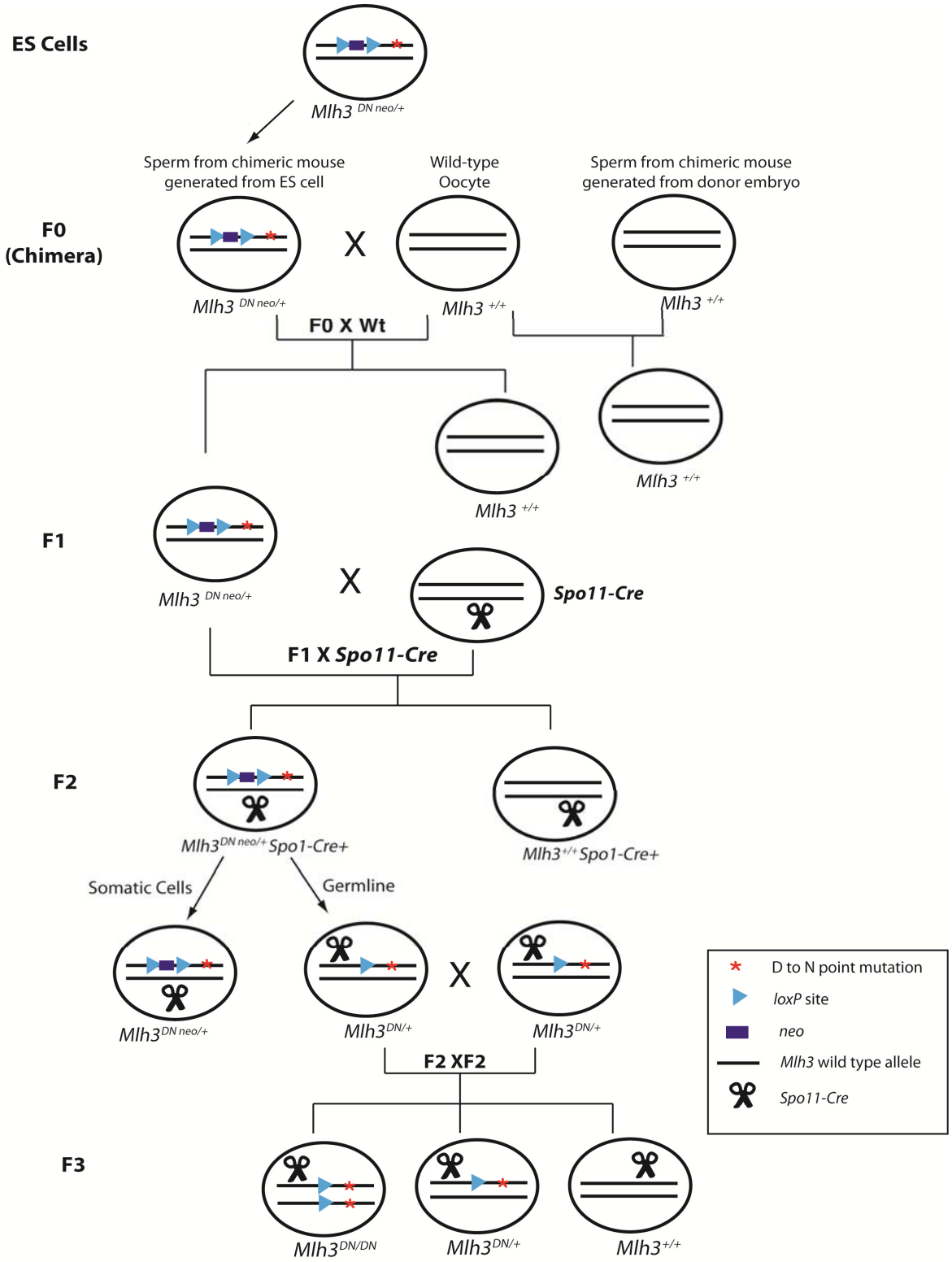
ES Cells
Mlh3 DN neo/+
Sperm from chimeric mouse generated from ES cell
Wild-type Oocyte
Sperm from chimeric mouse generated from donor embryo
F0 (Chimera)
X
Mlh3 DN neo/+
Mlh3 +/+
Mlh3 +/+
F0 X Wt
Mlh3 +/+
Mlh3 +/+
F1
Mlh3 DN neo/+
X
Spo11-Cre
F1 X Spo11-Cre
F2
Mlh3DN neo/+ Spo1-Cre+
Mlh3+/+ Spo1-Cre+
Somatic Cells
Germline
Mlh3DN neo/+
Mlh3DN/+
X
Mlh3DN/+
F2 XF2
F3
Mlh3DN/DN
Mlh3DN/+
Mlh3+/+
D to N point mutation
loxP site
neo
Mlh3 wild type allele
Spo11-Cre

Figure 2-6. Identification of chimeric mice and transgenic offsprings.

(A) To genotype F0 and F1 generations, genomic DNA was prepared from tails, and PCR primers were designed to amplify a 304 bp fragment inside neomycin gene to confirm the insertion of neo cassette into the genome, and a 702 bp region flanking the potential endonuclease domain to check the point mutation site. Then the 702 bp PCR products were either purified and sent to DNA sequencing, or further digested by Sau96I, as shown in **(B)**. When the PCR product is digested with Sau96I, wild-type allele yields two bands, one of 439 bp and the other of 263 bp, while the mutant allele has only one band of 702 bp due to elimination of Sau96I site by the point mutation. In the gel displayed, two clones (lane 2 and 5) are heterozygous while the other two are wild-type (lane 3 and 4). **(C)** One of the five chimeras (F_0 generation) is shown. This male shows > 80% coat color chimerism.

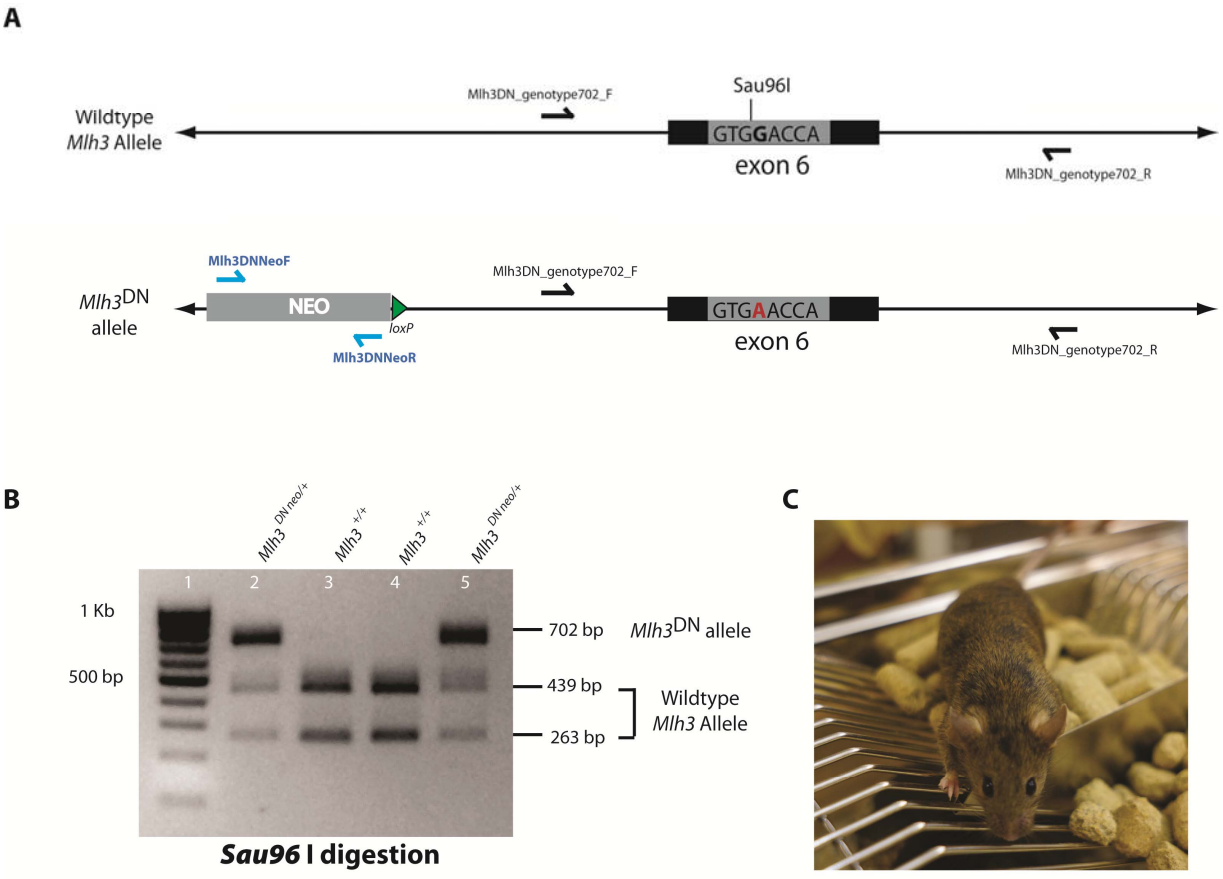
A
Wildtype
Mlh3 Allele
Mlh3DN_genotype702_F
Sau96I
GTGGACCA
exon 6
Mlh3DN_genotype702_R
Mlh3DNNeoF
Mlh3DN
allele
NEO
loxP
Mlh3DNNeoR
Mlh3DN_genotype702_F
GTGAACCA
exon 6
Mlh3DN_genotype702_R
B
Mlh3 DN neo/+
Mlh3 +/+
Mlh3 +/+
Mlh3 DN neo/+
1
2
3
4
5
1 Kb
500 bp
702 bp
Mlh3DN allele
439 bp
263 bp
Wildtype
Mlh3 Allele
Sau96 I digestion
C

(one in 439 bp and the other in 263 bp), but only one 702 bp band in the mutant allele since Sau96I site was eliminated due to the point mutation. The insertion of *neo* cassette in the genome was also confirmed by PCR (primers: Mlh3NeoF 5'-GTT CTG CCC TCT GAT CTA AAG -3' and Mlh3NeoCasR 5'-AGG CCA CTT GTG TAG CG-3').

3.5 Chromosome analysis of *Mlh3* $^{DN\ neo/-}$ mouse oocytes throughout prophase I

To rapidly generate mutants for the *Mlh3*^{DN} allele, *Mlh3*$^{DN\ neo/+}$ males were mated with *Mlh3* $^{+/-}$ females, and copulation plugs were checked the next morning. Pregnant females were euthanized on embryonic day 19.5, and fetal ovaries were dissected from female embryos. Tails of the embryos were collected for genotyping. The genotyping strategy for the *Mlh3* null allele has been described previously (Lipkin et al. 2002), and *Mlh3* DN allele was identified by the method mentioned in section 3.4. This breeding strategy would result in pups bearing a combination of either a wild-type allele, or a full null (-) allele, or a DN allele (DN neo). We use the term *Mlh3* $^{DN\ neo/-}$ to indicate the presence of one *Mlh3*^{DN} allele with the neomycin reporter cassette and one *Mlh3* null allele. Fetal ovaries were prepared for chromosome spreads using techniques described previously (Peters et al. 1997; Lipkin et al. 2002; Kolas et al. 2005; Lenzi et al. 2005). The primary antibodies were either generated in our lab, or commercially available, or gifts from other labs. The primary antibodies used to detect the synaptonemal complex of meiotic cells were SYCP1 (1:1000), rabbit SYCP3 (1:5000) and mouse SYCP3 (1:5000). Centromeres were identified by CREST human autoimmune serum (1:30,000). Early meiotic events were evaluated by mouse γH2AX (1:5000) and rabbit RAD51 (1:300). Rabbit MSH5 (1:1000), monoclonal human MLH1 (1:100) and polyclonal rabbit MLH3 (1:300) (Lipkin et al. 2002) were used to identify early and late meiotic nodules. Secondary antibodies used were goat anti-mouse Alexa

Fluor 488, goat anti-rabbit Alexa Fluor 555 and goat anti-human Alexa Fluor 647 (all 1:1000; Invitrogen).

3.6 Bioinformatic analysis

Multi-species comparison of MLH3 potential endonuclease domain was performed using ClustalX2. The potential functional motifs of mouse MLH3 were predicted by NCBI PSI-BLAST and Ensembl database.

4. Results

To determine the *in vivo* function of the potential endonuclease domain of mouse MLH3, we generated *Mlh3*^{DN} chimeric mice, which contain a single amino acid change on the first amino acid of the conserved 'DQHAAHERIRLE' domain (Aspartic acid (D) to Asparagine (N)) in one *Mlh3* allele, which is analogous to human PMS2 D699N mutation and yeast *MLH3* D523N mutation (Nishant et al. 2008). The point mutation in human PMS2 leads to disruption of MutLα endonuclease activities, and defects in mismatch repair (Kadyrov et al. 2006). In *S.* cerevisiae, the single amino acid alteration in this conserved domain does not affect the stability of the protein or the dimerization between endogenous MLH1 and mutated MLH3. However, this mutant demonstrates similar level of defects as *mlh3-null* mutant in meiotic crossover, repair of frame shift mutation and spore viability (Nishant et al. 2008).

To get preliminary data on how the D to N mutation would affect the function of MLH3 during mammalian meiosis, *Mlh3* $^{DN\ neo\ /+}$ males (F1 generation) were mated with Mlh3$^{+/-}$ females and

female chromosome spreads were made using wild-type and *Mlh3*$^{DN\ neo\ /-}$ fetal ovaries from 19 dpc (day postcoitum) embryos (Figure 2-7). To check the repair of the DSBs, which begins in the leptotene stage of meiosis, chromosome spreads were stained with antibodies against SYCP3 and γH2AX. As a marker of genomic damage, γH2AX signal peaks in leptonema and zygonema (Mahadevaiah et al. 2001), and then decreases to background level by mid-pachynema. When the *Mlh3* wild-type alleles were replaced by a single *Mlh3*^{DN} allele (to give *Mlh3*$^{DN\ neo\ /-}$), γH2AX showed a similar dynamic as seen in wild-type (Figure 2-8 A, B). The progression of DSB repair was also assessed by RAD51, a marker for early recombination process (Hunter and Kleckner 2001). Again, the oocytes demonstrated similar level of RAD51 signal in pachynema as wild-type oocytes (Figure 2-8 C, D). The synapsis of homologous chromosomes was also intact in the mutants, illustrated by the nicely merged SYCP1 and SYCP3 signals during pachynema (Figure 2-8 E, F). Then the formation of meiotic recombination intermediates was examined by the appearance of early and late recombination nodules, using antibodies against MSH5 (Figure 2-8 G, H), MLH1 (Figure 2-8 I, J), and MLH3 (Figure 2-8 K, L). Oocytes from wild-type and *Mlh3*$^{DN\ neo\ /-}$ fetuses accumulated MSH5 foci at similar frequency, indicating the formation of early recombination nodules was normal in the mutants. However, MLH3 and MLH1 foci were significantly reduced in the mutants compared with wild type. While most of the oocytes from the mutants showed one or two MLH3 foci per nucleus, more than 60% of the mutant oocytes displayed no detectable MLH1 foci in pachynema, suggesting Class I CO pathway was disrupted in the mutants. It should be noted that this observation is very preliminary, however, and requires more thorough quantitation to be statistically sound.

Figure 2-7. Breeding strategy to obtain *Mlh3*$^{DN\ neo\ /-}$ fetus.

Chimeras (F_0 generation) with one correctly targeted allele were mated with wild-type C57/B6 mice to generate *Mlh3*$^{DN\ neo\ /+}$ mice (F1). Then the *Mlh3*$^{DN\ neo\ /+}$ males were mated with *Mlh3*$^{+/-}$ females, and 19.5 dpc embryos were collected for the experiment.

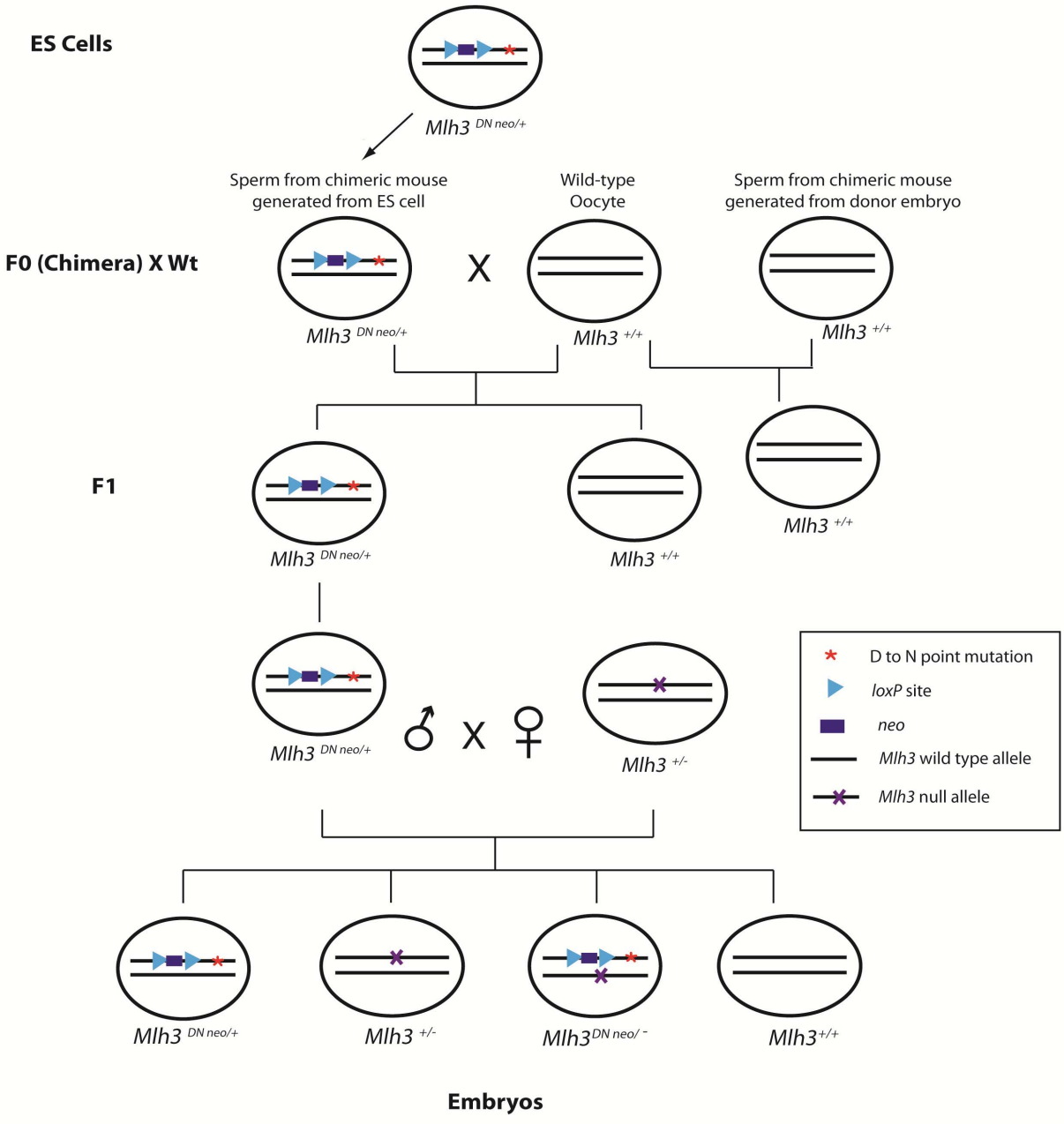

Figure 2-8. Meiotic progression in wild-type and *Mlh3*$^{DN\ neo\ /-}$ mouse oocytes.

(A, B) Meiotic chromosome spreads from wild-type (A) and *Mlh3*$^{DN\ neo\ /-}$ mutant (B) oocytes were stained with antibodies against SYCP3 (red) and γH2AX (green). **(C, D)** Meiotic chromosome spreads from wild-type (C) and *Mlh3*$^{DN\ neo\ /-}$ mutant (D) oocytes were stained with antibodies against SYCP3 (green), RAD51 (red), and CREST (blue). **(E, F)** Meiotic chromosome spreads from wild-type (E) and *Mlh3*$^{DN\ neo\ /-}$ mutant (F) oocytes were stained with antibodies against SYCP3 (green), SYCP1 (red), and CREST (blue). **(G, H)** Meiotic chromosome spreads from wild-type (G) and *Mlh3*$^{DN\ neo\ /-}$ mutant (H) oocytes were stained with antibodies against SYCP3 (green), MSH5 (red), and CREST (blue). **(I, J)** Meiotic chromosome spreads from wild-type (I) and *Mlh3*$^{DN\ neo\ /-}$ mutant (J) oocytes were stained with antibodies against SYCP3 (red), and MLH1 (green). Residual MLH1 foci are indicated as white arrows. **(K, L)** Meiotic chromosome spreads from wild-type (K) and *Mlh3*$^{DN\ neo\ /-}$ mutant (L) oocytes were stained with antibodies against SYCP3 (green), MLH3 (red), and CREST (blue). White arrows point to residual MLH3 foci.

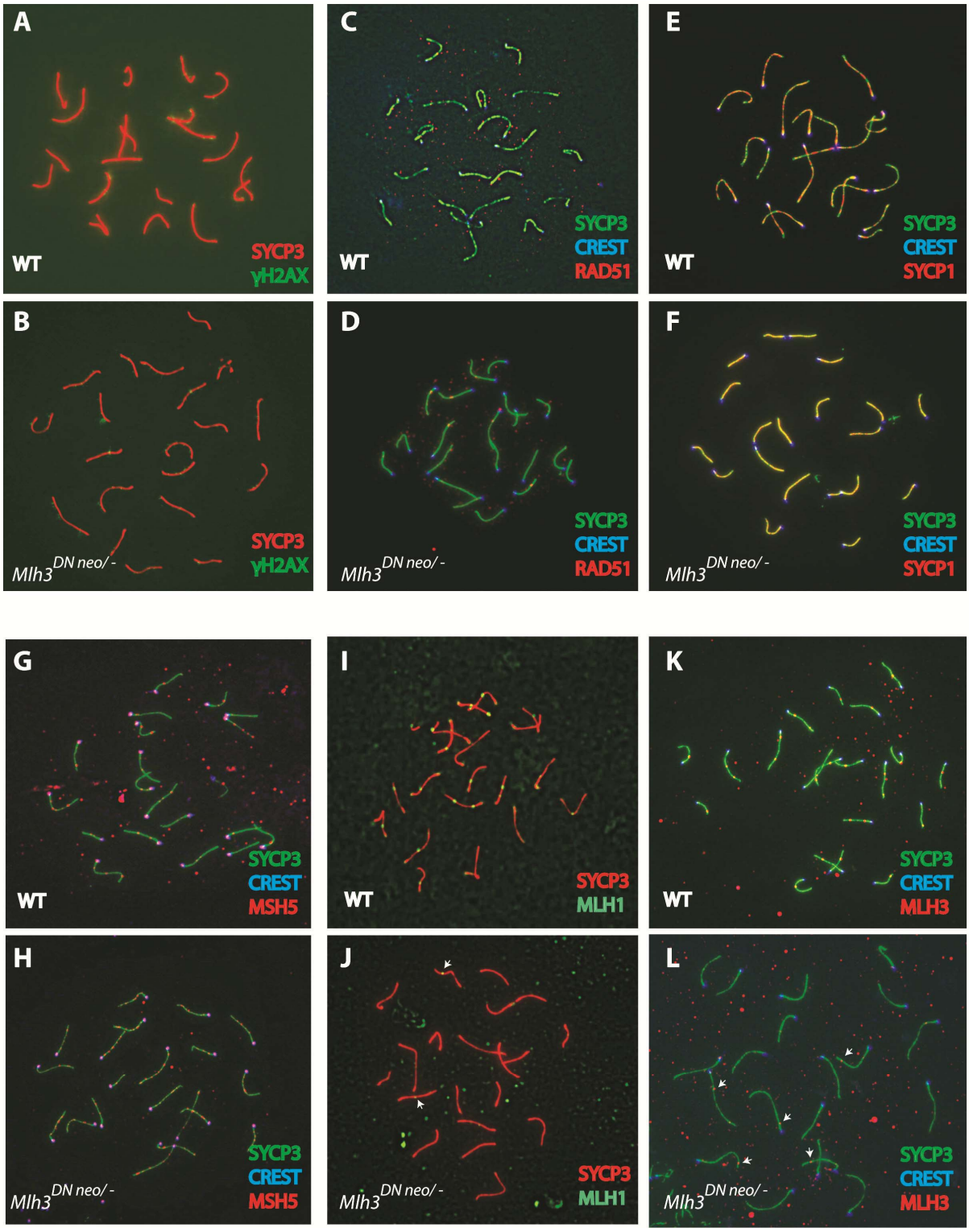
A
WT
SYCP3
γH2AX
C
WT
SYCP3
CREST
RAD51
E
WT
SYCP3
CREST
SYCP1
B
Mlh3DN neo/ -
SYCP3
γH2AX
D
Mlh3DN neo/ -
SYCP3
CREST
RAD51
F
Mlh3DN neo/ -
SYCP3
CREST
SYCP1
G
WT
SYCP3
CREST
MSH5
I
WT
SYCP3
MLH1
K
WT
SYCP3
CREST
MLH3
H
Mlh3DN neo/ -
SYCP3
CREST
MSH5
J
Mlh3DN neo/ -
SYCP3
MLH1
L
Mlh3DN neo/ -
SYCP3
CREST
MLH3

5. Discussion

MutL homolog proteins usually have a well-conserved N-terminal region, which contains ATP binding/hydrolysis domains, and a dimerization domain localizing in the C-terminal region, which is critical for homo- or hetero-dimerization of MutL proteins (Guarne et al. 2004). Consistent with this, mouse MLH3 is predicted to have three functional domains (20-149 aa, 206-349 aa, 1153-1334 aa) (Figure 2-2 B). The N-terminal region of this protein contains the ATP-binding domain (20 -149 aa), which can be found in several ATP-binding proteins, such as histidine kinase and topoisomerases. The C-terminal domain is predicted to be a MutL C-terminal dimerization domain (1153-1334 aa). Although mouse MLH3 has been reported to form heterodimers with MLH1 and can be co-immunoprecipitated with MSH4 (Santucci-Darmanin et al. 2002), there is no direct research evidence to pinpoint these interactions to any of these domains. Interestingly, the 12-residue long 'DQHAAHERIRLE' (1185-1196 aa) domain, encoded by exon 6, is localized within the predicted dimerization domain near C-terminal. While the sequences of MutL C-terminal dimerization region are usually highly divergent among its homologs (Guarne et al. 2004), the 'DQHAAHERIRLE' domain is surprisingly conserved across various species.

In this study, an *Mlh3*^{DN} transgenic mouse line with one point mutation in the conserved 'DQHAAHERIRLE' domain was generated. To obtain preliminary data on the meiotic progression in *Mlh3*^{DN} mice, chromosome spreading was performed on *Mlh3*$^{DN\ neo\ /-}$ oocytes containing one copy of the *Mlh3* null allele and one copy of the point mutant allele. The results from the immunofluorescent staining of these spreads demonstrate that DSB repair, synapsis, and the formation of early meiotic nodules in mutants are comparable to the wild type, which is

similar to what was observed in *Mlh3* null mice (Lipkin et al. 2002). Interestingly, although the mutated MLH3 only has one residue change compared with wild- type protein, most of the MLH3 foci are missing from the mutant. Since the *neo* cassette has not been removed from these mutants, the reduction of MLH3 foci on pachytene chromosomes can be caused by the interference from the expression of neomycin gene. Or this observation may imply that the stability of MLH3 was affected by the point mutation. In yeast, the analogous point mutation in MLH3 (*mlh3-D523N*) does not affect the stable expression of the protein (Nishant et al. 2008). But considering the significant difference between yeast *MLH3* and mouse MLH3, future experiments will be needed to confirm the expression of mutated mouse MLH3 *in vivo*. It is also possible that the MLH3 endonuclease domain may be involved in facilitating the interaction between MLH3 and its upstream interactor, such as MSH4/MSH5 and hence stabilizing the binding of MLH3 on the chromosome core. The point mutation may interrupt such interaction and leads to the loss of MLH3 foci. On the other hand, I found that the MLH1 foci detected on pachytene chromosome were also dramatically decreased in our $Mlh3^{DN\ neo/-}$ mutants, and most of the mutant oocytes lacked MLH1 foci completely. This can be partly explained by the absence of most of the MLH3 foci in mutants, as was observed in *Mlh3* null mice (Lipkin et al. 2002). However, when the number of residual MLH1 foci was compared with the number of residual MLH3 foci, fewer MLH1 foci were detected, which implies a possible defect in dimerization between MLH1 and mutated MLH3. This observation is not consistent with results from previous studies in yeast, showing that the analogous yeast mutation does not affect the interaction between mutated MLH3 and wild-type MLH1 (Nishant et al. 2008). Thus, future experiments should be done to determine the interaction between MLH1 and mutated MLH3 in mouse. Again, since the *neo* cassette inserted in the mutant *Mlh3* allele was not removed from

these mutant animals, the expression of the exogenous neomycin gene could also affect the formation of MLH1-MLH3 heterodimer. Currently, we are crossing the *Mlh3*$^{DN\ neo\ /-}$ mice with the *Spo11-Cre* line to remove *neo* cassette from the genome. Importantly, however, these preliminary studies demonstrate that this point mutant does affect MLH3 function and thus gives confidence that the *Mlh3*^{DN} mutant is likely to be highly informative with respect to MLH3 function in meiosis.

Since the preliminary data imply a late prophase I phenotype in the mutants, after the generation of *Mlh3*$^{DN/DN}$ mutant mice, future experiments will be focused on studying crossover formation during diakinesis in both sexes, and metaphase progression in mutant females. Additionally, while MLH3 is a key player in Class I CO pathway, the level of Class II COs generated from MUS81-related pathway should also be examined. The interplay between Class I and Class II crossover pathway has been implicated by the observation that MLH3 foci were found to be increased in *Mus81*$^{-/-}$ pachytene cells (Holloway et al. 2008). It will be interesting to see whether MUS81 foci increase in *Mlh3*$^{DN/DN}$ cells during pachynema. Importantly, the changes in meiotic progression detected in *Mlh3*$^{DN/DN}$ mutants should be compared with *Mlh3*$^{-/-}$ mutant, in the hope that the comparison of meiotic phenotype of these two *Mlh3* transgenic lines, together with the comparisons of histological phenotypes of these two mouse line will provide us useful information on how the 'DQHAAHERIRLE' domain affects the function of mouse MLH3.

6. References

Acharya S, Wilson T, Gradia S, Kane MF, Guerrette S, Marsischky GT, Kolodner R, Fishel R. 1996. hMSH2 forms specific mispair-binding complexes with hMSH3 and hMSH6. *Proc Natl Acad Sci U S A* **93**(24): 13629-13634.

Aebi S, Kurdi-Haidar B, Gordon R, Cenni B, Zheng H, Fink D, Christen RD, Boland CR, Koi M, Fishel R et al. 1996. Loss of DNA mismatch repair in acquired resistance to cisplatin. *Cancer Res* **56**(13): 3087-3090.

Buermeyer AB, Deschenes SM, Baker SM, Liskay RM. 1999. Mammalian DNA mismatch repair. *Annual Reviews of Genetics* **33**: 533-564.

Cenni B, Kim HK, Bubley GJ, Aebi S, Fink D, Teicher BA, Howell SB, Christen RD. 1999. Loss of DNA mismatch repair facilitates reactivation of a reporter plasmid damaged by cisplatin. *Br J Cancer* **80**(5-6): 699-704.

Chambers SR, Hunter N, Louis EJ, Borts RH. 1996. The mismatch repair system reduces meiotic homeologous recombination and stimulates recombination-dependent chromosome loss. *Mol Cell Biol* **16**(11): 6110-6120.

Chen YT, Bradley A. 2000. A new positive/negative selectable marker, puDeltatk, for use in embryonic stem cells. *Genesis* **28**(1): 31-35.

Cohen PE, Pollack SE, Pollard JW. 2006. Genetic analysis of chromosome pairing, recombination, and cell cycle control during first meiotic prophase in mammals. *Endocr Rev* **27**(4): 398-426.

de Vries SS, Baart EB, Dekker M, Siezen A, de Rooij DG, de Boer P, te Riele H. 1999. Mouse MutS-like protein Msh5 is required for proper chromosome synapsis in male and female meiosis. *Genes Dev* **13**(5): 523-531.

Edelmann W, Cohen PE, Kneitz B, Winand N, Lia M, Heyer J, Kolodner R, Pollard JW, Kucherlapati R. 1999. Mammalian MutS homologue 5 is required for chromosome pairing in meiosis. *Nat Genet* **21**(1): 123-127.

Feschenko VV, Rajman LA, Lovett ST. 2003. Stabilization of perfect and imperfect tandem repeats by single-strand DNA exonucleases. *Proc Natl Acad Sci U S A* **100**(3): 1134-1139.

Flores-Rozas H, Kolodner RD. 1998. The Saccharomyces cerevisiae MLH3 gene functions in MSH3-dependent suppression of frameshift mutations. *Proc Natl Acad Sci U S A* **95**(21): 12404-12409.

Genschel J, Littman SJ, Drummond JT, Modrich P. 1998. Isolation of MutSbeta from human cells and comparison of the mismatch repair specificities of MutSbeta and MutSalpha. *J Biol Chem* **273**(31): 19895-19901.

Greig D, Travisano M, Louis EJ, Borts RH. 2003. A role for the mismatch repair system during incipient speciation in Saccharomyces. *J Evol Biol* **16**(3): 429-437.

Guarne A, Ramon-Maiques S, Wolff EM, Ghirlando R, Hu X, Miller JH, Yang W. 2004. Structure of the MutL C-terminal domain: a model of intact MutL and its roles in mismatch repair. *EMBO J* **23**(21): 4134-4145.

Guillon H, Baudat F, Grey C, Liskay RM, de Massy B. 2005. Crossover and noncrossover pathways in mouse meiosis. *Mol Cell* **20**(4): 563-573.

Hall MC, Matson SW. 1999. The Escherichia coli MutL protein physically interacts with MutH and stimulates the MutH-associated endonuclease activity. *J Biol Chem* **274**(3): 1306-1312.

Handel MA, Schimenti JC. 2010. Genetics of mammalian meiosis: regulation, dynamics and impact on fertility. *Nat Rev Genet* **11**(2): 124-136.

Harfe BD, Jinks-Robertson S. 2000. DNA mismatch repair and genetic instability. *Annu Rev Genet* **34**: 359-399.

Hollingsworth NM, Ponte L, Halsey C. 1995. MSH5, a novel MutS homolog, facilitates meiotic reciprocal recombination between homologs in Saccharomyces cerevisiae but not mismatch repair. *Genes Dev* **9**(14): 1728-1739.

Holloway JK, Booth J, Edelmann W, McGowan CH, Cohen PE. 2008. MUS81 generates a subset of MLH1-MLH3-independent crossovers in mammalian meiosis. *PLoS Genet* **4**(9): e1000186.

Horst JP, Wu TH, Marinus MG. 1999. Escherichia coli mutator genes. *Trends Microbiol* **7**(1): 29-36.

Hunter N, Chambers SR, Louis EJ, Borts RH. 1996. The mismatch repair system contributes to meiotic sterility in an interspecific yeast hybrid. *EMBO J* **15**(7): 1726-1733.

Hunter N, Kleckner N. 2001. The single-end invasion: an asymmetric intermediate at the double-strand break to double-holliday junction transition of meiotic recombination. *Cell* **106**(1): 59-70.

Jiricny J, Su SS, Wood SG, Modrich P. 1988. Mismatch-containing oligonucleotide duplexes bound by the E. coli mutS-encoded protein. *Nucleic Acids Res* **16**(16): 7843-7853.

Kadyrov FA, Dzantiev L, Constantin N, Modrich P. 2006. Endonucleolytic function of MutLalpha in human mismatch repair. *Cell* **126**(2): 297-308.

Kan R, Sun X, Kolas NK, Avdievich E, Kneitz B, Edelmann W, Cohen PE. 2008. Comparative analysis of meiotic progression in female mice bearing mutations in genes of the DNA mismatch repair pathway. *Biol Reprod* **78**(3): 462-471.

Kat A, Thilly WG, Fang WH, Longley MJ, Li GM, Modrich P. 1993. An alkylation-tolerant,

mutator human cell line is deficient in strand-specific mismatch repair. *Proc Natl Acad Sci U S A* **90**(14): 6424-6428.

Kneitz B, Cohen PE, Avdievich E, Zhu L, Kane MF, Hou H, Jr., Kolodner RD, Kucherlapati R, Pollard JW, Edelmann W. 2000. MutS homolog 4 localization to meiotic chromosomes is required for chromosome pairing during meiosis in male and female mice. *Genes Dev* **14**(9): 1085-1097.

Kolas NK, Cohen PE. 2004. Novel and diverse functions of the DNA mismatch repair family in mammalian meiosis and recombination. *Cytogenet Genome Res* **107**(3-4): 216-231.

Kolas NK, Svetlanov A, Lenzi ML, Macaluso FP, Lipkin SM, Liskay RM, Greally J, Edelmann W, Cohen PE. 2005. Localization of MMR proteins on meiotic chromosomes in mice indicates distinct functions during prophase I. *J Cell Biol* **171**(3): 447-458.

Kunkel TA, Erie DA. 2005. DNA mismatch repair. *Annu Rev Biochem* **74**: 681-710.

Lenzi ML, Smith J, Snowden T, Kim M, Fishel R, Poulos BK, Cohen PE. 2005. Extreme heterogeneity in the molecular events leading to the establishment of chiasmata during meiosis i in human oocytes. *Am J Hum Genet* **76**(1): 112-127.

Lipkin SM, Moens PB, Wang V, Lenzi M, Shanmugarajah D, Gilgeous A, Thomas J, Cheng J, Touchman JW, Green ED et al. 2002. Meiotic arrest and aneuploidy in MLH3-deficient mice. *Nat Genet* **31**(4): 385-390.

Lipkin SM, Wang V, Jacoby R, Banerjee-Basu S, Baxevanis AD, Lynch HT, Elliott RM, Collins FS. 2000. MLH3: a DNA mismatch repair gene associated with mammalian microsatellite instability. *Nat Genet* **24**(1): 27-35.

Macpherson P, Humbert O, Karran P. 1998. Frameshift mismatch recognition by the human MutS alpha complex. *Mutat Res* **408**(1): 55-66.

Mahadevaiah SK, Turner JM, Baudat F, Rogakou EP, de Boer P, Blanco-Rodriguez J, Jasin M, Keeney S, Bonner WM, Burgoyne PS. 2001. Recombinational DNA double-strand breaks in mice precede synapsis. *Nat Genet* **27**(3): 271-276.

Matic I, Babic A, Radman M. 2003. 2-aminopurine allows interspecies recombination by a reversible inactivation of the Escherichia coli mismatch repair system. *J Bacteriol* **185**(4): 1459-1461.

Nishant KT, Plys AJ, Alani E. 2008. A Mutation in the Putative MLH3 Endonuclease Domain Confers a Defect in Both Mismatch Repair and Meiosis in Saccharomyces cerevisiae. *Genetics* **179**(2): 747-755.

Peters AH, Plug AW, van Vugt MJ, de Boer P. 1997. A drying-down technique for the spreading of mammalian meiocytes from the male and female germline. *Chromosome Res* **5**(1): 66-68.

Santucci-Darmanin S, Neyton S, Lespinasse F, Saunieres A, Gaudray P, Paquis-Flucklinger V. 2002. The DNA mismatch-repair MLH3 protein interacts with MSH4 in meiotic cells, supporting a role for this MutL homolog in mammalian meiotic recombination. *Hum Mol Genet* **11**(15): 1697-1706.

Svetlanov A, Cohen PE. 2004. Mismatch repair proteins, meiosis, and mice: understanding the complexities of mammalian meiosis. *Exp Cell Res* **296**(1): 71-79.

van Oers JM, Roa S, Werling U, Liu Y, Genschel J, Hou H, Jr., Sellers RS, Modrich P, Scharff MD, Edelmann W. 2010. PMS2 endonuclease activity has distinct biological functions and is essential for genome maintenance. *Proc Natl Acad Sci U S A* **107**(30): 13384-13389.

Wang TF, Kleckner N, Hunter N. 1999. Functional specificity of MutL homologs in yeast:

evidence for three Mlh1-based heterocomplexes with distinct roles during meiosis in recombination and mismatch correction. *Proc Natl Acad Sci U S A* **96**(24): 13914-13919.

Winand NJ, Panzer JA, Kolodner RD. 1998. Cloning and characterization of the human and Caenorhabditis elegans homologs of the Saccharomyces cerevisiae MSH5 gene. *Genomics* **53**(1): 69-80.

Yamaguchi M, Dao V, Modrich P. 1998. MutS and MutL activate DNA helicase II in a mismatch-dependent manner. *J Biol Chem* **273**(15): 9197-9201.

Zalevsky J, MacQueen AJ, Duffy JB, Kemphues KJ, Villeneuve AM. 1999. Crossing over during Caenorhabditis elegans meiosis requires a conserved MutS-based pathway that is partially dispensable in budding yeast. *Genetics* **153**(3): 1271-1283.

CHAPTER 3

Exploring the possible roles of a mammalian-specific domain in mouse MLH3

1. Abstract

In addition to its roles during meiosis, MLH3 has also been found to participate in mismatch repair (MMR)-related process. Earlier research in the Cohen lab identified the association between mouse MLH3 and satellite sequences at centromere and non-pseudoautosomal region of the Y chromosome during pachynema, which suggests possible roles of MLH3 in MLH1-independent process. Mouse MLH3 is significantly bigger than other mammalian MutL homologs. Further comparison shows that a large piece of extra sequence within exon 2, which is conserved in mammals, is responsible for the increase in size. However, no functional motif has been predicted for this unique exon 2 region. Given the strict conservation of MMR proteins, together with the large size of the mammalian-specific region, I hypothesize that this unique region may have some functions in meiosis and/or mismatch repair process. The goal of this study is to identify possible functions of the MLH3 exon 2-unique region, and also to develop appropriate experimental methods to realize this task. I used two different approaches to examine this exon 2 region. To find possible interaction partners of this region, I first cloned part of this region into pBTM116 and used it as bait in yeast two-hybrid assay, in the hope that the prey recruited by the bait could provide clues to the molecular function of the unique region. A few possible interaction partners of this region were identified from the yeast two-hybrid screening. To further screen for key sub-motifs within this region, a microsatellite instability reporter assay

was developed. It is expected that this study will allow us more insights into the function of mouse MLH3 in maintaining genome integrity as a member of MMR family.

2. Introduction

Mismatch repair (MMR) proteins participate in a variety of cellular events, and play important roles in maintaining genomic stability. Their inactivation can result in the accumulation of point mutations in the genome. In mammals, the importance of MMR proteins has been underscored by the observation that the loss of MMR activity is associated with the initiation and development of carcinogenesis (Loeb et al. 2003). One good example is hereditary non−polyposis colorectal cancer (HNPCC). HNPCC is an autosomal dominant genetic disorder characterized by genomic instability at short tandem repeats and inability to repair replication errors at these repeats, which is often related to mutations in mismatch repair genes, such as MLH1 and MSH2 (Liu et al. 1996; Pedroni et al. 2001; Wei et al. 2003; Kolas and Cohen 2004). The most recently identified MutL homolog, MLH3, has been suggested to play a role in the repair of insertion-deletion mismatch repairs (Flores-Rozas and Kolodner 1998). Mutations in yeast *MLH3* causes a mutator phenotype characterized by an increase in the rate of accumulation of frameshift mutations (Wang et al. 1999). When *Mlh3* is inactivated in mice, tail genomic DNA extracted from the mutants show significantly elevated microsatellite instability (MSI) compared with DNA from wild-type mice (Chen et al. 2005). Additionally, in response to DNA damaging reagents, spontaneously immortalized mouse embryonic fibroblast (MEF) cells generated from *Mlh3* knockout mice display increased resistance compared to wild-type MEF cells (Chen et al. 2005). In humans, although pathogenic germ line mutations of MLH3 are identified in only a small fraction of inherited colorectal cancer (HNPCC), about 25% of sporadic colorectal cancers with microsatellite instability have somatic MLH3 mutations (Taylor et al. 2006). Taken together, these data suggest other MMR-related functions of MLH3, besides the meiotic roles discussed in

Chapter 2. Indeed, previous research done in our lab has identified the association between MLH3 and certain repetitive sequences in the mouse genome (Kolas et al. 2005). Independent of its well-known dimerization partner MLH1, MLH3 was found to be localized in minor/major satellite sequences during pachynema at the centromere and on the nonpseudoautosomal region of the Y chromosome, both of which consist of highly repetitive sequences, and are resistant to meiotic recombination. Noticeably, this association has never been reported in yeast, probably due to the relatively short centromere (~120bp in yeast Vs 6~20 Mb in mice) (Choo 1997; Talbert and Henikoff 2010). Moreover, the localization of MLH3 in these regions was illustrated to be dependent on MSH2 and MSH3, which are related to insertion-deletion mismatch repairs, but not dependent on meiosis- specific MSH4-MSH5.

Bioinformatic studies on mouse *Mlh3* reveal a unique region in exon 2, a region that is highly conserved in mammals. However, while several possible MutL dimerization sites are found elsewhere on the protein, no functional domains have been predicted for this unique region. Given the immense size of this unique region and its conservation among mammalian species, it is believed that such a big piece of DNA must have some novel function in order to have been maintained through evolution.

In this chapter, based on the bioinformatic analysis and the previous discoveries made in our lab, I hypothesize that the unique region in exon 2 is important for the function of mouse MLH3 in maintaining genome integrity, and confers mammalian- specific functions to MLH3 in higher eukaryotes. The experiments described in this chapter were intended to 1) discover possible interacting partners of this unique region and 2) explore a proper experimental method for identifying functionally critical nucleotides in this region, the mutation of which will disrupt the MMR-related function of mouse MLH3 and lead to genomic instability in the cell.

3. Materials and Methods

3.1 Bioinformatic analysis

The comparison among MLH3 orthologues was performed using protein-protein BLAST (blastp) analysis. The potential functional motifs of mouse MLH3 were predicted by NCBI protein-protein BLAST and Ensembl database. The regional conservation of vertebrate MLH3 orthologues was analyzed using ClustalX2.

3.2 Yeast two-hybrid screen

Plasmids and strains

Complementary DNA fragments encoding relevant exon 2 regions of mouse MLH3 were isolated by DNA amplification from wild-type C57B6 cDNA with primers Mlh3-1435F(BamHI) 5'-AAA GGA TCC GCC AAA ACA TCA CAC TCC GGA G -3' and Mlh3-2724R(EcoRI) 5'-AAA GAA TTC GCA CTG GCT ATT ATC TTT CCA - 3', and then cloned into yeast two-hybrid vector pBTM116 by the use of two unique restriction endonuclease sites BamHI and EcoRI, which leads to the generation of the bait vector pBTM116-Mlh3(1435-2724). The mouse testis cDNA library in pGAD10 vector (Clontech) was used as the prey for the protein-protein interaction screen.

Yeast two-hybrid assay

The interactions between proteins were monitored by the activation of both the *His3* and *lacZ* gene in the reporter strain L40 (genotype: *MATa his3*Δ200*trp1–901 leu2–3112 ade2 LYS2*::(4*lex*Aop-*HIS3*)*URA3*:: (*8lex*Aop-*lacZ*)*GAL4*), which is mutant for chromosomal copies

of LEU2, TRP1, and HIS3. The activation of both genes can lead to histidine-independent growth and β-Galactosidase activity.

The pBTM116-Mlh3(1435-2724) and testis cDNA library were co-transformed into L40 cells by the polyethylene glycol-lithium acetate method. The interactions with mouse MLH3 exon 2 region were first selected by colony growth on histidine-deficient plates supplemented with 5 mM ~10 mM 3-amino-1,2,4-triazole (3-AT), which inhibits leaky *His3* expression. The colonies that survived the first round of selection were tested for β-galactosidase (β-gal) activity, which was measured qualitatively by X-gal colony filter lift assay, as described previously (Mockli and Auerbach 2004), with a slight modification. Briefly, colonies from selective plates were transferred onto Whatman #5 paper filters, which were pre-soaked in 0.05% X-gal solution (w/v). Then the wet filters with colonies were immersed in liquid nitrogen. When completely frozen (within ~20 seconds), the filters were removed and thawed at room temperature. The thawed filters were placed on the top of fresh pre-soaked paper filters, and incubated at 30^{o}C to develop color. The colonies producing β-galactosidase, indicated by their blue color, were picked. PCR was used to identify the inserts with primers pGAD10F 5'–CTA TTC GAT GAT GAA GAT ACC CCA CCA AAC CC–3' and pGAD10R 5'–GTG AAC TTG CGG GGT TTT TCA GTA TCT ACG AT–3'.

3.3 Spontaneously-immortalized MEF cell lines and cell culture

The microsatellite instability assays (MSI) mentioned in this chapter were conducted on spontaneously immortalized MEF cells (>20 passages). The *Mlh1*$^{-/-}$ MEF line was kindly provided by Dr. Winfried Edelmann's lab. *Mlh3* MEFs were prepared from 13.5 dpc embryos from timed matings between *Mlh3*$^{+/-}$ mice, whose genotyping strategies have been previously

described (Lipkin et al. 2002). Briefly, embryos were dissected from deciduum, mechanically dissociated by brief homogenization, and cultured on 100 mm culture plates in DMEM supplemented with 10% (v/v) FBS, 1 mM L-glutamine, 0.1 mM MEM nonessential amino acids, 100 U/ml penicillin, and 100 μg/ml streptomycin. These plates were marked as passage zero (p0), and the cells were allowed to grow on the plates until confluent before splitting at a dilution of 1:3 to 1:6. Unless during growth-crisis stage, MEFs were passaged and maintained on a 3T3 culture schedule, in which 1×10^6 cells were passed onto a 100 mm culture plate every three days.

3.4 Microsatellite instability (MSI) reporter assay

For the MSI reporter plasmid, an insertion containing an out-of–frame GFP reporter gene, whose initial ATG start codon was replaced by microsatellite repetitive sequences **ATG**GC$(A)_{17}$ or **ATG**GC$(CA)_{25}$, an IRES sequence and a mCherry gene were integrated into doxycycline inducible lentiviral vector pTet-O-FUW (pTet-O-FUW_MSI_A17 or pTet-O-FUW_MSI_CA25) (Figure 3-2 A). Doxycycline inducible lentiviral vectors were prepared by co-transfecting viral packaging plasmids psPAX2 and pMD2.G with MSI reporter into 293T cells using TransIT-Lt1 transfection reagent (Mirus). For viral infection, self-immortalized MEFs seeded at 10^4 cells per 35 mm culture dish were prepared 24 hours before infection with MSI vectors. 24 hours after infection, doxycycline (Sigma-Aldrich) was added (final concentration 2ug/ml), and the cells were cultured for 5 days before infected MEF cells were sorted with a fluorescence-activated high speed flow cytometer (BD-Biosciences LSR II analyzer) for mCherry positive cells. mCherry positive MEF cells were then cultured for another 8 generations, and then sorted again for GFP and mCherry positive cells. The percentage of GFP- and mCherry-expressing cells was

analyzed with BD FACS Diva. The calibration of the flow cytometer and the gate for each fluorescent channel were set using uninfected, or single fluorescent (GFP or mCherry) MEFs as controls.

4. Results

4.1 One region in *Mlh3* exon 2 is highly conserved in mammals

Due to the importance of MMR system in maintaining genomic stability, the size of MMR homologs is generally conserved in various species. However, one MutL homolog, mouse MLH3, is significantly bigger when compared with other eukaryotic MutL homologs. The 12 exons of this gene encode a protein consisting of 1411 amino acids, almost twice the size of other MutL homologs (Figure 3-1A). Further multispecies comparison demonstrates that mouse MLH3 has gained some extra sequence within exon 2 (from 350 aa to 1000 aa), and this region is highly matched in mammalian species, *including Rattus norvegicus, Homo sapiens, Macaca mulatta, Bos taurus, Canis familiaris, Pan troglodytes, Monodelphis domestica and Pongo pygmaeus* (Figure 3-1 B). Interestingly, in spite of its conservation, this unique exon 2 region contains no known functional motifs. In contrast, four conserved protein domains are identified in either N- or C- terminal of mouse MLH3 (Figure 3-1 C).

Given the strict conservation of MMR family members, together with the large size of this region, I hypothesize that this extra region may have some unique functions that are specific for mammalian species.

Figure 3-1. One region in the exon 2 of mouse MLH3 is highly conserved in mammals, but contains no predicted functional motif.

(A) The size of MutL homologs from mouse, human and yeast is compared. Note that the size of MLH3 is almost doubled in human and mouse compared with yeast. **(B)** NCBI blastp results comparing MLH3 orthologues across different species are shown. **(C)** Predicted functional domains of mouse MLH3 are shown. While four conserved functional domains are found in N- or C- terminal of the protein, no prediction is made for the unique exon 2 region (labeled as a two way arrow and a question mark).

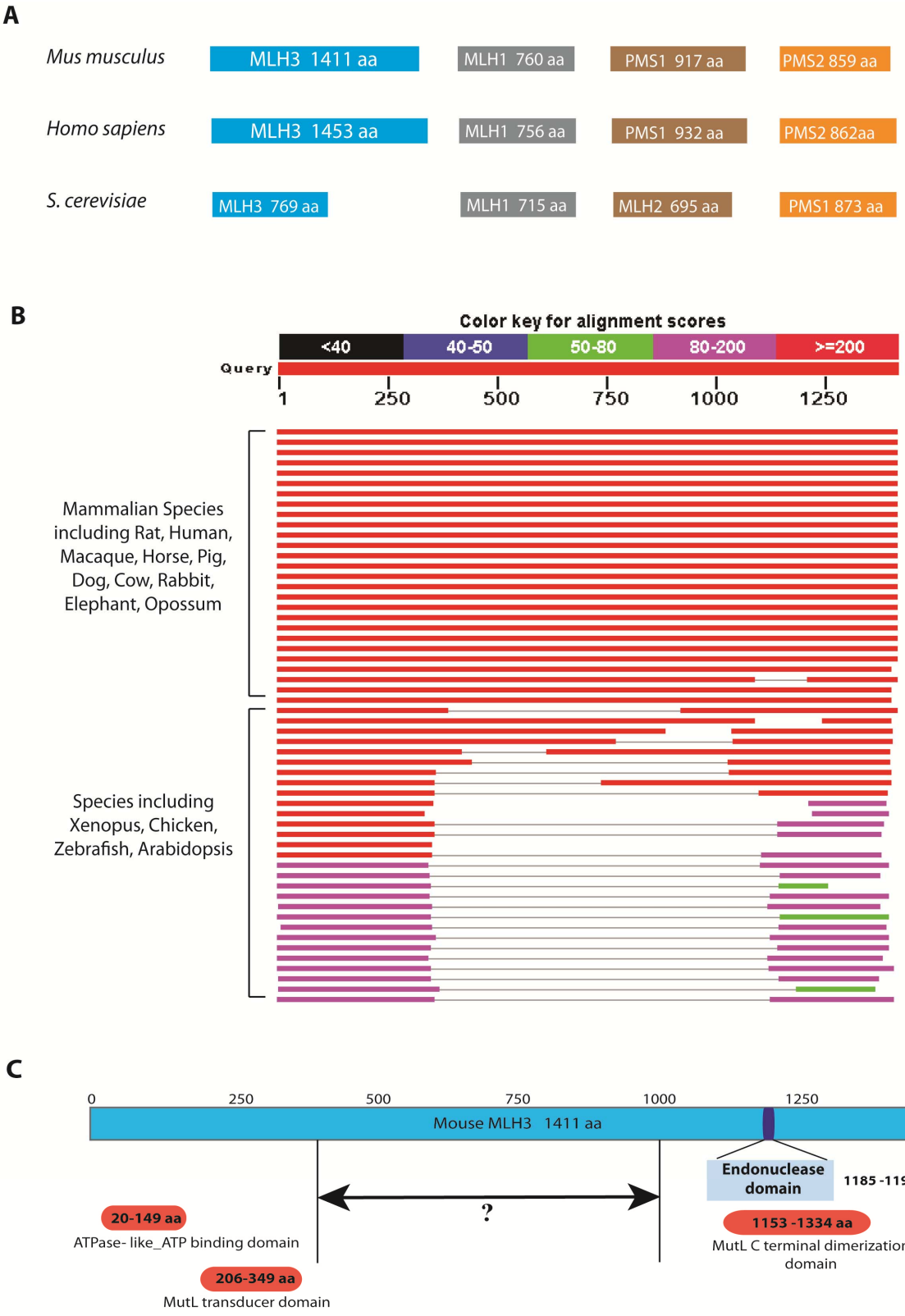
A
Mus musculus
MLH3 1411 aa
MLH1 760 aa
PMS1 917 aa
PMS2 859 aa
Homo sapiens
MLH3 1453 aa
MLH1 756 aa
PMS1 932 aa
PMS2 862aa
S. cerevisiae
MLH3 769 aa
MLH1 715 aa
MLH2 695 aa
PMS1 873 aa
B
Color key for alignment scores
<40
40-50
50-80
80-200
>=200
Query
1
250
500
750
1000
1250
Mammalian Species including Rat, Human, Macaque, Horse, Pig, Dog, Cow, Rabbit, Elephant, Opossum
Species including Xenopus, Chicken, Zebrafish, Arabidopsis
C
0
250
500
750
1000
1250
1411
Mouse MLH3 1411 aa
Endonuclease domain
1185 -1196 aa
?
20-149 aa
ATPase- like_ATP binding domain
206-349 aa
MutL transducer domain
1153 -1334 aa
MutL C terminal dimerization domain

4.2 Identification of potential interaction partners of the *Mlh3* unique region

To investigate the possible function of this unique region, the yeast two-hybrid system was used to screen for the potential interacting proteins of this region. Due to the big size of the unique region (~2 kb totally), one part of this region (1.2kb DNA fragment corresponding to 1435 bp to 2724bp of *Mlh3* cDNA, encoding 478 aa to 908 aa of mouse MLH3) was chosen based on the high conservation in mammalian species, This 1.2 kb fragment was cloned into pBTM116 as the "bait" (pBTM116-Mlh3(1435-2724)), and screened against a mouse testis cDNA library in pGAD10. The potential interaction partners were identified by assaying for the transcriptional activation of two reporters, *His3* and *lacZ*. Among approximately 10^5 transformants surviving on histidine-deficient plates supplemented with 3-AT, nine clones turned blue when tested for β-galactosidase activity in the presence of the chromogenic substrate X-gal. These yeast clones were isolated, and the sequences of the inserts in pGAD10 were determined by PCR amplification. However, none of these potential interacting genes are yet known to have a direct role in gametogenesis (See Table 3-1). *Fhd15* and *Hmgb4* are known to function in nucleus, and HMGB4, especially, was found to be expressed in the adult mouse testis. It has been shown that, while HMGB4 is present in the euchromatin of late pachytene spermatocytes, stronger expression is observed at the basal pole of the elongating spermatid nucleus (Catena et al. 2009). It is not clear whether HMGB4 is involved in meiotic events.

4.3 MSI reporter assay to screen for critical sub-regions in the *Mlh3* unique region

Previous studies have found the association of MLH3 with minor/major satellite sequences at centromere of meiotic chromosomes, which is not seen in lower eukaryotes, such as yeast (Kolas et al. 2005). Additionally, microsatellite instability (MSI) has been detected in *Mlh3* knockout

Table 3-1. Potential interactors of the 1.2 kb region of mouse MLH3 identified in the yeast two-hybrid screen

Gene symbol (Name)	Process/ Function	Cellular Component	Roles in Gametogenesis
Tns1 (Tensin 1)	Cell-substrate junction assembly, fibroblast migration/ actin binding, metal ion binding	Cell-substrate junction	Not defined
Phospho2 (Phosphatase orphan 2)	Dephosphorylation, metabolic process/ hydrolase activity, metal ion binding, phosphatase activity, pyridoxal phosphatase activity	Not defined	Not defined
Slc36a3 (Solute carrier family 36 (proton/amino acid symporter), member 3)	Proton/amino acid transporters	Cell membrane	Not defined
Ccdc27 (coiled-coil domain containing 27)	Not defined	Not defined	Not defined
Tmem135 (Transmembrane protein 135)	Peroxisome organization/ fat storage and energy expenditure	Integral to membrane, membrane, peroxisome	Not defined
Fhl5 (Four and a half LIM domains 5)	Regulation of RNA biosynthetic processes, transcription, DNA-dependent/ transcription coactivator activity, metal ion binding	Nucleus	Its interacting partner cAMP-responsive element modulator(CREM) is essential for differentiation of spermatids into mature spermatozoa (Kimmins et al. 2004).
Ddx19b (DEAD (Asp-Glu-Ala-Asp) box polypeptide 19b)	ATP binding, helicase activity, hydrolase activity/export of mRNA from the nucleus	Cytoplasm, cytoplasmic fibrils of the nuclear pore complex	Some members of this protein family are believed to be involved in spermatogenesis (Tsai-Morris et al. 2010).
Ndufa2 (NADH dehydrogenase (ubiquinone) 1 alpha subcomplex, 2)	Transport, electron transport chain/NADH dehydrogenase (ubiquinone) activity	Inner mitochondrial membrane, mitochondrial respiratory chain complex I	Not defined
Hmgb4 (High mobility group box 4)	DNA binding	Chromosome, nucleus	This protein specifies distinct chromatin domains at the basal poles of the elongating spermatid nucleus (Catena et al. 2009).

mice by previous researchers (Lipkin et al. 2000; Chen et al. 2005). Thus, I chose to use microsatellite instability (MSI) reporter assay to test 1) whether deficiency in this exon 2 unique region will cause an increase in MSI, which is the hallmark of a defective mismatch repair system, and 2) which sub-regions of this unique region are more important for this function.

Immortalized MEF cells were chosen as the system for the MSI reporter assay to allow sustainable selection in a somatic cell background. To generate *Mlh3* MEF cell line, 13.5 dpc embryos were harvested from timed matings between $Mlh3^{+/-}$ mice and mechanically dissociated. The dissociated cells were grown on the plates (p0) until confluent before further splitting. These MEF cells entered growth-crisis stage around passage 4 and recovered around passage 10 (Figure 3-2 C). After that, MEFs were maintained on a 3T3 culture schedule, in which 1×10^6 cells were passed onto a 100 mm culture plate every three days. The spontaneously immortalized mouse embryonic fibroblasts (MEFs) were generated from $Mlh3^{+/+}$, $Mlh3^{+/-}$, $Mlh3^{-/-}$ and $Mlh1^{-/-}$ embryos (Figure 3-2 C). Interestingly, the MEFs derived from $Mlh3^{+/-}$ embryos proliferated at a higher rate compared with either wild-type or $Mlh1^{-/-}$ MEFs, which may suggest certain growth advantage of these heterozygous MEF cells.

Transfection efficiency of MEFs were first tested by using lipid-based transfection reagents commercially available, which resulted in low yield (<5%). To increase the transfection efficiency in MEFs, the MSI reporter was reconstructed based on a doxycycline inducible lentiviral vector using pTet-O-FUW as backbone. The inserted fragments were composed of a disrupted GFP gene, whose open reading frame is interrupted by the insertion of either mononucleotide repeats ($(A)_{17}$) or dinucleotide repeats ($(CA)_{25}$) after the start codon, an IRES sequence and one mCherry gene (pTet-O-FUW_MSI_A17 or pTet-O-FUW_MSI_CA25) (Figure 3-2 A).

Figure 3-2. MSI reporter assay is used to screen for critical sub-regions in the *Mlh3* exon 2 region.

(A) and **(B)** are the maps of MSI reporter construct and Mlh3 expression vector. **(C)** *Mlh3* MEF lines were generated through spontaneous immortalization. The growth curves of $Mlh3^{+/+}$, $Mlh3^{+/-}$ and $Mlh3^{-/-}$ MEF lines are shown. The growth rate of each generation is calculated by $\ln(X_{n+1}/X_n)/\ln 2$. X is the total cell number; n represents the number of the passage. **(D)** The experiment procedure of the MSI reporter assay is illustrated. Please refer to the main text for detailed explanation.

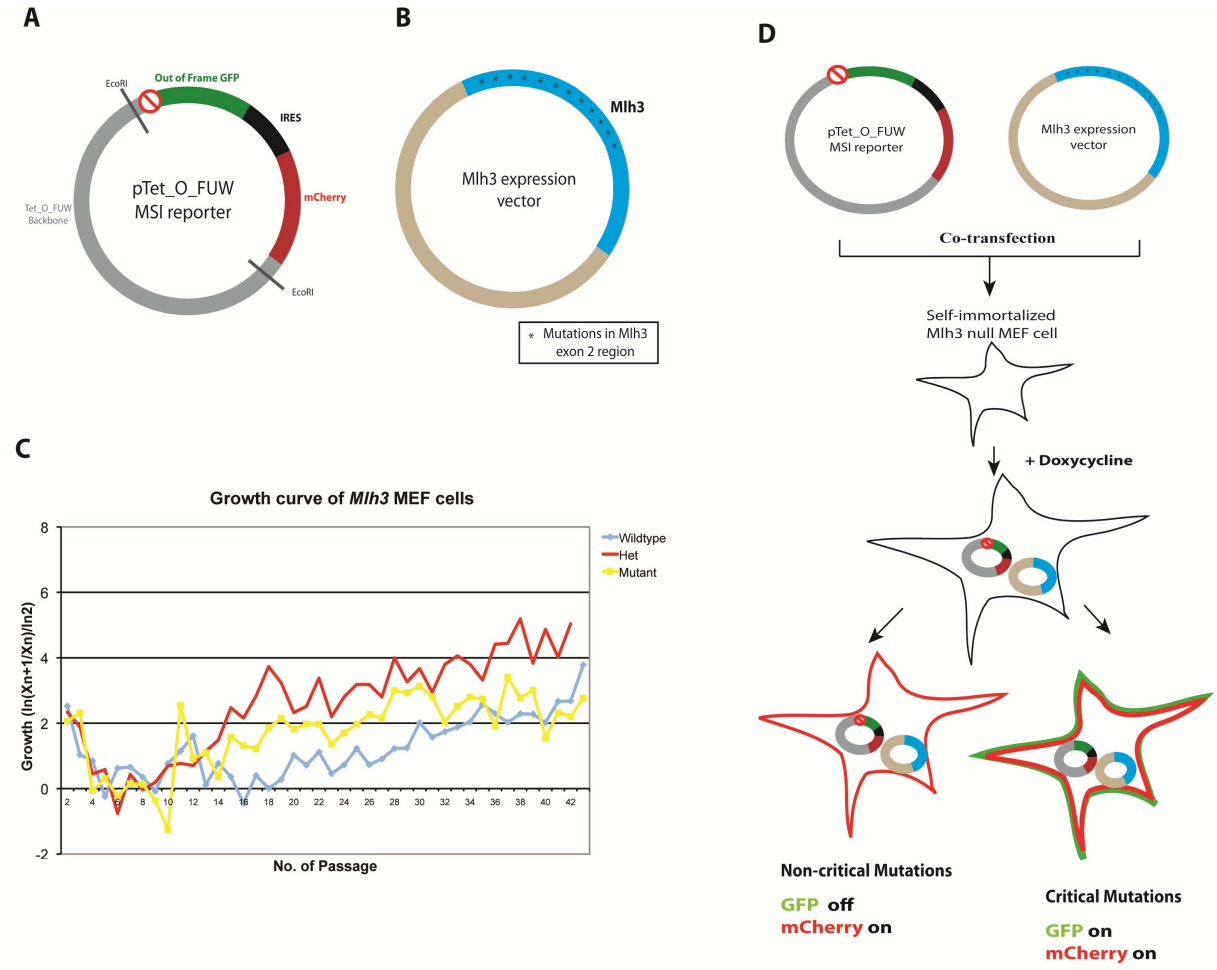

In the MSI reporter assay, *Mlh3*$^{-/-}$ MEFs are first co-transfected with pTet-O-FUW_MSI reporter and *Mlh3* expression vector containing full-length Mlh3 cDNA with mutations in the exon 2 region (Figure 3-2 D). The mCherry gene in the reporter is an indicator of successful transfection while MSI status of the cell is monitored by the out of frame GFP gene. If the mutated sites in the exon 2 region are not critical, MEFs will be GFP negative but mCherry positive. On the contrary, when the mutations interrupt the normal function of this gene and MSI is induced, GFP gene may be back to in-frame, and MEFs will turn on both GFP and mCherry expression.

To test the feasibility of the use of *Mlh3*$^{-/-}$ MEF cells as the screening system, control experiments have been conducted by transfecting *Mlh3*$^{+/+}$, *Mlh3*$^{+/-}$, *Mlh3*$^{-/-}$ and *Mlh1*$^{-/-}$ MEFs with the MSI reporter pTet-O-FUW_MSI_A17 without *Mlh3* expression vector. Among these MEF lines, *Mlh1*$^{-/-}$ MEF cells were used as a positive control since MLH1 is the major MuL homolog in eukaryotic MMR. Five days after transfection, these MEFs were sorted for mCherry signal. Then the mCherry positive MEFs were allowed to grow for another 8 generations before entering the second round of sorting for GFP and mCherry signals (Figure 3-3 A), and MSI status of each cell line was determined based on the proportion of GFP positive cells to total fluorescent cells (GFP or mCherry positive). Of note, since errors occurring during DNA replication could also disrupt the expression of mCherry, some cells could be mCherry negative but GFP positive at this point (Figure 3-3 A). As expected, *Mlh1*$^{-/-}$ MEFs had the highest level of MSI, which is consistent with the critical role MLH1 plays in mismatch repair system (23.8% in *Mlh1*$^{-/-}$, 10.7% in wild type). However, to our surprise, *Mlh3*$^{+/-}$ line, not the *Mlh3*$^{-/-}$ MEFs, had the second highest MSI level (14.1%). Furthermore, the GFP percentage in *Mlh3*$^{-/-}$ was only 7.7%, even lower than wild-type MEFs (10.7%). It is to be determined whether the decreased GFP signal in *Mlh3*$^{-/-}$ MEF results from the increase of apoptotic cells, which may be GFP

Figure 3-3 Spontaneously-immortalized MEF is tested as the system for MSI reporter assay. (A) The experimental flow chart of the control experiment of MSI is shown. Please refer to the main text for more details. (B) A snapshot of mCherry positive MEFs after the first round of sorting is displayed. (C) A sample of the FACS results after the second round of sorting. (D) The proportion of GFP positive population in GFP or mCherry positive population is calculated for each MEF line according to the FACS results.

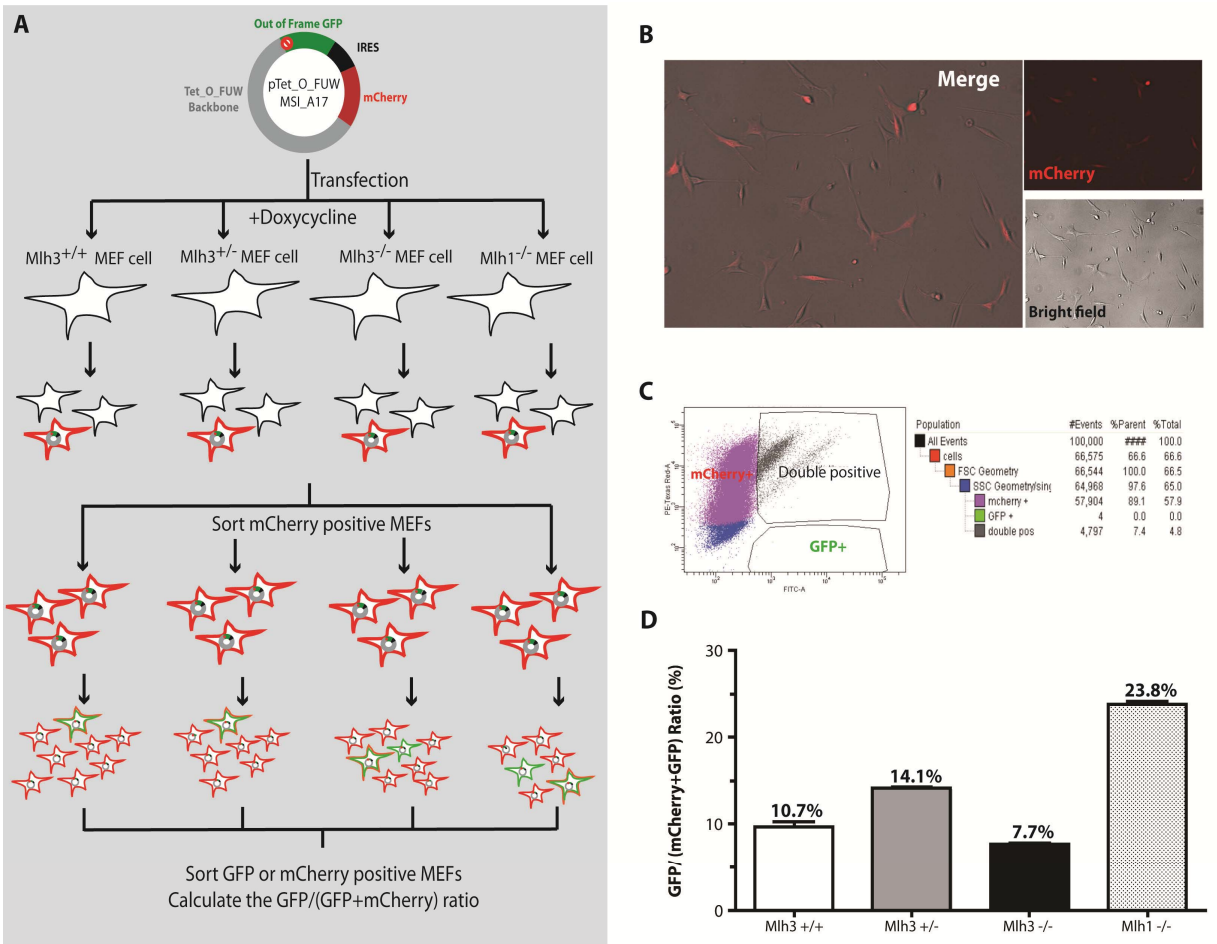

positive. On the other hand, these results indicates that *Mlh3*$^{-/-}$ may not be the best choice for the MSI reporter assay. It can be predicted that, if *Mlh3*$^{-/-}$ MEFs are used for the screening, the introduction of one copy of exogenous wild-type *Mlh3* may lead to an increase in MSI, just as we observed in *Mlh3*$^{+/-}$ MEFs. More importantly, if that single copy of *Mlh3* contains critical mutation, it will be hard to predict the change of the MSI level in these cells, which makes it difficult to interpret the screening results correctly.

5. Discussion

The preliminary studies presented herein explore the possible functions of one unique region of mouse MLH3 in mammals. While the size of MutL homologs is generally conserved in various species, mammalian MLH3 is significantly bigger than other MutL homologs in mammals and other eukaryotic organisms. A closer study of mouse MLH3 demonstrates that this expansion, encoded by exon 2, is highly conserved in mammals, but no functional domain has been found in this region.

To elucidate the functions of this region, two different approaches were employed. The first was the yeast two-hybrid screen. It was conducted to identify potential interacting proteins of known function in the hope that these proteins could provide clues to the molecular function of the unique region. Although none of the identified proteins have been known to be involved in meiosis or mismatch repair, two of them, FHL5 and DDX19B, may play a direct or indirect role during gametogenesis (Kimmins et al. 2004; Tsai-Morris et al. 2010), and one of the proteins, HMGB4, is found to be strongly and preferentially expressed in mouse testis. HMGB4 is a member of HMGB (High-Mobility Group Box) family and specific to mammalian species. As a

newly identified HMGB family member, HMGB4 is shown to function as transcriptional regulator, and also play a key role in organizing polar chromatin domains in the nucleus (Catena et al. 2009) . Although the strong expression of HMGB4 was observed in elongating spermatids, this protein was found to be associated with chromatin, and can be detected on chromosomes of spermatocytes during late pachynema, which overlaps the period when MLH3 functions in meiosis (Lipkin et al. 2002; Catena et al. 2009). However, with our current knowledge of MLH3 and its unique region, it is still hard to establish logical linkage between MLH3 and HMGB4. Thus, further validation will be needed to confirm the interaction between MLH3 and HMGB4, and meanwhile, more rounds of the yeast two-hybrid screen may be necessary to identify more potential interacting proteins, which may help add missing pieces to the puzzle.

Previous studies have suggested that mammalian MLH3 may play a role in maintaining genomic stability and participate in repair of DNA insertion/deletion loops (Fishel and Wilson 1997; Nakagawa et al. 1999; Lipkin et al. 2000). The interruption of MLH3 can cause defects in maintaining repetitive sequence length and lead to MSI. Furthermore, mouse MLH3 was found to be associated with repetitive sequences at centromere and certain region of Y chromosome in mice (Kolas and Cohen 2004). Similar to the unique region, this localization of MLH3 is also absent in lower eukaryotic species, such as yeast. Considering the error-prone nature of repetitive sequences in the genome, we decided to test whether the MLH3 unique region is related with the mismatch repair, and to ask which sub-regions of the unique domain are responsible for this function. To this end, I devised a novel screening method, which integrated an MSI reporter assay into self-immortalized MEF cells. The basis for the experiment was that critical mutations in the MLH3 unique region could lead to an elevation of MSI level in *Mlh3*$^{-/-}$ MEFs, which would be reflected on the increase in the reporter gene expression. However, when the *Mlh3*$^{+/+}$,

Mlh3$^{+/-}$, *Mlh3*$^{-/-}$ and *Mlh1*$^{-/-}$MEF lines were tested for its ability to turn on MSI-sensitive reporter genes, only *Mlh1*$^{-/-}$ and *Mlh3*$^{+/-}$ MEFs exhibited particularly elevated MSI levels. The MSI level in *Mlh3*$^{-/-}$ MEFs is even lower than *Mlh3*$^{+/+}$. These data may imply a dosage-dependent phenotype in *Mlh3* MEF lines. When the MEF cell has both copies of *Mlh3*, MSI level is relatively low. In *Mlh3*$^{+/-}$ MEF cells, where there is only one functional *Mlh3* allele, MMR system seems to be disrupted, indicated by the increase of MSI level. However, when both *Mlh3* alleles are absent, the MMR system is further impaired, and activates compensatory machinery from the other members of the mismatch repair system. Both MLH1-PMS2 (MutLα) and MLH1-MLH3 (MutLγ) can repair insertion-deletion mismatches (Kunkel and Erie 2005). In the absence of MLH3, the activity of MLH1-PMS2 (MutLα) may be upregulated in the cell. Future experiments should be set up to monitor the change in MLH1 and PMS2 protein level in *Mlh3*$^{-/-}$ MEF line compared with wild-type MEF line. Alternatively, it is possible that the relatively low MSI level observed in *Mlh3*$^{-/-}$ MEF cells is the result of increased apoptosis in these cells compared with *Mlh3*$^{+/-}$ and wild-type MEF. TUNEL (TdT-mediated dUTP Nick End Labeling) staining of *Mlh3*$^{-/-}$, *Mlh3*$^{+/-}$ and wild-type MEF cells will be necessary to test this possibility. Of note, the relatively high MSI level in *Mlh3*$^{+/-}$ MEFs did not affect the growth of these cells. It was observed that the growth rate in these heterozygous MEF cells was higher than both the wild-type and *Mlh3*$^{-/-}$ MEFs, indicating perhaps that the high MSI level allows *Mlh3*$^{+/-}$ MEFs to gain more chance to accumulate advantageous mutations for survival.

Taken together, our MSI assay indicates the need for other MEF line for the screening. One option is to use a *Pms2* and *Mlh3* double null MEF line. The results from previous studies in mice demonstrate that, while *Mlh3*$^{-/-}$ mice show slightly elevated MSI compared with wild-type level, *Mlh3*$^{-/-}$; *Pms2*$^{-/-}$ double null mice have similar MSI level as *Mlh1*$^{-/-}$ mice, about 40-fold

higher than wild type (Chen et al. 2005). It is expected that this double null MEF line will exclude, or at least alleviate, the compensation effect observed in *Mlh3*$^{-/-}$ MEF cells and make for a better system for MSI screening. However, the apoptosis level of these double null MEF cells should be determined before the screening. It may cause a similar problem as *Mlh3*$^{-/-}$ MEFs if apoptosis level in these double null MEFs is significantly higher than wild-type MEFs. Then other mismatch repair deficient MEF lines may be needed

After the validation of the screening system, the full-length *Mlh3* expression vector will be introduced into the screening system in the hope that the exogenous copy of *Mlh3* can rescue the phenotype, at least to some extent. Then the next problem will be to decide which nucleotides are critical, and should be targeted for mutation. A more careful comparison of the big unique region reveals ten mammalian-specific conserved sub-regions in mouse MLH3 (Figure 3-4). Each sub-region in *Mlh3* cDNA can be mutated by deletion or nucleotide-substitution, and be integrated into an expression vector. Each *Mlh3* expression vector containing a specific mutation from these ten regions will be transfected into mismatch repair-deficient MEFs with the MSI reporter. The proportion of cells with MSI reporter genes turned on in each clone can be compared. It can be predicted that the mutations introduced into a critical sub-region of MLH3 unique region will induce significantly higher MSI in the MEF cells. Ultimately, we hope that this study will shed some light on the function of this MLH3 unique region either in meiosis or in other somatic process and improve our current understanding of mouse MLH3.

Meanwhile, possible functions of this region can also be tested by inserting this region into other related MMR proteins, which do not contain these sequences, and see whether any new functions are brought in by the insertion. For example, while this unique exon 2 region is highly conserved in mammals and some other eukaryotic organisms, it is absent from yeast MLH3. It will be

Figure 3-4. Multispecies comparison of *Mlh3* exon 2 region.

The sequence of mouse MLH3 exon 2 unique region is compared with the corresponding region of MLH3 homologs from *Homo sapiens, Pan troglodytes, Bos taurus, Canis familiaris, Gallus gallus, Xenopus tropicalis* and *Danio rerio* using ClustalX2. The regions, which are highly conserved only in mammalian species, are shaded in light grey and labeled as 1 to 10.

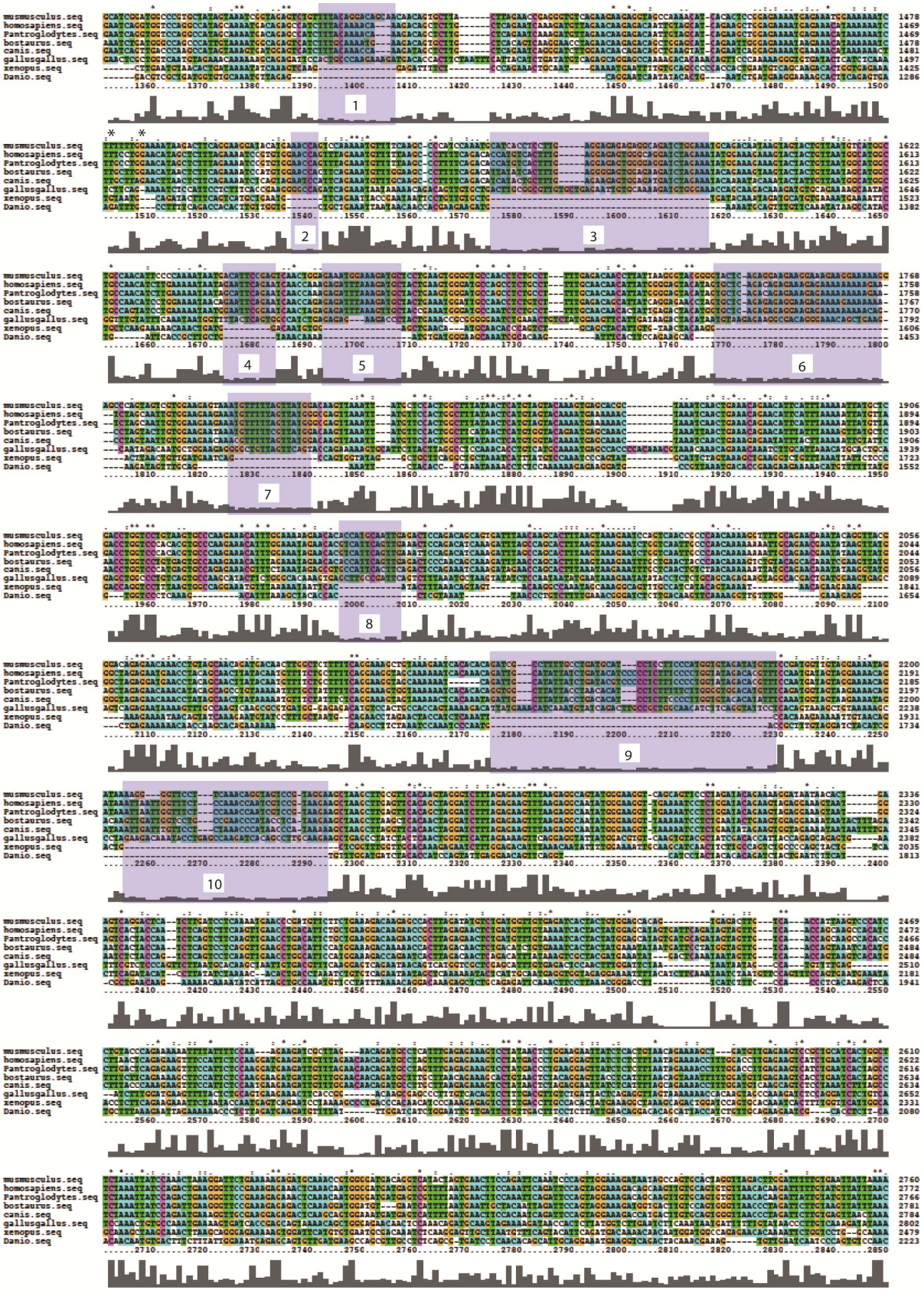
musmusculus.seq
homosapiens.seq
Pantroglodytes.seq
bostaurus.seq
canis.seq
gallusgallus.seq
xenopus.seq
Danio.seq
1
2
3
4
5
6
7
8
9
10

interesting to integrate this region into yeast MLH3 and put the construct into *mlh3* deficient yeast strain and examine how mismatch repair activity is rescued by the fusion protein. Similarly, this unique region is also missing from PMS2, a closely related MutL homolog. It will be intriguing to examine how the mismatch repair function of PMS will be altered after the insertion of this unique region.

6. References

Catena R, Escoffier E, Caron C, Khochbin S, Martianov I, Davidson I. 2009. HMGB4, a novel member of the HMGB family, is preferentially expressed in the mouse testis and localizes to the basal pole of elongating spermatids. *Biol Reprod* **80**(2): 358-366.

Chen PC, Dudley S, Hagen W, Dizon D, Paxton L, Reichow D, Yoon SR, Yang K, Arnheim N, Liskay RM et al. 2005. Contributions by MutL homologues Mlh3 and Pms2 to DNA mismatch repair and tumor suppression in the mouse. *Cancer Res* **65**(19): 8662-8670.

Choo KHA. 1997. The centromere. *Oxford University Press, Oxford*.

Fishel R, Wilson T. 1997. MutS homologs in mammalian cells. *Current Opinions in Genetics and Development* **7**: 105-113.

Flores-Rozas H, Kolodner RD. 1998. The Saccharomyces cerevisiae MLH3 gene functions in MSH3-dependent suppression of frameshift mutations. *Proc Natl Acad Sci U S A* **95**(21): 12404-12409.

Kimmins S, Kotaja N, Davidson I, Sassone-Corsi P. 2004. Testis-specific transcription mechanisms promoting male germ-cell differentiation. *Reproduction* **128**(1): 5-12.

Kolas NK, Cohen PE. 2004. Novel and diverse functions of the DNA mismatch repair family in mammalian meiosis and recombination. *Cytogenet Genome Res* **107**(3-4): 216-231.

Kolas NK, Svetlanov A, Lenzi ML, Macaluso FP, Lipkin SM, Liskay RM, Greally J, Edelmann W, Cohen PE. 2005. Localization of MMR proteins on meiotic chromosomes in mice indicates distinct functions during prophase I. *J Cell Biol* **171**(3): 447-458.

Kunkel TA, Erie DA. 2005. DNA mismatch repair. *Annu Rev Biochem* **74**: 681-710.

Lipkin SM, Moens PB, Wang V, Lenzi M, Shanmugarajah D, Gilgeous A, Thomas J, Cheng J,

Touchman JW, Green ED et al. 2002. Meiotic arrest and aneuploidy in MLH3-deficient mice. *Nat Genet* **31**(4): 385-390.

Lipkin SM, Wang V, Jacoby R, Banerjee-Basu S, Baxevanis AD, Lynch HT, Elliott RM, Collins FS. 2000. MLH3: a DNA mismatch repair gene associated with mammalian microsatellite instability. *Nat Genet* **24**(1): 27-35.

Liu B, Parsons R, Papadopoulos N, Nicolaides NC, Lynch HT, Watson P, Jass JR, Dunlop M, Wyllie A, Peltomaki P et al. 1996. Analysis of mismatch repair genes in hereditary non-polyposis colorectal cancer patients. *Nat Med* **2**(2): 169-174.

Loeb LA, Loeb KR, Anderson JP. 2003. Multiple mutations and cancer. *Proc Natl Acad Sci U S A* **100**(3): 776-781.

Mockli N, Auerbach D. 2004. Quantitative beta-galactosidase assay suitable for high-throughput applications in the yeast two-hybrid system. *Biotechniques* **36**(5): 872-876.

Nakagawa T, Datta A, Kolodner RD. 1999. Multiple functions of MutS- and MutL-related heterocomplexes [comment]. *Proc Natl Acad Sci U S A* **96**(25): 14186-14188.

Pedroni M, Sala E, Scarselli A, Borghi F, Menigatti M, Benatti P, Percesepe A, Rossi G, Foroni M, Losi L et al. 2001. Microsatellite instability and mismatch-repair protein expression in hereditary and sporadic colorectal carcinogenesis. *Cancer Res* **61**(3): 896-899.

Talbert PB, Henikoff S. 2010. Centromeres convert but don't cross. *PLoS Biol* **8**(3): e1000326.

Taylor NP, Powell MA, Gibb RK, Rader JS, Huettner PC, Thibodeau SN, Mutch DG, Goodfellow PJ. 2006. MLH3 mutation in endometrial cancer. *Cancer Res* **66**(15): 7502-7508.

Tsai-Morris CH, Sheng Y, Gutti RK, Tang PZ, Dufau ML. 2010. Gonadotropin-regulated testicular RNA helicase (GRTH/DDX25): a multifunctional protein essential for

spermatogenesis. *J Androl* **31**(1): 45-52.

Wang TF, Kleckner N, Hunter N. 1999. Functional specificity of MutL homologs in yeast: evidence for three Mlh1-based heterocomplexes with distinct roles during meiosis in recombination and mismatch correction. *Proc Natl Acad Sci U S A* **96**(24): 13914-13919.

Wei K, Clark AB, Wong E, Kane MF, Mazur DJ, Parris T, Kolas NK, Russell R, Hou H, Jr., Kneitz B et al. 2003. Inactivation of Exonuclease 1 in mice results in DNA mismatch repair defects, increased cancer susceptibility, and male and female sterility. *Genes Dev* **17**(5): 603-614.

CHAPTER 4

Investigating the role of *Cntd1* during mouse meiosis

1. Abstract

Mouse CNTD1, a cyclin-related protein, is the mammalian orthologue of *C. elegans* COSA-1. A recent study in *C. elegans* demonstrates that COSA-1 is associated with presumptive crossover (CO) sites during meiosis. Mutations in the worm gene cause frequent missegregaton of sex chromosomes and a high frequency of non-viable progeny in *C. elegans*. These mutants also display disrupted interhomolog crossing over with a significant reduction in genetic recombination, although homolog pairing, synapsis and double strand break formation during early stages of meiosis appear to be normal. To elucidate the role of mouse *Cntd1* during mammalian meiosis, we generated *Cntd1* mutant mice using a *Cntd1* gene trap ES cell line. *Cntd1* mutant animals demonstrated normal reproductive behavior, but both sexes were found to be infertile. In *Cntd1* mutant males, loss of normal levels of CNTD1 protein led to increased apoptosis of spermatocytes in the testis, and no spermatozoa in the epididymis. Homozygous mutant females showed a gradual depletion of the oocyte pool after puberty and displayed rudimentary ovarian morphology by 8 weeks of age. Examination of meiotic progression in these mutant animals revealed that DSB formation, pairing and synapsis were normal in these mutants. However, Class I COs, indicated by MLH1/MLH3 foci, were dramatically reduced, coupled with significantly decreased chiasmata number at diakinesis. Taken together, our results suggest that CNTD1 has essential functions during mouse gametogenesis and is critical for promoting and stabilizing reciprocal crossovers in prophase I.

2. Introduction

Meiosis is a specialized type of cell division that is a crucial step in generating haploid gametes in sexually reproducing organisms. A successful meiotic event ensures proper segregation of homologous chromosomes and sister chromatids, which results in an accurate chromosome complement in each gamete so that the integrity of the genome will be preserved in the offspring. Prophase I is the defining stage of meiosis, during which homologous chromosomes pair with each other, and reciprocal recombination occurs between them. Meiotic recombination is a highly regulated process and conserved from yeast through to humans. It begins with the formation of genetically programmed double-strand breaks (DSBs), which is catalyzed by the type II topoisomerase-like DNA transesterase SPO11(Keeney et al. 1997). The repair of DSBs can occur through various downstream pathways, resulting in either crossovers (COs) or noncrossovers (NCOs). In *S. cerevisiae*, the best studied organism in terms of meiotic recombination mechanisms, at least two pathways have been found to produce COs. One is the interference-dependent Class I CO pathway, also known as ZMM (for yeast protein Zip1/ Zip2/ Zip3, Msh4/Msh5 and Mer3) pathway. This pathway involves MutS homologs, Msh4 and Msh5, as well as MutL homologs, Mlh1 and Mlh3 (Borner et al. 2004). The other one is the interference-independent Class II CO pathway, requiring the activity of the endonuclease *MUS81*, which acts as a heterodimer with *MMS4* (de los Santos et al. 2003; Jessop and Lichten 2008; Oh et al. 2008). A third CO pathway, which is Msh4/Msh5/Mus81/Mms4-independent, has also been suggested in S. cerevisiae by the observation that residual COs can still be detected in the mutant defective for key proteins of both pathways (de los Santos et al. 2003; Argueso et al. 2004).

Different organisms rely on the two pathways to different degrees. In *C. elegans*, almost all COs

are generated from Class I CO pathway (Zalevsky et al. 1999). Yeast use Class I CO pathway for about 70% of all COs (Argueso et al. 2004). In mice, about 90%-95% of COs, as marked by MLH1/MLH3 foci on chromosome cores during pachynema, are generated from Class I CO pathway, and Mus81-dependent Class II CO pathway is responsible for only ~ 5%-10% of COs (Kolas et al. 2005; Holloway et al. 2008; Svetlanov et al. 2008).

While meiotic COs can be generated from different pathways, the number and the distribution of COs are strictly controlled. It has been found that each pair of homologous chromosomes needs to have at least one crossover to ensure proper segregation, and each CO tends to form away from others (interference) (Jones and Franklin 2006). The total number of COs is maintained by a mechanism called crossover homeostasis, which has been described in different organisms, including yeast, worms and mice (Hillers and Villeneuve 2003; Martini et al. 2006; Cole et al. 2012). Crossover homeostasis keeps the number of COs relatively consistent at the expense of NCOs even when the number of double strand breaks varies (Martini et al. 2006). In mice, the recombination process is induced by double strand breaks in the beginning of prophase I. Early recombination events are marked by strand invasion proteins such RAD51 and DMC1. More than 200 RAD1 foci can be detected per nucleus at leptonema/zygonema, a subset of which (~ 150 foci per nucleus) are processed by MSH4 and MSH5 (Cole et al. 2012). Only a small portion of these MSH4-MSH5 foci are stabilized by MLH1-MLH3 (~ 23 per nucleus), the marker for ~ 90%-95% of all CO events, while most of MSH4-MSH5 foci are repaired through NCOs pathway with a few through MLH1-independent CO pathway (Cohen et al. 2006).

CNTD1 (cyclin N-terminal domain-containing 1) is a cyclin-related protein that is highly conserved in various organisms, including *C. elegans*, mice and humans. A recent study on its *C. elegans* orthologue COSA-1 demonstrates that this protein is associated with presumptive COs,

and responsible for reinforcing the designation of meiotic CO sites (Yokoo et al. 2012). COSA-1 first appears as a diffuse signal in early pachytene stage, forms discrete foci on chromosome core from mid to late pachynema, and persists until late diplonema. The localization of the discrete COSA-1 foci during pachynema and diplonema mirrors presumptive CO sites, where CO-promoting proteins, such as MSH-5, are eventually concentrated (Yokoo et al. 2012). *cosa-1* mutants show frequent missegregation of both sex chromosomes and autosomes, producing 38% male progeny (compared with 0.2% in wild-type) and a high ratio of non-viable embryos (97%). A closer check of the mutant meiocytes displays that, while early meiotic events, such as DSB formation and synapsis, are normal in *cosa-1* mutants, cytological markers for interhomolog COs are missing, which results in unpaired chromosomes without chiasmata in diakinesis (Yokoo et al. 2012).

Consistent with the meiotic phenotype of C. elegans *cosa-1* mutants, mRNA expression data from humans and mice shows that *Cntd1* transcripts are highly enriched in testis (genome.ucsc.edu), and also detected in fetal mouse ovaries, peaking from E14 to E18, the time when the female germ cells are progressing through prophase I of meiosis (Harding et al. 2011), suggesting its possible function during mammalian meiosis.

In this study, a mouse line with a promoterless Frt-*lacZ-loxP-neo*-Frt-*loxP* cassette inserted between exon 1 and exon 2 of the *Cntd1* gene was generated using the ES cells from UC Davis KOMP (Knockout Mouse Project) Repository. We show that the disruption of *Cntd1* results in infertility in both male and female mice. The mutant males display significantly decreased testis size with no spermatids or spermatozoa, which may result from an increased level of apoptosis in late-stage spermatocytes. Adult female mutants display normal mating behavior, but no pregnancies are observed. Histological sections from the mutant females reveal gradual oocyte

depletion between 4 weeks and 8 weeks of age, reminiscent of human premature ovarian failure syndrome. Examination of meiotic progression in both *Cntd1* mutant males and females reveals that Class I COs, indicated by MLH1 and MLH3 foci, are completely missing in these mutants, coupled with significantly reduced chiasmata number. Taken together, our results suggest that CNTD1 is a key regulator for meiotic CO control in mouse germ line, and is required for gametogenesis in mice.

3. Materials and Methods

3.1 Animals and genotyping

Cntd1 mice were generated from one embryonic stem (ES) cell line obtained from UC Davis KOMP (Knockout Mouse Project) Repository, which contains a gene trap cassette (FRT-*lacZ*-*loxP*-*neo*-FRT-*loxP*) in the first intron of mouse *Cntd1* gene (EPD0190_3_E03, Cntd1$^{tm1e(KOMP)Wtsi}$). The term *Cntd1* $^{lacZ\ neo/+}$ is used to indicate that the insertion of *lacZ* gene and *loxP* flanked neomycin (neo) gene into one of the *Cntd1* alleles. A *Spo11*-Cre mouse line (Rebecca Holmes and Paula Cohen, unpublished) was crossed with *Cntd1* $^{lacZ\ neo/+}$ mice to remove *neo* cassette, which leads to the generation of *Cntd1* $^{lacZ/+}$ mice. Intercrosses of these *Cntd1* $^{lacZ/+}$ mice can give rise to *Cntd1* $^{lacZ/lacZ}$ mutants. *Cntd1* $^{lacZ\ neo/lacZ\ neo}$ and *Cntd1* $^{lacZ/lacZ}$ mice were genotyped using primers CNTD1lacZ_F 5'- CGA CTC CTG GAG CCC GTC AG-3' and CNTD1loxP_1R 5'- GCG CGC CGT TTA AAC ATA ACT- 3' to amplify the *lacZ* gene in the mutated allele, CNTD1WtF 5'- CTG ACA TTC GCT CTC GTT TCC- 3' and CNTD1WtR 5'- CGG CTG ACA AAA GGT TTG G- 3' to amplify the wild-type allele, and CNTD1neo_F 5'- TTC TTC TGA GCG GGA CTC TG- 3' and CNTD1intron_2R 5'- CTC GGC TGA CAA AAG GTT TGG- 3'to amplify the *neo* insertion.

3.2 Bioinformatic analysis

The potential functional motifs of mouse CNTD1 were predicted by NCBI protein-protein BLAST (blastp) and Ensembl database. The protein structure was predicted using I-TASSER server. I-TASSER used the structure of human cyclin B1 (PDB ID: 2jgzB) as its top template to generate protein models of mouse CNTD1. Bovine cyclin A2 (PDB ID: 3ddq) and human cyclin B1 were returned as the top 2 most structurally similar proteins to mouse CNTD1. Predicted protein structure models of mouse CNTD1 were generated using I-TASSER (Zhang 2008; Roy et al. 2010). The visualization of the protein structure was done in RasMol (Sayle and Milnerwhite 1995).

3.3 cDNA analysis of *Cntd1* transcripts

Total RNA was isolated with Trizol (Invitrogen) from adult mouse testis. Complementary DNA was generated from 3 μg of total RNA using SuperScript III First-Strand Synthesis Kit (Invitrogen) with random hexamer as primer. PCR reactions were performed using the following primers: Cntd1Ex1_2F 5'- GCC GTG GTG GAC ATT ATG- 3' and Cntd1Ex1_2R 5'- TTT CTA CAG CCT GGT AGC TCA- 3' to amplify exon 1- exon 2 region; Cntd1Ex2_6F 5'- AAT GGT GTC TGG AGA AAT CGG- 3' and Cntd1Ex2_6R 5'- TTT GGA TGA AGG CAC TCG C- 3' to amplify exon 2- exon 6 region; Cntd1Ex1_IRESF 5'- TGA CTT TCA GTT CGG AGT GG- 3' and Cntd1Ex1_IRESR 5'- CCC TTG TTG AAT ACG CTT GAG- 3' to amplify exon 1- *lacZ* region.

3.4 Western blotting

Whole testis protein lysate was prepared by sonicating the decapsulated testes of appropriate genotype in RIPA plus buffer (PBS with 1% NP40, 0.5% sodium deoxycholate, 0.1% SDS, 1 mM PMSF, 10 μg/ml aprotinin, 2 mM Sodium orthovanadate (Na_3VO_4) and 1X Complete protease inhibitor cocktail (Roche)) on ice, and then cleared by centrifuge. Protein levels were determined using Bradford protein assay. Proteins were separated on SDS-PAGE and then transferred onto a PVDF membrane (Millipore). Blots were blocked using blocking buffer containing 5% milk, and then washed in 1XTBST (1XTBS with 0.1% tween-20). Primary antibodies used were rabbit CNTD1 (Sigma-Aldrich; 1:500), rabbit β-galactosidase (Rockland Immunochemicals; 1: 3,000) and donkey actin (Santa Cruz; 1: 3000). Secondary antibodies were goat anti-rabbit or goat anti-donkey IgG-HRP (Santa Cruz; 1:3,500). The antigens were visualized using chemiluminescence (Pierce ECL Western Blotting Substrate; Thermo scientific). The chemiluminescent signals were captured by a charge-coupled device (CCD) camera placed on the top of Bio-Rad universal hood II gel imager (serial number 721BR03949).

3.5 Histology and immunohistochemistry

Testes or ovaries removed from 4 or 8 week- old mice were fixed in Bouins fixative for 6 hours at room temperature or 10% formalin overnight at 4^{o}C, and then washed in 70% ethanol. Then the tissues were embedded in paraffin and sectioned at 4 μm onto poly-lysine coated glass slides. Hematoxylin and eosin (H&E) staining was performed on Bouins-fixed sections following standard procedures. Immunohistochemistry was performed on formalin-fixed sections to detect apoptotic cells using the Apoptag Peroxidase In Situ Apoptosis Detection Kit (Millipore) (TUNEL staining), or on Bouins-fixed sections for staining of spermatogonia and early

spermatocytes using rat monoclonal hybridoma supernatant against germ cell nuclear antigen-1 (GCNA-1) (Wang and Enders 1996). Stained slides were then mounted with Permount (Fisher Chemicals) and allowed to dry for at least 2 hours before visualization.

3.6 Sperm counts

The cauda epididymides were removed from adult mice of appropriate genotype and placed in prewarmed DMEM containing 4% bovine serum albumin (Sigma-Aldrich). Each epididymis was squeezed with tweezers to extrude the sperm and then incubated at 32^{o}C/5% CO_2 for 20 minutes to allow the sperm to swim out. The sperm-containing suspension was mixed well, and 20 µl aliquot was resuspended in 480 µl 10% formalin. The density of sperm cells was counted using a hemacytometer.

3.7 Chromosome analysis and immunofluorescent staining

Chromosome preparations and immunofluorescence were performed using the techniques described previously (Peters et al. 1997; Kolas et al. 2005; Lenzi et al. 2005). Briefly, testes from adult males or fetal ovaries from 19.5 dpc embryos were kept in hypotonic extraction buffer (HEB; 30 mM Tris, pH 8.2, 50 mM sucrose, 17 mM trisodium citrate, 5 mM EDTA, 0.5 mM DTT, and 0.1 mM PMSF) on ice, for 20 minutes (for fetal ovaries) or 60 minutes (for testes). Then either one fragment of testicular tubules, or a whole ovary, were transferred to 100 mM sucrose solution and further minced before spreading on slides coated in 1% paraformaldehyde and 0.25% Triton X-100. The slides were dried slowly in a humidified chamber for 3 hours at room temperature, or overnight at 4^{o}C, and then washed in PBS containing 0.4% Photoflo before staining. The primary antibodies used were either generated in our lab, or commercially available,

or gifts from other lab (Kolas et al. 2005). They were mouse SYCP1 (1:1000), rabbit SYCP3 (1:5000), mouse SYCP3 (1:5000), CREST human autoimmune serum (1:30,000), mouse γH2AX (1:5000), rabbit RAD51 (1:300, Calbiochem), rabbit MSH5 (1:1000), monoclonal human MLH1 (1:100, BD Biosciences) and polyclonal rabbit MLH3 (1:300, (Lipkin et al. 2002)). Secondary antibodies used were goat anti-mouse Alexa Fluor 488, goat anti-rabbit Alexa Fluor 555 and goat anti-human Alexa Fluor 647 (all 1:1000, Invitrogen).

3.8 Spindle preparation of oocytes

Spindle analysis of metaphase I oocytes was done using a modification of the techniques published previously (Woods et al. 1999; Hodges et al. 2001; Kan et al. 2008). Briefly, ovaries were removed from unstimulated females at 24 days of age. Oocytes were released by puncturing ovaries with 30-gauge needles in Waymouth media (Gibco, Invitrogen) supplemented with 100 units/ml penicillin, 10 μg/ml streptomycin, 10% fetal bovine serum (Sigma-Aldrich), and 0.23 mM sodium pyruvate. Primary oocytes at the germinal vesicle stage were cultured in 20 μl drops of KSOM (Millipore, Bedford, MA) overlaid with mineral oil and incubated at 37^{o}C in an atmosphere of 5% CO_2. After 2.5 hours in culture, oocytes with germinal vesicle broken down were transferred to fresh KSOM drops. In order to observe meiotic division at metaphase I, oocytes were further cultured in KSOM for 8.5 hours, and fixed in fibrin clots. To make fibrin clots, up to 10 oocytes were transferred from KSOM to 1 μl fibrinogen solution containing 1.25% fibrinogen (Calbiochem), 154 mM NaCl, 5.63 mM KCl, and 2.25 mM $CaCl_2$ under mineral oil on microscope slides pre-coated with poly-L-lysine. Then 1.2 μl thrombin (Sigma-Aldrich) was added into the fibrinogen drop and mixed gently. The mineral oil was washed off using 2% Triton X-100 in PBS, and the slides were placed in the fixative containing 2% paraformaldehyde,

1% Triton X-100, 0.1 mM PIPES, 5 mM $MgCl_2$, and 2.5 mM EGTA for 30 minutes at 37^{o}C. Slides were washed in 0.1% normal goat serum for 15 minutes at 37^{o}C and further incubated in 10% normal goat serum for an hour at 37^{o}C before stained for β-tubulin (mouse monoclonal antibody at 1:500 dilution, Sigma-Aldrich). Tubulin was detected with goat anti-mouse Alexa Fluor 488 (1: 1000, Invitrogen), and DNA was counterstained by 4',6'-Diamidino-2-phenylindole (DAPI).

3.9 Spermatocyte metaphase preparation

The metaphase chromosome spreading was processed using the techniques described previously (Evans et al. 1964; Uroz et al. 2008), with a slight modification (Holloway et al. 2010). In brief, testes were minced in hypotonic buffer (1% sodium citrate), and incubated at room temperature for 20 minutes. After removal of large pieces of tubules, the suspension containing cells were centrifuged, and the supernatant was discarded. Cells were fixed twice: the first time in methanol/glacial acetic acid/chloroform (30:10:0.15), and the second time in methanol/glacial acetic acid (3:1). Then the cells were centrifuged again, and resuspended in methanol/glacial acetic acid (3:1). Fixed cells were dropped onto slides and dried in the air. For staining, slides were stained in Giemsa solution for 3 minutes, washed and air dried.

3.10 Image acquisition

All slides were visualized using the Zeiss Imager Z1 microscope (Carl Zeiss, Inc.) under a 5 x/ 0.15 or 20×/ 0.5 NA EC Plan-Neofluar air immersion magnifying objective lens (Carl Zeiss, Inc.), or a 63×/ 1.4 NA Plan Apochromat oil immersion differential interference contrast objective lens (Carl Zeiss, Inc.). Images were captured using a high resolution microscopy camera AxioCam

MRm (Carl Zeiss, Inc.) and processed with AxioVision software (version 4.7.2; Carl Zeiss, Inc.).

3.11 Examination of reproductive performance

Adult male or female mice of appropriate genotype aged between eight and ten weeks were caged with wild-type adult females or males for 4 consecutive nights. Mating was determined by the presence of a copulation plug the next morning. Pregnancy was confirmed either by gentle abdominal palpation after gestation day 11 or the delivery of litters.

3.12 Embryo collection and *in vitro* culture

For natural matings, adult females of appropriate genotype were mated with wild-type males. Copulation plugs were checked the following morning and fertilized oocytes were harvested from oviducts. For superovulation, 4-week-old female mice were injected (i.p.) with 5 IU PMSG followed by 5 IU hCG 48 hours later before removal of oocytes the following morning.

The fertilized oocytes were incubated in KSOM (Millipore, Bedford, MA) droplets under light mineral oil at 37^{o}C in an atmosphere of 5% CO_2/5% O_2 for up to 5 days, and developmental progression was examined.

4. Results

4.1 Generation of *Cntd1* gene targeted mice

Mouse *Cntd1* is a gene consisting of 7 exons, which encodes a 37 kDa protein (334 amino acids) (Figure 4-1A). Similar to *C. elegans* COSA-1, CNTD1 is predicted to have a cyclin-like structure with a cyclin N- terminal domain according to the analysis using Ensembl genome browser and I-TASSER protein structure prediction server (Figure 4-1 B-D).

Figure 4-1. CNTD1 is the mouse orthologue of *C. elegans* COSA-1.

(A) Mouse *Cntd1* gene has 7 exons encoding a 334 amino acid protein. Exons and introns are shown as yellow rectangles and solid lines, respectively. 3' and 5' UTRs are indicated as unfilled boxes. **(B)** As its name implies, mouse CNTD1 protein contains a Cyclin N-terminal domain. The range of the domain is indicated as red bar. **(C)** One predicted structure model of mouse CNTD1 generated by I-TASSER is shown. **(D)** Predicted structure of mouse CNTD1 (blue) is threaded with human Cyclin B1 (red) (See materials and method section 3.2).

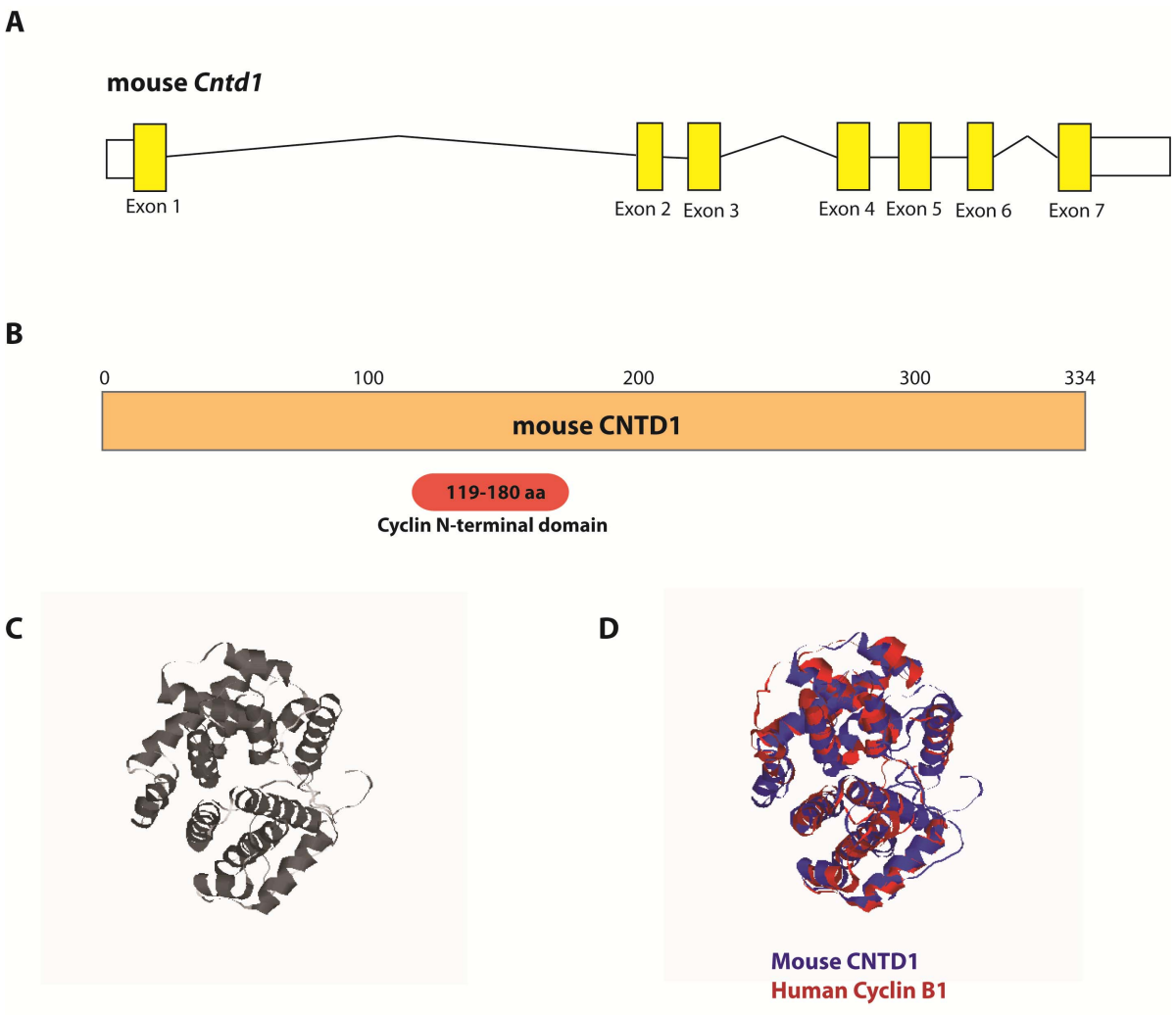

To study the function of mouse *Cntd1* during mammalian meiosis, an ES cell line with a promoterless FRT- *lacZ*-*loxP*-*neo*-FRT-*loxP* cassette inserted into intron 1 of mouse *Cntd1* was obtained from UC Davis KOMP (Knockout Mouse Project) Repository (Figure 4-2A). The targeted ES cell line was injected into blastocysts derived from C57BL/6 donors and transferred into pseudopregnant females, which yielded seven chimeric animals (F_0 generation, 5 males and 2 females). Then these chimeras were mated with wild-type animals (F_0 X WT), which generated pups of F1 generation. F1 mice either mated with *Spo11-Cre* mice to remove the neo cassette (Figure 4-2B) or with F1 mice to get F2 $^{neo+}$ mice (Figure 4-2C).

4.2 *Cntd1* gene expression is altered in *Cntd1* mutants

The cassette inserted into the targeted *Cntd1* allele is designed to act as a gene trap. It is expected that the splice acceptor sequence before *lacZ* gene will fuse exon 1 with *lacZ* during transcription and produce exon1-*lacZ* fusion protein, so that the transcription and translation of *Cntd1* gene (exon 1 through exon 7) will be aborted or reduced.

RT-PCR was used to check the transcriptional profile of *Cntd1* exons in mutant and wild-type mouse testes. Consistent with our expectation, exon1-*lacZ* fusion transcripts were only found in heterozygous and mutant *Cntd1* mice. However, transcription beyond exon 1 of *Cntd1* was still detected in *Cntd1* mutant, albeit at a lower levels (Figure 4-3). Furthermore, it was observed that exon1-exon7 transcript found in the mutant contained an additional 111 bp insert between exon 1 and exon 2, which is derived from the gene trap cassette. Since this 111 bp insert contains no stop codon, the protein product of the extended mutant transcript will have 37 extra amino acids compared to wild-type CNTD1. Collectively, two *Cntd1*-related transcripts were detected in *Cntd1* mutant mice: one is the expected exon1-*lacZ* fusion transcript, and the other is the

Figure 4-2. Generation of *Cntd1* gene targeted mice.

(A) The organization of the gene trap construct is shown. **(B,C)** The breeding strategies to produce *Cntd1* $^{lacZ/lacZ}$ (B) and *Cntd1*$^{lacZ\ neo/lacZ\ neo}$ (C) mutant mice are displayed.

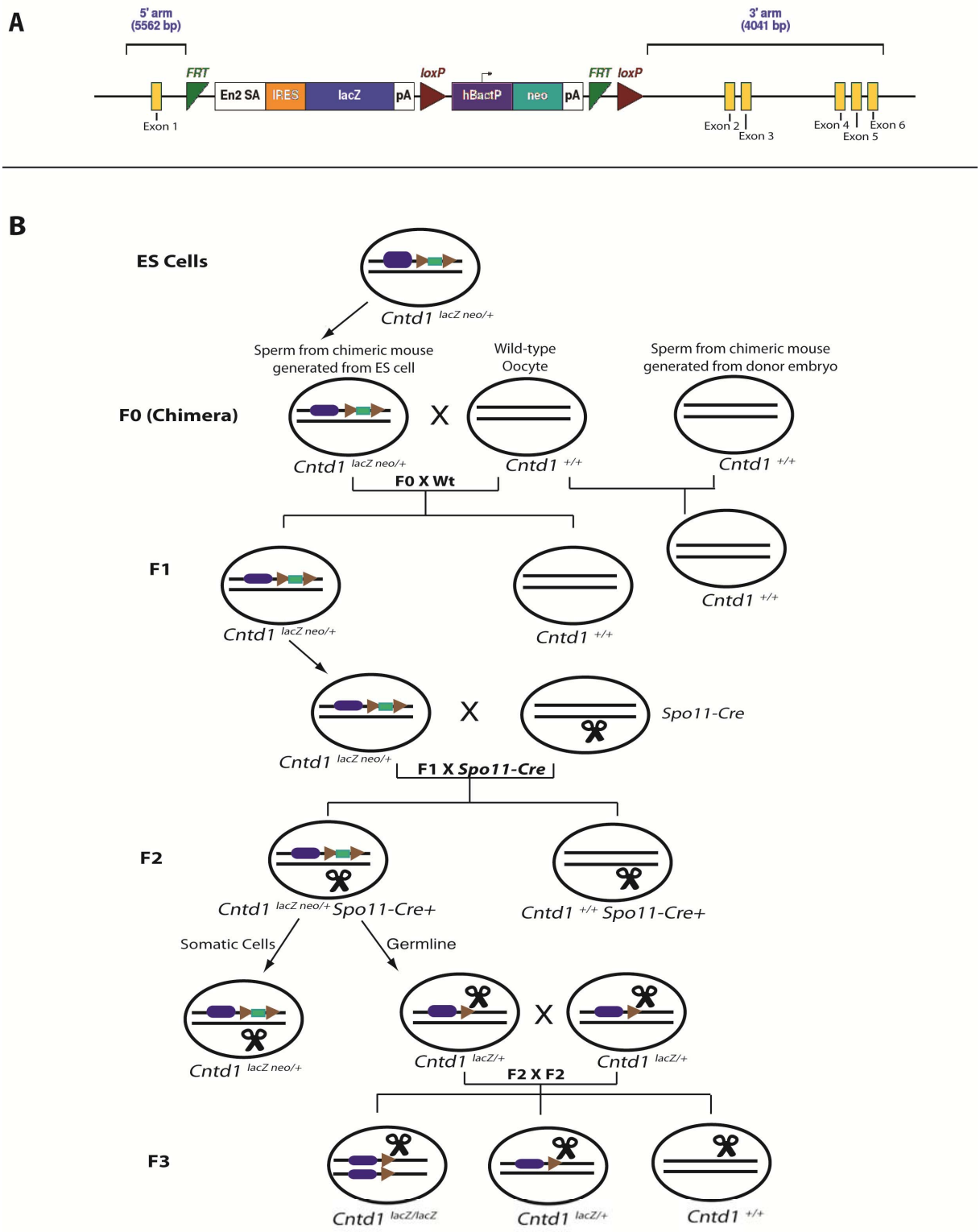
A
5' arm
(5562 bp)
3' arm
(4041 bp)
FRT
En2 SA
IRES
lacZ
pA
loxP
hBactP
neo
pA
FRT
loxP
Exon 1
Exon 2
Exon 3
Exon 4
Exon 5
Exon 6
B
ES Cells
Cntd1 lacZ neo/+
Sperm from chimeric mouse generated from ES cell
Wild-type Oocyte
Sperm from chimeric mouse generated from donor embryo
F0 (Chimera)
X
Cntd1 lacZ neo/+
Cntd1 +/+
Cntd1 +/+
F0 X Wt
F1
Cntd1 lacZ neo/+
Cntd1 +/+
Cntd1 +/+
Cntd1 lacZ neo/+
X
Spo11-Cre
F1 X Spo11-Cre
F2
Cntd1 lacZ neo/+ Spo11-Cre+
Cntd1 +/+ Spo11-Cre+
Somatic Cells
Germline
Cntd1 lacZ neo/+
Cntd1 lacZ/+
X
Cntd1 lacZ/+
F2 X F2
F3
Cntd1 lacZ/lacZ
Cntd1 lacZ/+
Cntd1 +/+

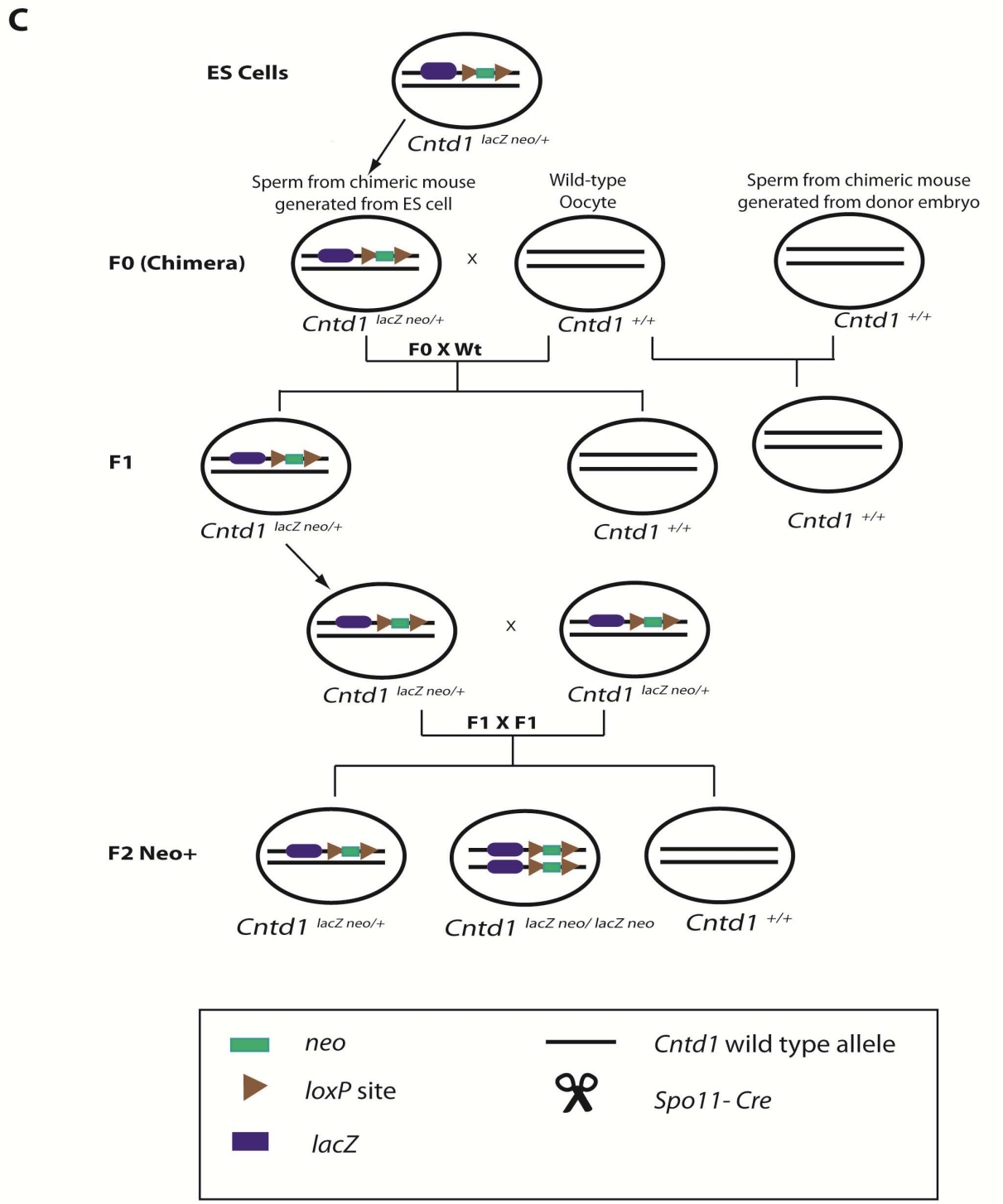
C
ES Cells
Cntd1 lacZ neo/+
Sperm from chimeric mouse generated from ES cell
Wild-type Oocyte
Sperm from chimeric mouse generated from donor embryo
F0 (Chimera)
x
Cntd1 lacZ neo/+
Cntd1 +/+
Cntd1 +/+
F0 X Wt
F1
Cntd1 lacZ neo/+
Cntd1 +/+
Cntd1 +/+
x
Cntd1 lacZ neo/+
Cntd1 lacZ neo/+
F1 X F1
F2 Neo+
Cntd1 lacZ neo/+
Cntd1 lacZ neo/ lacZ neo
Cntd1 +/+
neo
loxP site
lacZ
Cntd1 wild type allele
Spo11- Cre

Figure 4-3. cDNA analysis of *Cntd1* gene targeted mice.

(A, B) *Cntd1* transcripts from *Cntd1 neo+* and *Cntd1 neo-* gene targeted mice were analyzed using RT-PCR. PCR primers were designed to detect the transcription of the exons of *Cntd1* and the sequences from the gene trap cassette. The positions of each set of primers are indicated in (A). Different colors represent different RT-PCR products (F; forward primer, R; reverse primer). Blue arrows in (B) indicate the position of 1 kb standard band. **(C)** *Cntd1* transcripts detected in wild-type, heterozygous ($Cntd1^{lacZ\ neo/+}$ and $Cntd1^{lacZ/+}$), mutant ($Cntd1^{lacZ\ neo/lacZ\ neo}$ and $Cntd1^{lacZ/lacZ}$) mouse testis by RT-PCR analysis are illustrated.

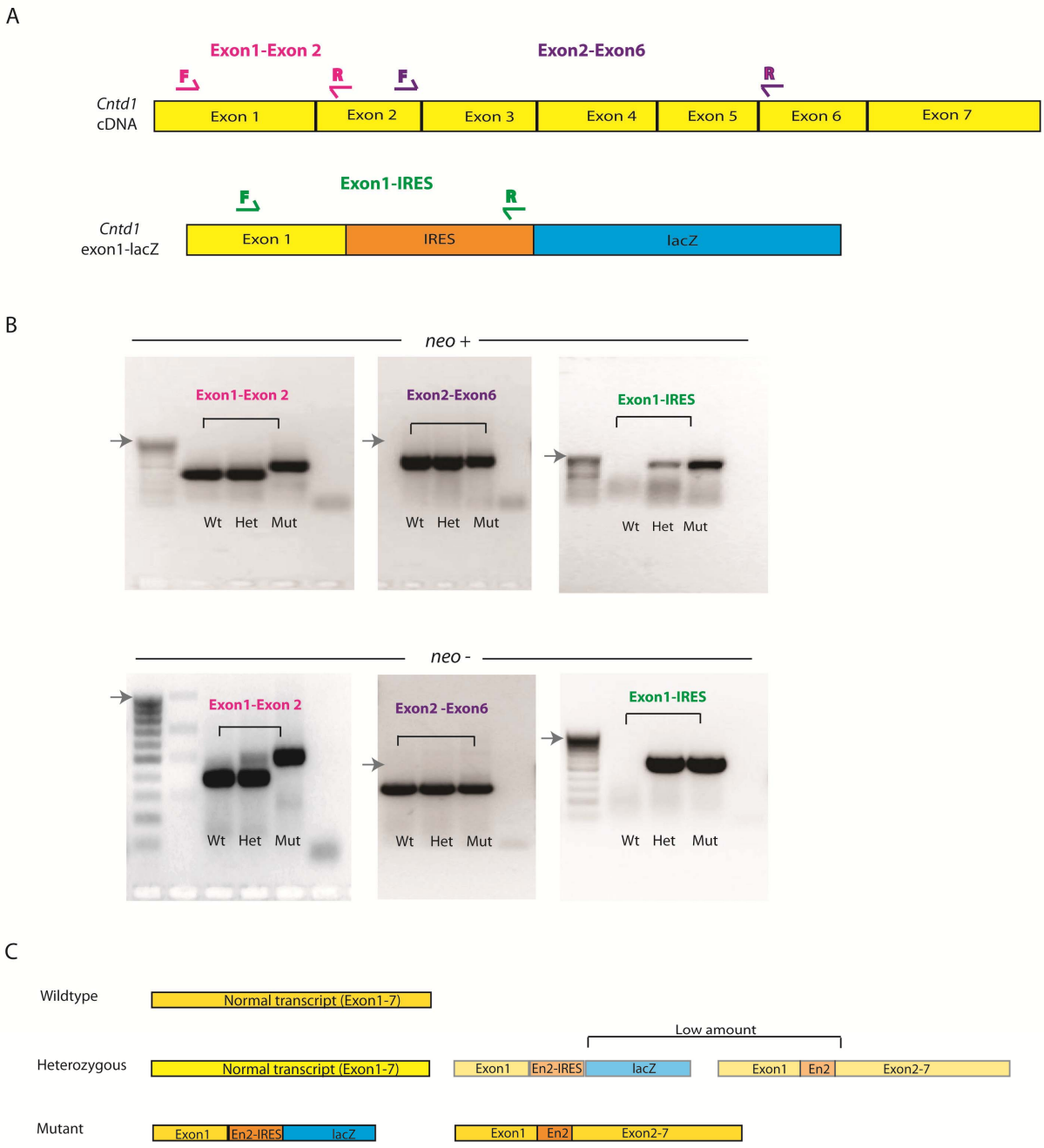
A
Exon1-Exon 2
Exon2-Exon6
F
R
F
R
Cntd1
cDNA
Exon 1
Exon 2
Exon 3
Exon 4
Exon 5
Exon 6
Exon 7
Exon1-IRES
F
R
Cntd1
exon1-lacZ
Exon 1
IRES
lacZ
B
neo +
Exon1-Exon 2
Exon2-Exon6
Exon1-IRES
Wt Het Mut
Wt Het Mut
Wt Het Mut
neo -
Exon1-Exon 2
Exon2 -Exon6
Exon1-IRES
Wt Het Mut
Wt Het Mut
Wt Het Mut
C
Wildtype
Normal transcript (Exon1-7)
Low amount
Heterozygous
Normal transcript (Exon1-7)
Exon1
En2-IRES
lacZ
Exon1
En2
Exon2-7
Mutant
Exon1
En2-IRES
lacZ
Exon1
En2
Exon2-7

extended exon 1-exon 7 transcript with 111 bp extra insertion. Although the latter one may not be translated into a fully functional CNTD1 protein, it may still become our big concern if this extended transcript can be translated into stable proteins and expressed at a comparable level to wild-type *Cntd1*. Thus, it became critical to examine the CNTD1 protein levels in these mice.

To explore the status of CNTD1 protein in the wild-type, heterozygous, and mutant testes, western blotting was performed using whole testis protein lysates (Figure 4-4). An antibody raised against the C-terminus of mouse CNTD1 was utilized (Sigma-Aldrich). In the wild-type testis lysate, this antibody recognized CNTD1 protein at 37 kDa. It was found that CNTD1 protein level was similar in testis lysate from wild-type and heterozygous mice ($Cntd1^{lacZ\ neo/+}$ and $Cntd1^{lacZ/+}$), while the expression of *Cntd1* was greatly reduced in homozygous mutants ($Cntd1^{lacZ\ neo/lacZ\ neo}$ and $Cntd1^{lacZ/lacZ}$). Furthermore, the size of the weak band in the lane containing testis lysate from the mutant is at 37 kDa, the same as the wild-type CNTD1. If the extended exon1-exon7 transcript with 111 bp insertion, as detected by RT-PCR, was translated into a mature protein in *Cntd1* mutant mice, the size of this protein should be at 41 kDa. But we failed to detect the 4 kDa shift in the mutant lane. One possibility is that the protein product of this extended transcript is not stable and the presence of a weak 37 kDa protein band in *Cntd1* mutant testis sample represents another variation of *Cntd1* transcript gene in the mutant testis, which is a wild-type *Cntd1* transcript(exon1 through exon 7 with no insertion). This transcript may have been produced due to certain leakiness of the gene trap cassette. But the level of this wild-type *Cntd1* transcript must be very low in homozygous mutant animals compared with the extended exon1-exon7 transcript, and RT-PCR failed to pick it up as PCR template. Alternatively, this extended transcript could be stable but the 111 bp insert gets excised during splicing for some reason, which could also result in a 37 kDa protein. As expected, testis lysates from *Cntd1*

Figure 4-4. CNTD1 protein level is significantly reduced in *Cntd1* mutant mice.

Western blot analysis of whole testis protein lysates from *Cntd1* wild-type (lane 1, 4), heterozygous (*Cntd1*$^{lacZ/+}$ in lane 2, *Cntd1*$^{lacZ\ neo/+}$ in lane 5) and mutant (*Cntd1*$^{lacZ/lacZ}$ in lane 3, *Cntd1*$^{lacZ\ neo/lacZ\ neo}$ in lane 6) mice using antibodies against CNTD1, β-galactosidase and actin (protein control) is shown.

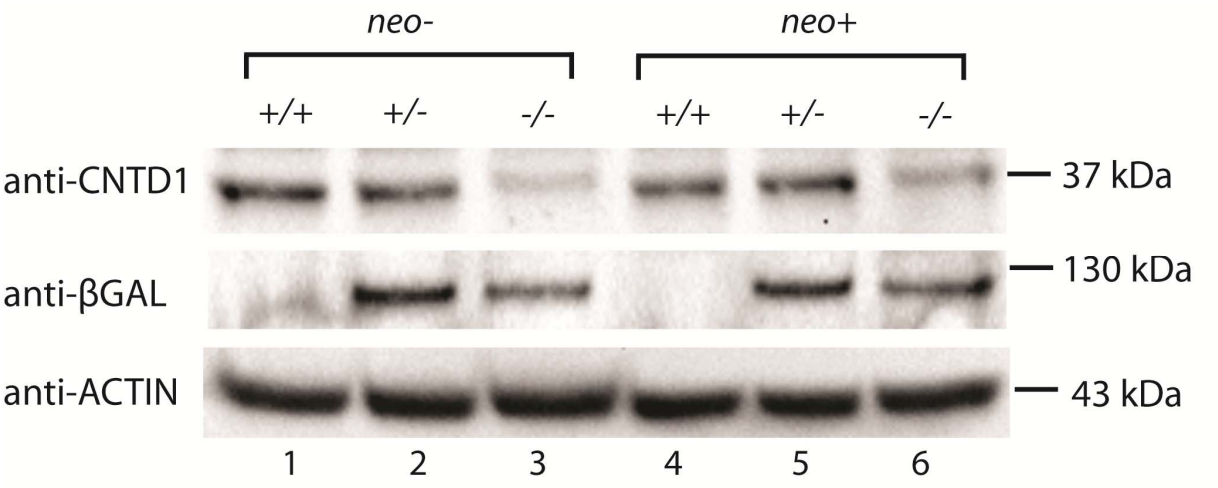

heterozygous (*Cntd1*$^{lacZ\ neo/+}$ and *Cntd1*$^{lacZ/+}$) and homozygous mutants (*Cntd1*$^{lacZ\ neo/lacZ\ neo}$ and *Cntd1*$^{lacZ/lacZ}$) displayed positive staining for β-galactosidase while no β-galactosidase bands were detected in wild-type mouse testes.

Taken together, the RT-PCR and western blotting data show that the expression of CNTD1 is dramatically reduced in *Cntd1* mutant mice. The *lacZ* gene is also transcribed and expressed, either as exon 1-lacZ fusion or as a distinct protein, in heterozygous and homozygous mutant

animals.

4.3 *Cntd1* mutant animals are viable but sterile

Cntd1 mutant mice are viable and appear to develop normally into adulthood. The body weight of homozygous mutants is comparable to their wild-type littermates at all ages studied. Adult mutant animals were able to mate normally with wild-type mice, and firm copulation plugs were found the following morning. However, no pregnancies were found either in *Cntd1* mutant females after mating with wild-type males or in wild-type females after mating with *Cntd1* mutant males, indicating that *Cntd1* mutant animals are sterile. To determine the cause of infertility, *Cntd1* mutant males and females were euthanized at 4 weeks and 8 weeks of age, and the reproductive organs were examined.

Both $Cntd1^{lacZ\ neo/lacZ\ neo}$ and $Cntd1^{lacZ/lacZ}$ adult males displayed significantly decreased testicular size compared with wild-type or heterozygous littermates (Figure 4-5 A-C; two-tailed *t* test for C $p<0.0001$). The testis weight to body weight ratio in mutant mice is only one-third of the ratio found in wild-type or heterozygous littermates. The reduction of testicular size in *Cntd1* mutant mice is already evident in their juvenile stage (Figure 4-5 A). At 4 weeks, the testes to body weight ratio in mutant mice is about 50% of wild-type level. Furthermore, sperm counts using cauda epididymal extrusion revealed no spermatozoa present in *Cntd1* mutants, while wild-type and heterozygous males contained similar numbers of sperm ($1.76 \times 10^7 \pm 1.4 \times 10^6$ and $1.52 \times 10^7 \pm 1.1 \times 10^6$ sperm per mouse; two-tailed *t* test $p=0.21$) (Figure 4-5 D). Consistent with this, H& E staining of testis sections from wild-types and *Cntd1* mutants at 4 weeks and 8 weeks of age showed that, instead of spermatozoa as seen in wild-type mice, the center of the seminiferous tubule lumen of $Cntd1^{lacZ\ neo/lacZ\ neo}$ mutants was filled with vacuoles (Figure 4-6 A, B, G, H).

Figure 4-5. *Cntd1* mutant males have decreased testicular size with no epididymal sperm.

(A) The reduction in testicular size is already detectable in testes from 4-week-old *Cntd1*$^{lacZ/lacZ}$ mutant mice compared with wild-type littermates. **(B)** Testes from 8-week-old *Cntd1*$^{lacZ/lacZ}$ mice are significantly reduced in size compared with wild-type and heterozygous littermates. **(C)** The ratio of testicle weight to body weight was calculated for 4-week-old and 8-week-old wild-type (white), heterozygous (vertical stripe) and mutant (horizontal stripe for *neo*+; grey for *neo*-) *Cntd1* mice. **(D)** Epididymal sperm numbers were counted for wild-type, heterozygous (*Cntd1*$^{lacZ\ neo/+}$), and mutant *Cntd1* mice (*Cntd1*$^{lacZ\ neo/lacZ\ neo}$ and *Cntd1*$^{lacZ/lacZ}$).

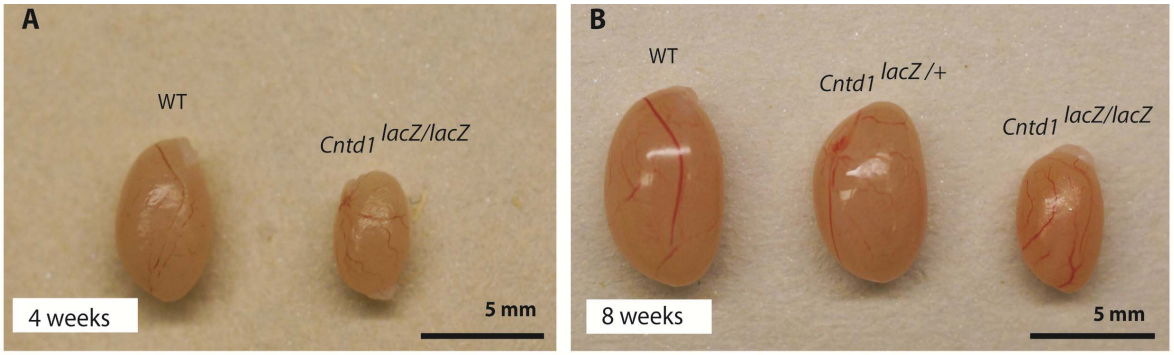
A
WT
Cntd1 lacZ/lacZ
4 weeks
5 mm
B
WT
Cntd1 lacZ /+
Cntd1 lacZ/lacZ
8 weeks
5 mm

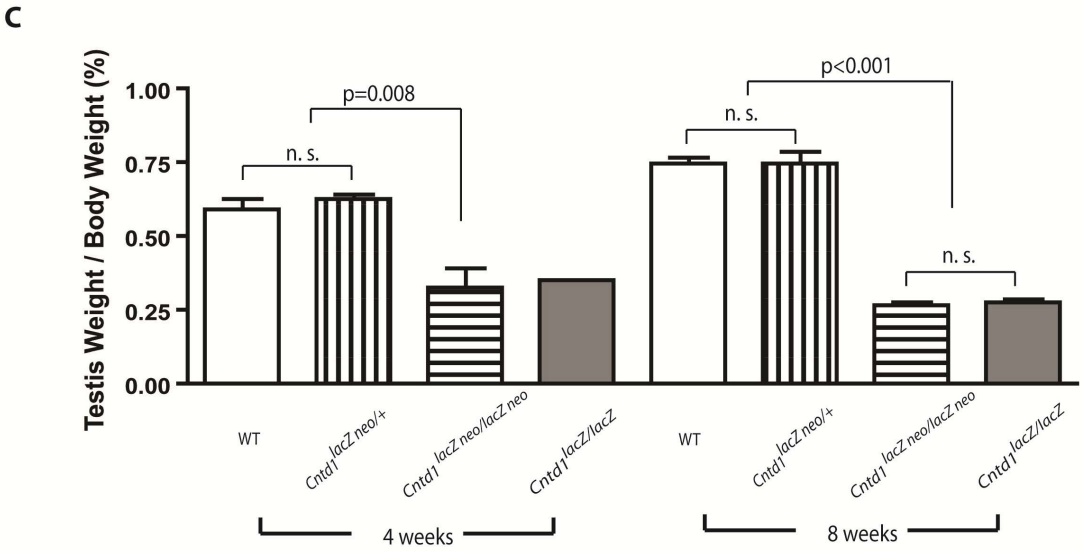
C
Testis Weight / Body Weight (%)
1.00
0.75
0.50
0.25
0.00
p=0.008
n. s.
p<0.001
n. s.
n. s.
WT
Cntd1 lacZ neo/+
Cntd1 lacZ neo/lacZ neo
Cntd1 lacZ/lacZ
WT
Cntd1 lacZ neo/+
Cntd1 lacZ neo/lacZ neo
Cntd1 lacZ/lacZ
4 weeks
8 weeks

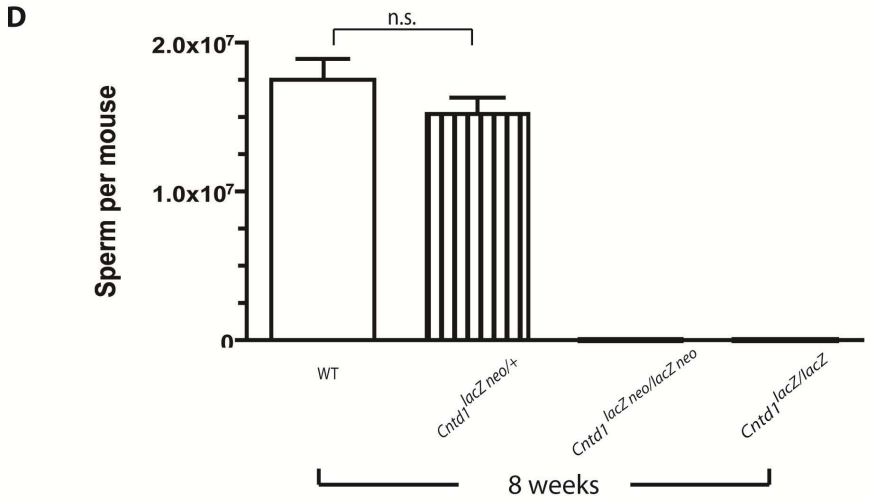
D
Sperm per mouse
2.0x10⁷
1.0x10⁷
0
n.s.
WT
Cntd1 lacZ neo/+
Cntd1 lacZ neo/lacZ neo
Cntd1 lacZ/lacZ
8 weeks

Figure 4-6. *Cntd1* mutant males demonstrate increased apoptosis in testes.

(A-F) Testis sections from 4-week-old wild-type (A, C, E), or *Cntd1*$^{lacZ\ neo/lacZ\ neo}$ mutant mice (B, D, F) were stained with either H&E (A, B) or an antibody against GCNA-1 (C,D; brown), or TUNEL (E, F; brown). **(G-L)** Testis sections from 8-week old wild-type (G, I, K), or *Cntd1*$^{lacZ\ neo/lacZ\ neo}$ mutant mice (H, J, L) were stained with either H&E (G, H) or an antibody against GCNA-1 (I, J; brown), or TUNEL (K, L; brown). While the level of GCNA-1 staining is comparable between wild-type and mutant mice, apoptosis is increased in both 4-week and 8-week old *Cntd1*$^{lacZ\ neo/lacZ\ neo}$ mutants. The apoptotic cells are indicated by dark grey (E, K) and red (F, L) arrows. Scale bar is 50 μm.

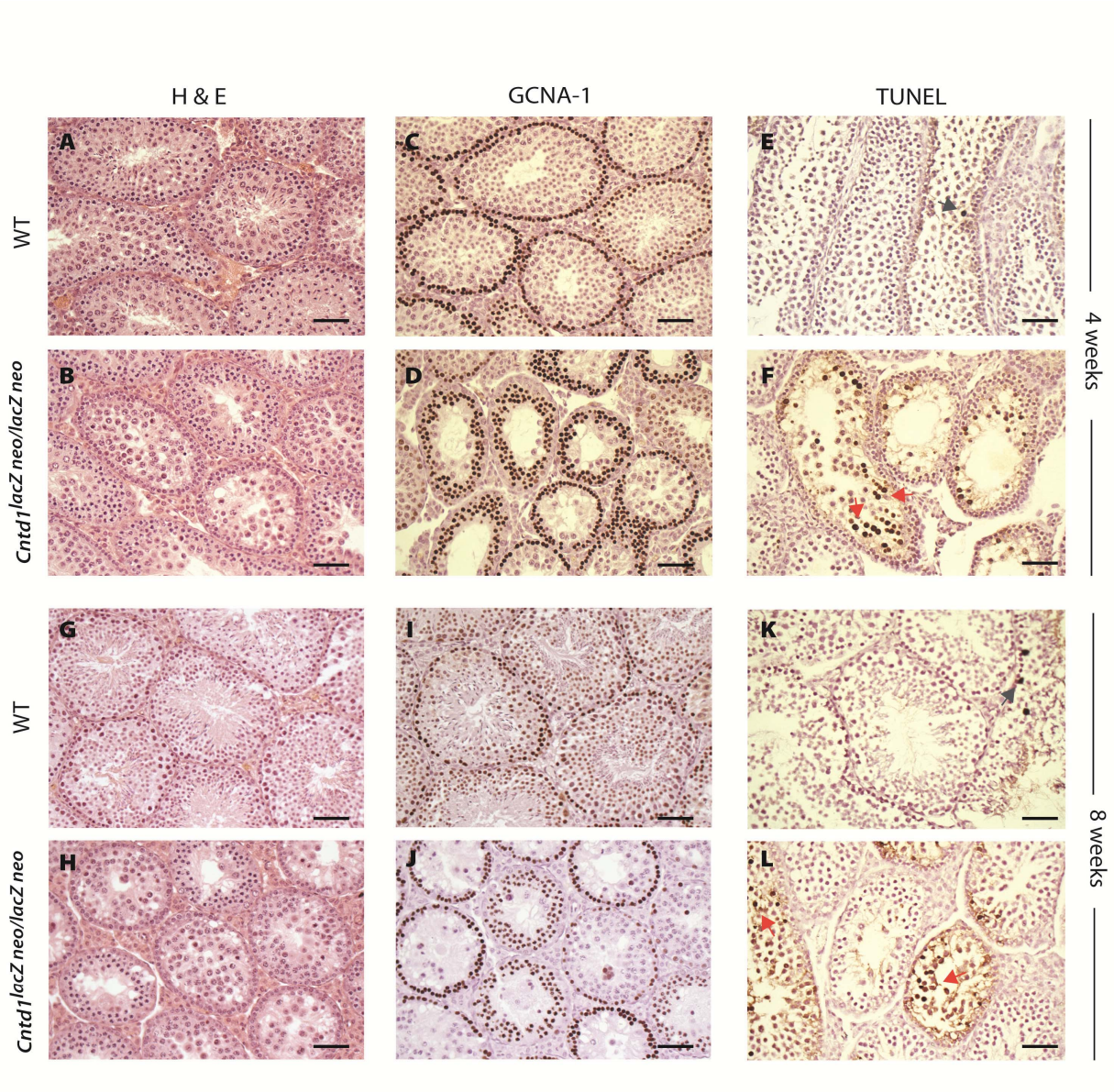
H & E
GCNA-1
TUNEL
WT
Cntd1lacZ neo/lacZ neo
WT
Cntd1lacZ neo/lacZ neo
A
B
C
D
E
F
G
H
I
J
K
L
4 weeks
8 weeks

While the populations of spermatogonia and early spermatocytes were not affected in mutants, as indicated by GCNA-1 staining (Figure 4-6 C, D, I, J), increased TUNEL labeling of apoptotic cells was detected in the testis sections of *Cntd1*$^{lacZ\ neo/lacZ\ neo}$ mice compared with wild-type mice (Figure 4-6 E, F, K, L). The majority of these TUNEL labeled cells were localized close to the center region of the lumen (See red arrows in Figure 4-6 F, L), suggesting that these cells were undergoing apoptosis at around the end of meiosis I. These results demonstrate loss of post-prophase I germ cell population in *Cntd1* mutant animals, which implies possible meiotic defects in these mutant males.

In *Cntd1* mutant females, hematoxylin and eosin (H&E) staining of ovary sections from wild-type, *Cntd1*$^{lacZ/+}$, and *Cntd1*$^{lacZ/lacZ}$ mice at 4 weeks of age displayed similar ovarian morphology with comparable numbers of developing follicles (Figure 4-7 A-F, arrowheads). However, at 8 weeks of age, while ovary sections from wild-type and *Cntd1*$^{lacZ\ neo/+}$ females contained follicles at all developmental stages, ovaries from *Cntd1*$^{lacZ/lacZ}$ mice appeared rudimentary with few or no follicles or oocytes (Figure 4-7 G-L). These data indicate that oocytes from *Cntd1* mutant females are able to reach dictyate arrest, but most of them are eliminated over time in the ovary with almost no oocytes left by adulthood.

Figure 4-7. Ovaries from *Cntd1* mutant females become depleted of oocytes or follicles over time.

(A-F) H&E staining of ovary sections from 4-week-old wild-type (A, B), *Cntd1*$^{lacZ/+}$ (C, D), and *Cntd1*$^{lacZ/lacZ}$ mutant (E, F) mice is shown. Overall ovarian morphology is shown at 5X (A, C, E). Developing follicles are shown at higher magnification (20X) (B, D, F). **(G-L)** H&E staining of ovary sections from 8-week-old wild-type (G, H), *Cntd1* heterozygous (*Cntd1*$^{lacZ\ neo/+}$) (I, J), and homozygous mutant (*Cntd1*$^{lacZ/lacZ}$) (K, L) mice are shown. Overall ovarian morphology is shown at 5X (G, I, K). Developing follicles are shown at 20X (H, J, L). Primary follicles; green arrowheads, early secondary follicles; blue arrowheads, late secondary follicles; orange arrowheads, antral follicles; red arrowheads. Scale bar is 100 μm.

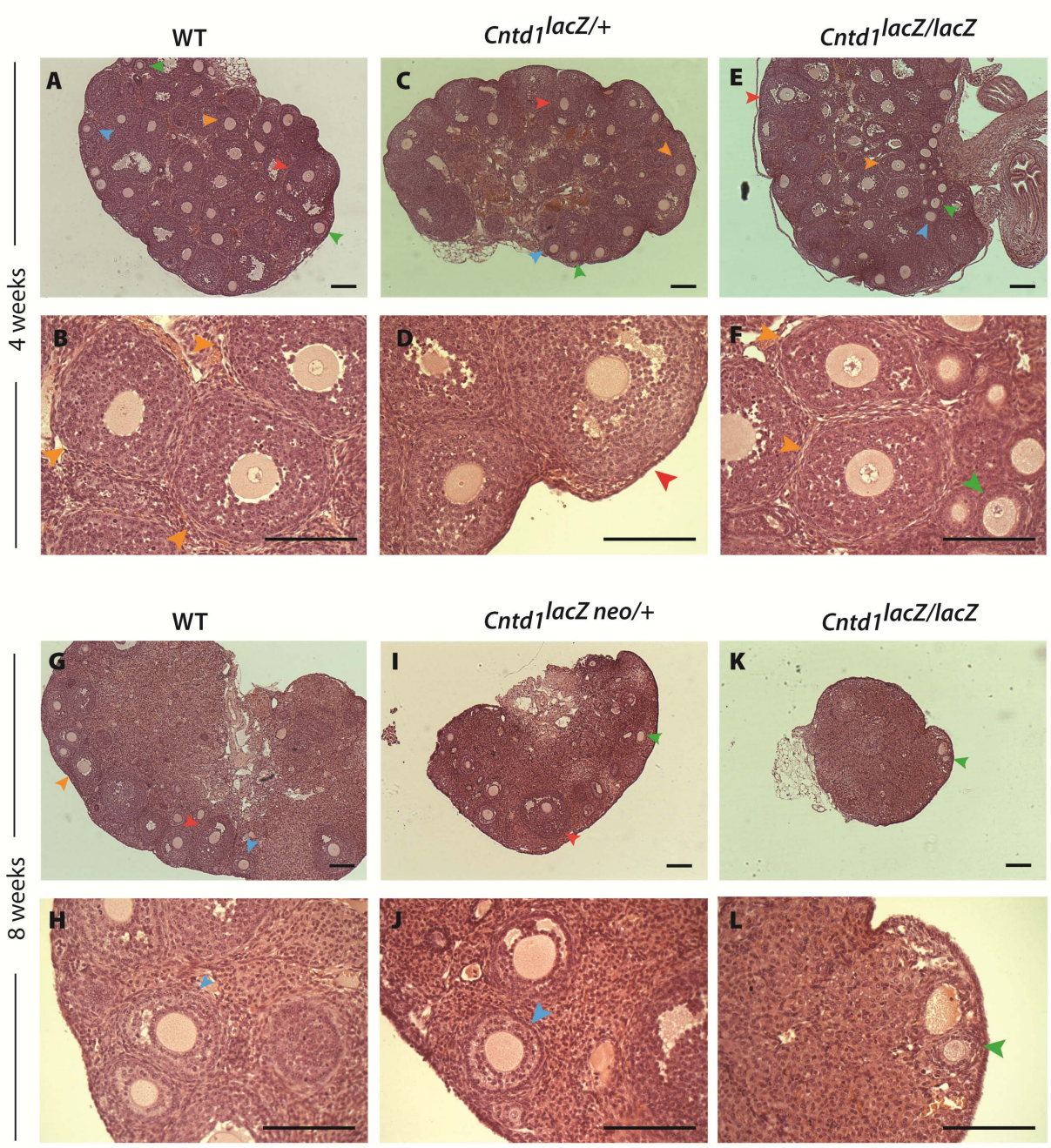
WT
Cntd1lacZ/+
Cntd1lacZ/lacZ
4 weeks
A
B
C
D
E
F
WT
Cntd1lacZ neo/+
Cntd1lacZ/lacZ
8 weeks
G
H
I
J
K
L

4.4 Class I CO markers are undetectable in immunofluorescent staining of *Cntd1* mutant meiocytes during pachynema

To better examine the degree of meiotic progression in *Cntd1* mutant animals, chromosome spreads were made from adult spermatocytes and oocytes from 19 dpc embryos. Prophase I progression in *Cntd1* mutant animals was checked by immunostaining chromosome spreads for SYCP3 and SYCP1, the components of the axial/lateral elements and transverse filaments of the synaptonemal complex (SC). Meiocytes of various meiotic stages, from leptonema to diplonema, were observed in the mutants. No significant difference was observed for the percentages of meiocytes from different substages between wild-type and mutant animals. To check for repair of the DSB, which begins in the leptotene stage of meiosis, the chromosome spreads were stained with antibodies against SYCP3 and γH2AX. As a marker of genomic damage, γH2AX signal peaks in leptotene and zygotene meiocytes (Mahadevaiah et al. 2001), and then decreases in pachynema. In both wild-type and *Cntd1* mutants, it was observed that, by mid-pachynema, γH2AX localization was restricted to sex body in spermatocytes while only background staining can be seen in oocytes (Figure 4-8 A, B and 4-9 A, B). The progression of DSB repair is also assessed by RAD51, a marker for early recombination process (Hunter and Kleckner 2001). RAD51 foci first appear in leptonema, and the number of foci declines to one or less focus per chromosome by late pachynema, when paired homologous chromosomes are fully synapsed (Moens et al. 1997). In *Cntd1* mutant meiocytes, RAD51 signal demonstrated similar dynamics as seen in wild-type (Figure 4-8 C, D and 4-9 C, D), which confirms that early steps in meiotic DSB repair are normal in *Cntd1* mutants. The synapsis of homologous chromosomes was also intact in the mutants, as illustrated by the nicely merged SYCP1 and SYCP3 signals during pachynema (Figure 4-8 E, F and 4-9 E, F).

Then the formation of meiotic recombination intermediates was examined, using antibodies against MSH5 (Figure 4- 8 G, H and 4-9 G, H), MLH1 (Figure 4-8 I, J and 4-9 I, J), and MLH3 (Figure 4-8 K, L). In wild-type meiocytes, MSH5 loads onto meiotic chromosomes from zygonema (Figure 4-8 G, 4-9 G), and a subset of these foci are believed to be stabilized by MLH1-MLH3, which appears on chromosome core from early pachynema (Kolas et al. 2005) (Figure 4-8 I, K and 4-9 I). MLH1 and MLH3 are associated with late recombination nodules and believed to mark the sites for meiotic crossovers (COs) generated from Class I CO pathway (Marcon and Moens 2003; Kolas et al. 2005). Meiocytes from wild-type and *Cntd1* mutants accumulated MSH5 foci at similar frequency during early pachynema (Figure 4-8 G, H and 4-9 G, H), suggesting the formation of intermediate recombination nodule is normal in mutants. However, no MLH1 or MLH3 foci were found on pachytene chromosomes of *Cntd1* mutants, while each wild-type pachytene meiocyte had at least one MLH1/MLH3 focus per chromosome (Figure 4-8 I-N and 4-9 I-J). These results indicate that, although pairing, synapsis and early steps of DSB repair are normal in *Cntd1* mutants, meiotic recombination through Class I CO pathway is disrupted.

Figure 4-8. Early meiotic events in *Cntd1* mutant spermatocytes are normal, but Class I CO markers are missing during pachynema.

(A, B) Meiotic chromosome spreads from wild-type (A) and *Cntd1*$^{lacZ/lacZ}$ mutant (B) spermatocytes were stained with antibodies against SYCP3 (red) and γH2AX (green). **(C, D)** Meiotic chromosome spreads from wild-type (C) and *Cntd1*$^{lacZ/lacZ}$ mutant (D) spermatocytes were stained with antibodies against SYCP3 (green), RAD51 (red), and CREST (blue). **(E, F)** Meiotic chromosome spreads from wild-type (E) and *Cntd1*$^{lacZ/lacZ}$ mutant (F) spermatocytes were stained with antibodies against SYCP3 (green), SYCP1 (red), and CREST (blue). **(G, H)** Meiotic chromosome spreads from wild-type (G) and *Cntd1*$^{lacZ/lacZ}$ mutant (H) spermatocytes were stained with antibodies against SYCP3 (green), MSH5 (red), and CREST (blue). **(I, J)** Meiotic chromosome spreads from wild-type (I) and *Cntd1*$^{lacZ/lacZ}$ mutant (J) spermatocytes were stained with antibodies against SYCP3 (red), and MLH1 (green). **(K, L)** Meiotic chromosome spreads from wild-type (K) and *Cntd1*$^{lacZ/lacZ}$ mutant (L) spermatocytes were stained with antibodies against SYCP3 (green), MLH3 (red), and CREST (blue). **(M)** MLH1 focus counts per cell in wild-type (black square) and *Cntd1* homozygous mutants (dots around baseline) are shown. **(N)** MLH3 focus counts per cell in wild-type (black square) and *Cntd1* homozygous mutants (dots around baseline) are shown.

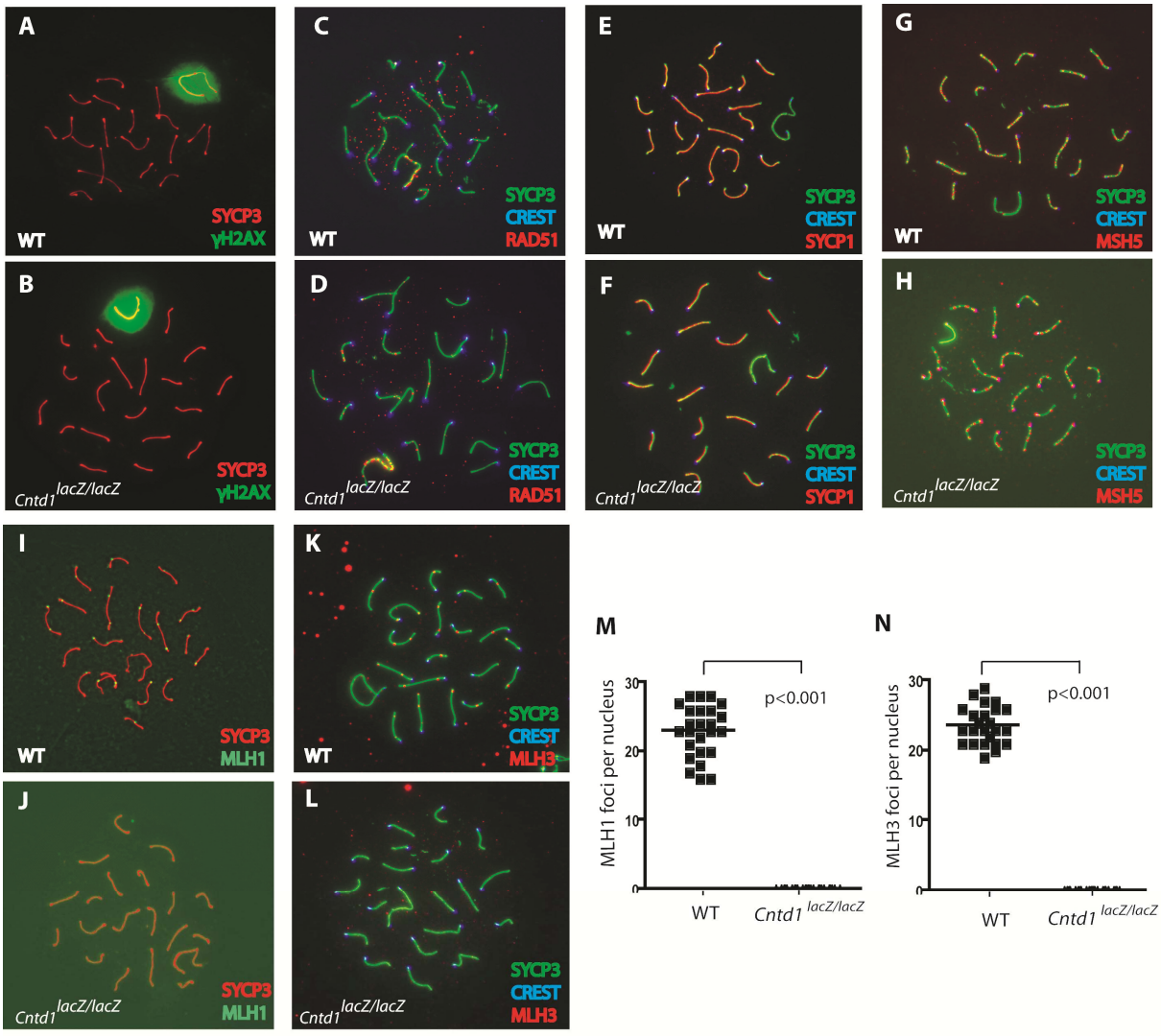
A
WT
SYCP3
γH2AX
B
Cntd1lacZ/lacZ
SYCP3
γH2AX
C
WT
SYCP3
CREST
RAD51
D
Cntd1lacZ/lacZ
SYCP3
CREST
RAD51
E
WT
SYCP3
CREST
SYCP1
F
Cntd1lacZ/lacZ
SYCP3
CREST
SYCP1
G
WT
SYCP3
CREST
MSH5
H
Cntd1lacZ/lacZ
SYCP3
CREST
MSH5
I
WT
SYCP3
MLH1
J
Cntd1lacZ/lacZ
SYCP3
MLH1
K
WT
SYCP3
CREST
MLH3
L
Cntd1lacZ/lacZ
SYCP3
CREST
MLH3
M
MLH1 foci per nucleus
30
20
10
0
p<0.001
WT
Cntd1lacZ/lacZ
N
MLH3 foci per nucleus
30
20
10
0
p<0.001
WT
Cntd1lacZ/lacZ

Figure 4-9. Early meiotic events in *Cntd1* mutant oocytes are normal, but Class I CO marker is missing during pachynema.

(A, B) Meiotic chromosome spreads from wild-type (A) and *Cntd1*$^{lacZ/lacZ}$ mutant (B) oocytes were stained with antibodies against SYCP3 (red) and γH2AX (green). **(C, D)** Meiotic chromosome spreads from wild-type (C) and *Cntd1*$^{lacZ/lacZ}$ mutant (D) oocytes were stained with antibodies against SYCP3 (green), RAD51 (red), and CREST (blue). **(E, F)** Meiotic chromosome spreads from wild-type (E) and *Cntd1*$^{lacZ/lacZ}$ mutant (F) oocytes were stained with antibodies against SYCP3 (green), SYCP1 (red), and CREST (blue). **(G, H)** Meiotic chromosome spreads from wild-type (G) and *Cntd1*$^{lacZ/lacZ}$ mutant (H) oocytes were stained with antibodies against SYCP3 (green), MSH5 (red), and CREST (blue). **(I, J)** Meiotic chromosome spreads from wild-type (I) and *Cntd1*$^{lacZ/lacZ}$ mutant (J) oocytes were stained with antibodies against SYCP3 (red), and MLH1 (green).

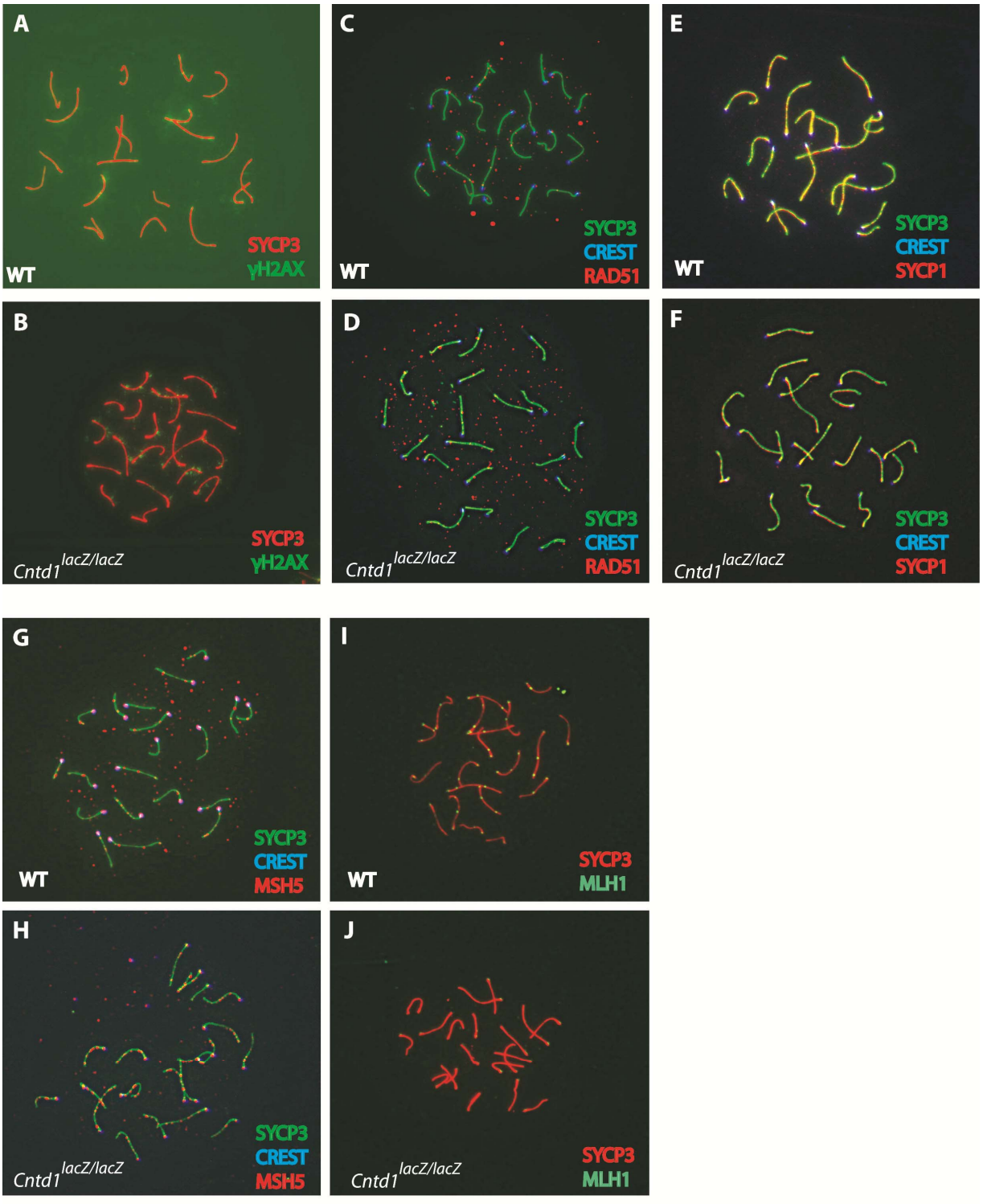
A
WT
SYCP3
γH2AX
C
WT
SYCP3
CREST
RAD51
E
WT
SYCP3
CREST
SYCP1
B
Cntd1lacZ/lacZ
SYCP3
γH2AX
D
Cntd1lacZ/lacZ
SYCP3
CREST
RAD51
F
Cntd1lacZ/lacZ
SYCP3
CREST
SYCP1
G
WT
SYCP3
CREST
MSH5
I
WT
SYCP3
MLH1
H
Cntd1lacZ/lacZ
SYCP3
CREST
MSH5
J
Cntd1lacZ/lacZ
SYCP3
MLH1

Figure 4-10. CNTD1 protein level is reduced only in mutants with defective Class I CO pathway.

Western blot analysis of whole testis protein lysates from wild-type (lane 1), *Cntd1*$^{lacZ/+}$ (lane 2), *Cntd1*$^{lacZ/lacZ}$ (land 3), *Msh4*$^{-/-}$ (land 4), *Mlh1*$^{-/-}$ (lane 5), and *Mus81*$^{-/-}$ (lane 6) mice using antibodies against CNTD1 and Actin (protein control) is shown.

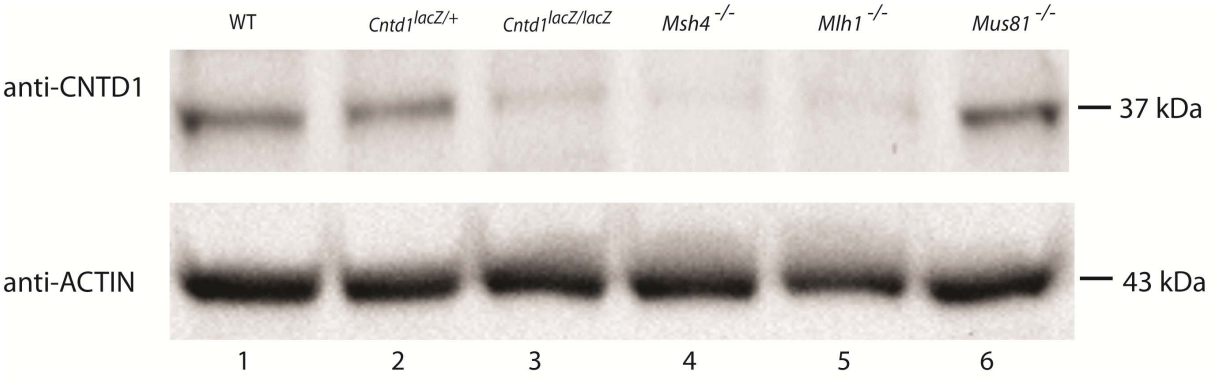

While the failure of the anti-CNTD1 antibody on chromosome spreads precluded our analysis of the distribution of CNTD1 during prophase I in wild-type and Class I CO-defective mutants, we were able to study the impact of these various mutations on the overall amount of CNTD1 protein in the testis by western blotting. As expected, in the absence of MLH1, CNTD1 protein level was severely reduced to the level close to that seen in *Cntd1* homozygous mutants (Figure 4-10 lane 5). However, when Class II CO pathway was disrupted due to the knockout of *Mus81*, CNTD1 level was not affected (Figure 4-10 lane 6). The band for CNTD1 is also missing from

the lane containing *Msh4* mutant protein extract. Since *Msh4* mutant meiocytes fail to go beyond pachynema, the absence of CNTD1 in *Msh4* mutant could be due to the absence of cell population of specific meiotic stage when, it is presumed, *Cntd1* is abundantly expressed (Figure 4-10 lane 4). To test this possibility, the localization of CNTD1 during prophase I needs to be determined by western blotting using purified germ cells of various meiotic stages.

4.5 *Cntd1* mutants fail to establish/maintain chiasmate pairing and demonstrate severe defects in chromosome segregation during metaphase I

To examine the impact of loss of *Cntd1* on the post-prophase I progression, air-dried diakinesis chromosome spreads were performed on wild-type, *Cntd1* heterozygous and homozygous mutant germ cells and stained with Giemsa. In wild-type and heterozygous spermatocytes, paired homologous chromosomes were found to separate from each other during diplonema, and by diakinesis, homologous chromosomes were associated only at sites of chiasmata (Figure 4-11 A-D arrows). By contrast, the formation of chiasmata was significantly impaired in $Cntd1^{lacZ\ neo/lacZ\ neo}$ and $Cntd1^{lacZ/lacZ}$ mutant spermatocytes, producing mostly univalent, with only a few residual bivalent chromosomes (25.62±0.32 in wild type vs. 4.35±0.23 in *Cntd1* mutants, $p<0.0001$, two-tailed *t* test) (arrow heads in Figure 4-11 E and F). Similar observations were also made in $Mlh1^{-/-}$ spermatocytes (Figure 4-11 G) (Kolas et al. 2005), although even fewer chiasmata remain in the absence of MLH1 (4.35 ± 0.23 in *Cntd1* mutants vs 2.04± 0.16 in *Mlh1* mutants, $p< 0.0001$, two-tailed *t* test). It is not clear whether this difference in residual chiasmata number is due to the different backgrounds of these two strains, or whether the loss of CNTD1 is affecting a different subset of class I CO events than the loss of MLH1.

Figure 4-11. Crossover formation was significantly reduced in *Cntd1* mutants and severe spindle configuration defects were found in MI oocytes from *Cntd1* mutant females.

(A-F) Diakinesis preparations from wild-type (A, B), *Cntd1*$^{lacZ\ neo/+}$ (C), *Cntd1*$^{lacZ/+}$ (D), *Cntd1*$^{lacZ\ neo/lacZ\ neo}$ (E) and *Cntd1*$^{lacZ/lacZ}$ (F) spermatocytes are shown. In wild type (A, B) and heterozygous (C, D), paired homologous chromosomes are associated at sites of chiasmata (arrows), while the formation of chiasmata was significantly impaired in *Cntd1* mutant spermatocytes (E, F), with only a few residual bivalent chromosomes (arrow heads). Chiasmata counts are shown for each group. **(G)** Chiasmata counts from metaphase preparation of wild-type, *Cntd1*$^{lacZ\ neo/+}$, *Cntd1*$^{lacZ/+}$, *Cntd1*$^{lacZ\ neo/lacZ\ neo}$, *Cntd1*$^{lacZ/lacZ}$, wild-type, and *Mlh1*$^{-/-}$ spermatocytes are shown. Significant differences are detected between wild-type and *Cntd1* heterozygous mice (wild-type vs. *Cntd1*$^{lacZ/+\ neo+}$ p= 0.007, two-tailed *t* test; wild-type vs. *Cntd1*$^{lacZ/+\ neo-}$ p= 0.003, two-tailed *t* test), and between *Cntd1* mutant and *Mlh1* mutant mice ($p< 0.0001$, two-tailed *t* test), and between two wild-type groups (p=0.019, two-tailed *t* test). **(H-J)** Metaphase I progression in wild-type (H), *Cntd1* heterozygous (*Cntd1*$^{lacZ/+}$) (I), *Cntd1* homozygous mutant (*Cntd1*$^{lacZ/lacZ}$) (J) oocytes were examined. One misaligned chromosome in the oocyte from *Cntd1* heterozygous mouse is indicated by arrow head (I). Spindle configuration and chromosome alignment are visualized by β-tubulin (green) and DAPI (magenta) staining.

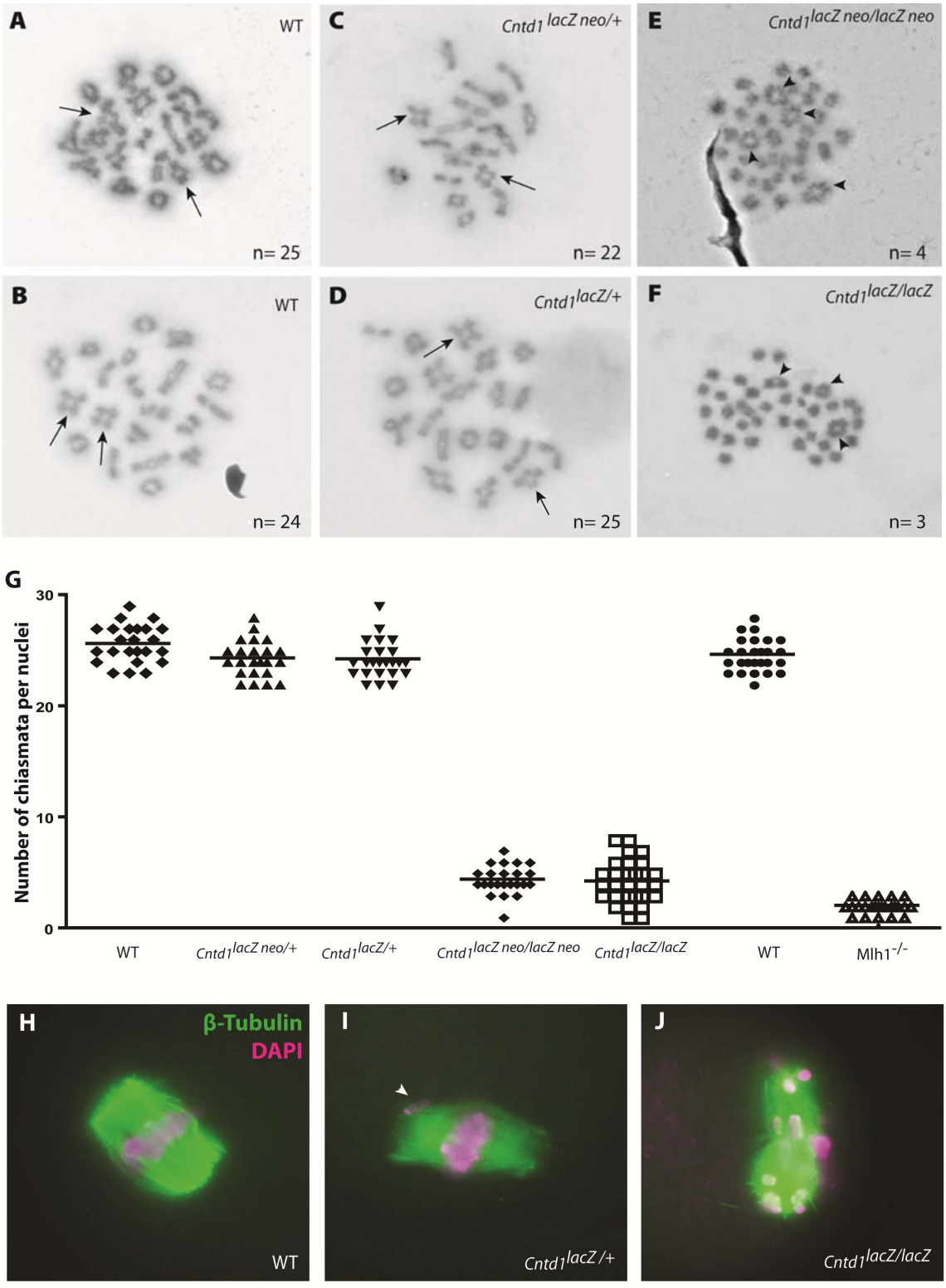
A
WT
n= 25
C
Cntd1 lacZ neo/+
n= 22
E
Cntd1lacZ neo/lacZ neo
n= 4
B
WT
n= 24
D
Cntd1lacZ/+
n= 25
F
Cntd1lacZ/lacZ
n= 3
G
Number of chiasmata per nuclei
30
20
10
0
WT
Cntd1lacZ neo/+
Cntd1lacZ/+
Cntd1lacZ neo/lacZ neo
Cntd1lacZ/lacZ
WT
Mlh1-/-
H
β-Tubulin
DAPI
WT
I
Cntd1lacZ /+
J
Cntd1lacZ/lacZ

To determine whether the loss of the majority of chiasmata can cause problems in chromosome segregation, I assessed the meiotic progression into metaphase I in *Cntd1* oocytes. Wild-type, *Cntd1* heterozygous and homozygous mutant oocytes were cultured *in vitro* for 8 hours after exhibiting germinal vesicle break down (GVBD). Then these oocytes were fixed and stained using an antibody against β-tubulin to illustrate the spindle configuration and DAPI to counterstain chromosomes. While the wild-type oocytes displayed a barrel-shaped bipolar spindle with chromosomes aligned around the metaphase plate (Figure 4-11 H), more than 80% of *Cntd1* mutant oocytes illustrated abnormal distribution of chromosomes around the metaphase I spindle (n=21) (Figure 4-11 J). Interestingly, while the loss of one copy of *Cntd1* did not affect prophase I progression in either spermatocytes or oocytes, *Cntd1* heterozygous oocytes showed an intermediate phenotype for chromosome congression in metaphase I. About 50% of the heterozygous oocytes had one or two chromosomes deviating from the metaphase plate (n=32) (arrow head in Figure 4-11 I). Taken together, these data indicate that the chiasmata number is dramatically reduced in *Cntd1* mutants, which results in abnormal metaphase progression in these germ cells.

4.6 *Cntd1* mutant oocytes cannot progress beyond 4-cell stage following fertilization

While ovary sections from 4 week old *Cntd1* mutant females demonstrate developing follicles similar to wild-type level, matings between young mutant females (4- to 5- weeks of age) and wild-type males did not yield any pregnancy. To determine the basis of female inferility, superovulation was performed on 4 week-old wild-type and $Cntd1^{lacZ\ neo/lacZ\ neo}$ females (Figure 4-12 A, B). After PMSG and hCG treatment, the mutant females ovulated at the same efficiency as their wild-type littermates (32 oocytes from wild-type and 46 oocytes from mutant, Table 4-1).

However, while 12 oocytes from the wild-type mice reached 2-cell stage and 8 of them developed into blastocyst stage after 4 days of *in vitro* culture, only 8 out of 46 oocytes from the mutant mice entered 2-cell stage, but none of them developed beyond 4-cell stage. These results indicate that the oocytes from *Cntd1* mutants are unable to support further development after fertilization, most likely due to the severe non-disjunction at the first meiotic division in these animals.

To determine whether the slightly disrupted chromosome alignment in the heterozygous females, as observed on metaphase I spindles (Figure 4-11 I), is sufficient to cause an effect on the efficiency of embryonic development, the *in vitro* development of fertilized oocytes harvested from wild-type and heterozygous females was checked (Figure 4-12 C). After 24 hours of *in vitro* culture, about 97.5% of the oocytes from wild-type females progressed into two-cell stage while only 57.1% of the oocytes from heterozygous animals displayed a similar progression. Interestingly, after 96 hours of *in vitro* culture, while about 72.5% of the oocytes from wild-type animals were at blastocyst stage, all the heterozygous oocytes reaching two-cell stage developed into blastocysts. These results suggest CNTD1 is very important for embryonic development, and loss of one copy of this gene in the genome can impair the survival rate of early embryos. However, this possibility should be further tested by checking embryonic development in wild-type females after mating with *Cntd1* heterozygous males.

Table 4-1. *In vitro* development of fertilized oocytes from superovulated 4-week-old wild-type and *Cntd1*$^{lacZ\ neo/lacZ\ neo}$ females

Genotype	Number of fertilized oocytes/embryos		
	Fertilized oocytes	2-cell stage	Blastocyst
WT	32	12	6
Cntd1$^{lacZ\ neo/lacZ\ neo}$	46	8	0

Figure 4-12. Fertilized oocytes from *Cntd1* mutant females display developmental defects during *in vitro* culture.

(A, B) H&E staining of ovary sections from superovulated 4-week-old wild-type and *Cntd1* mutant (*Cntd1*$^{lacZ\ neo/lacZ\ neo}$) females is illustrated. Scale bar is 50 μm. **(C)** Progression of fertilized oocytes from 8-week-old wild-type and *Cntd1* heterozygous females is compared at three developmental stage (fertilized oocytes, 2-cell stage and blastocyst stage).

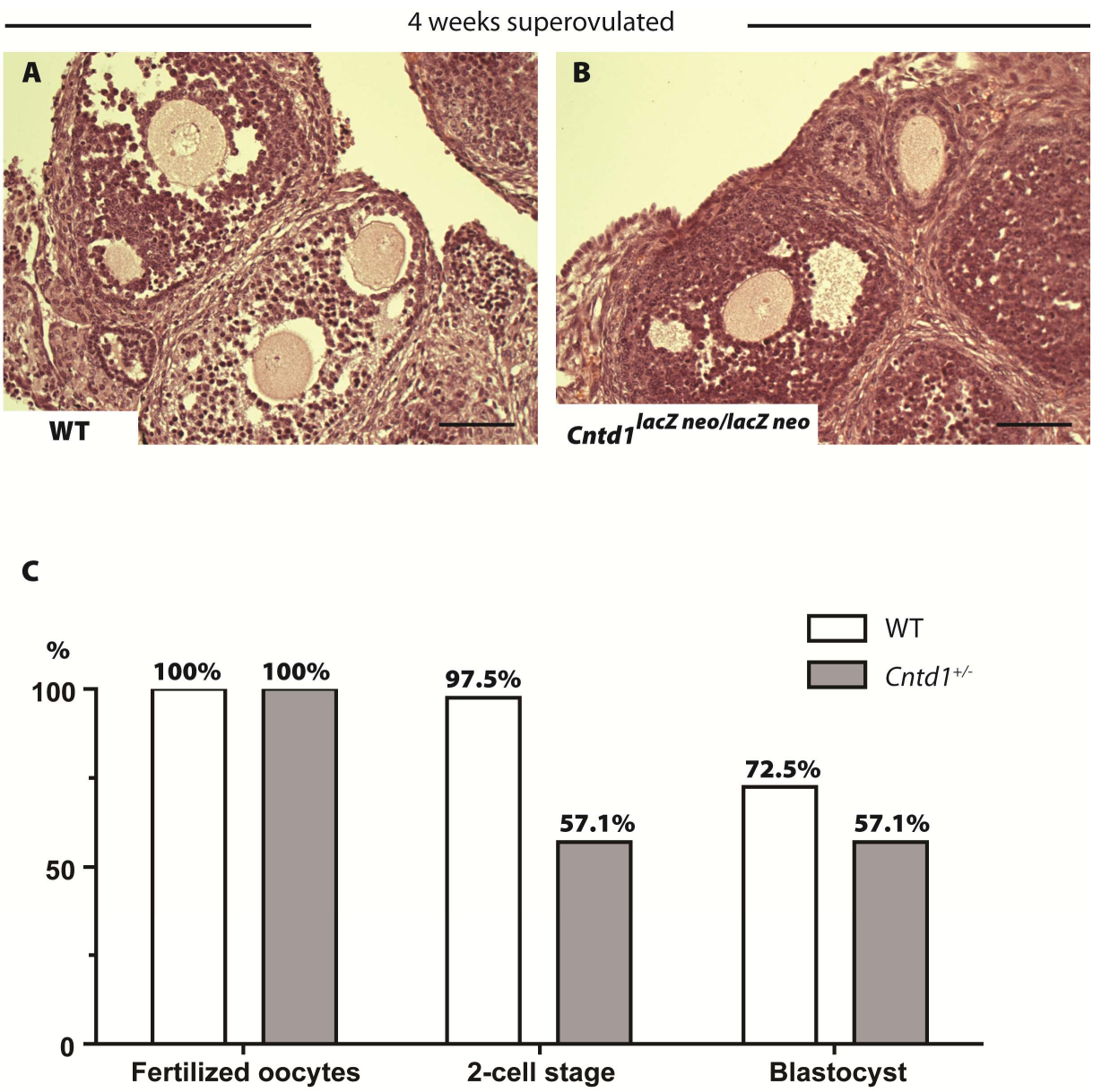
4 weeks superovulated
A
WT
B
Cntd1lacZ neo/lacZ neo
C
%
100
50
0
100%
100%
97.5%
57.1%
72.5%
57.1%
WT
Cntd1+/-
Fertilized oocytes
2-cell stage
Blastocyst

5. Discussion

Recent studies on *C. elegans* COSA-1 reveal its important roles in designation and reinforcement of meiotic COs and suggest that COSA-1 may function in conjunction with other conserved CO-promoting proteins (Yokoo et al. 2012). To explore the role of the mouse orthologue of COSA-1, CNTD1, in mouse gametogenesis, we generated *Cntd1* mutant mice using a *Cntd1* ES cell line obtained from UC Davis KOMP (Knockout Mouse Project) Repository. The insertion of a promoterless FRT- *lacZ-loxP-neo*-FRT-*loxP* cassette between exon 1 and exon 2 of mouse *Cntd1* results in the residual expression of CNTD1 as illustrated in western blotting. The detected protein can reflect either a fusion protein translated from the extended exon 1 to exon 7 transcripts detected in cDNA analysis, or an intact CNTD1 protein. The second possibility is favored because the size of residual CNTD1 detected in the mutant animal is the same as seen in wild-type. In the extended transcript, there is one 111 bp insertion between exon 1 and exon 2, which would lead to 4 kDa (37 amino acids) increase in protein size. But we did not detect such a shift between wild-type and mutant protein bands. The 37 kDa CNTD1 protein detected in the mutant mice could result from either a leaky transcription of *Cntd1* gene in the mutant mice, in which the targeted intron 1 region including FRT- *lacZ-loxP-neo*-FRT-*loxP* insert is excluded for some reason, or the removal of the 111 bp insertion from the extended transcript by a splicing event before translation, which also produce a CNTD1 protein of wild-type size. While it is very hard to distinguish between these two possibilities, the absence of the wild-type size *Cntd1* transcripts in our RT-PCR analysis seems to support the latter explanation. However, the absence could also result from the low transcriptional level of these transcripts, which may escape the detection by RT-PCR.

My studies show that the disruption of *Cntd1* results in infertility in both males and females, although *Cntd1* mutant animals develop normally and both sexes display normal mating behavior. *Cntd1* mutant males displayed dramatically smaller testes compared with wild-type animals at both 4 weeks and 8 weeks of age, and complete absence of epididymal sperm in adults. While histological analysis of testis section of *Cntd1* mutant males indicated that populations of spermatogonia and early spermatocytes were similar to wild-type, TUNEL staining demonstrated a significantly increased level of apoptosis in late-stage spermatocytes, which may be responsible for the depletion of spermatozoa and the decrease in testicular size.

Examination of meiotic prophase I progression in both males and females suggested that pairing, synapses and the early steps in DSB repair were normal in *Cntd1* mutant meiocytes. One thing to note is that the number of MSH5 foci, the marker for DSB repair progression through zygonema and also a key component of MutSγ, the DNA/substrate binding component of the meiotic MMR complex, was comparable to wild-type on zygotene/early-pachytene chromosomes from both male and female mutants, thus differs from the observation made in *C. elegans*. It was found that *C. elegans* COSA-1 foci were not observed in *msh-5* mutant, and MSH-5 foci were not detected in *cosa-1* mutant (Yokoo et al. 2012), implying that *Cosa-1* and *Msh-5* are interdependent in *C. elegans*, and suggesting that COSA-1 may facilitate or stabilize the association of MSH-5 with nascent recombination sites. The different observations made in mouse and *C. elegans* may reflect the variation in the regulation of CO formation between these two difference species. My results shows that MSH5 or MSH4 foci (data not shown) can bind to chromosome cores without the presence of CNTD1, indicating the stabilization of MSH5 or MSH4 on meiotic chromosome is not dependent on CNTD1 in mouse. But it is not clear whether the function of CNTD1 in meiocytes requires MSH4 or MSH5. CNTD1 protein was found to be missing in whole testis

lysates of *Msh4* mutants. If CNTD1 functions after pachynema in meiocytes, the absence of CNTD1 could result from the loss of spermatocytes after pachytene stage in *Msh4* mutants (Kneitz et al. 2000). Unfortunately, detailed analysis of CNTD1 localization in meiocytes is precluded by the lack of a CNTD1 antibody that works in immunocytochemistry. Further studies will be focused on purifying germ cells of various meiotic stages to determine the specific stages when CNTD1 appears. If CNTD1 is proved to be distributed in germ cells before pachytene stage, combined with the absence of CNTD1 in *Msh4* mutant testis, it may indicate that the localization of CNTD1 in meiotic cells depends on the presence of MSH4. However, if CNTD1 is shown to be localized on meiotic chromosomes during and after pachynema, the dependence of CNTD1 on MutS homologs during prophase I will need to reevaluated. One option is to take advantage of an *Msh5* defective strain, whose *Msh5* gene is disrupted by a point mutation and its germ cells can survive beyond pachyenma (personal communication, Cohen and Edelmann). If CNTD1 is absent in pachytene germ cells of these *Msh5* point mutants, it will imply that the function of CNTD1 during prophase I requires the presence of fully functional MSH5.

While the marker for intermediate recombination nodules, the MSH5 foci, were present, the two Class I CO markers signifying late recombination nodules, MLH1 and MLH3, were completely absent from pachytene chromosomes from *Cntd1* mutant meiocytes. This indicates impaired Class I CO formation and hence defective meiotic recombination in these mutants. As the major CO pathway in mammals, Class I CO pathway is responsible for ~90% of all CO events (Guillon et al. 2005; Svetlanov et al. 2008). Knockout mice deficient for major components of this pathway, such as *Mlh1* or *Mlh3*, can only retain about 10% chiasmata by the end of prophase I (Baker et al. 1996; Edelmann et al. 1996; Lipkin et al. 2002; Kan et al. 2008). As expected, we observed a dramatic reduction of chiasmata number in the mutants to the level close to *Mlh1* and

Mlh3 mutants, which may correlate with the failure in spermatocyte maturation observed in histological analysis. Furthermore, western blot analysis showed that CNTD1 protein was absent from the whole testis protein lysate from *Mlh1*$^{-/-}$ mouse, which suggests that MLH1 expression is necessary for the localization of CNTD1.

Based on these results, I hypothesize that CNTD1 may function downstream of MSH4/MSH5 in the same recombination pathway as MLH1 and MLH3. CNTD1 may help select proper MLH1/MLH3 sites for COs from MSH4/MSH5 sites through facilitating and stabilizing the binding of MLH1/MLH3 onto meiotic chromosomes. Importantly, the localization of CNTD1 and MLH1/MLH3 on meiotic chromosomes is interdependent. When CNTD1 is missing, the binding of MLH1 or MLH3 onto the meiotic chromosome will be unstable, coupled with disrupted CO formation, and *vice versa*.

Of note, our current results indicate that residual COs found in *Cntd1* mutant spermatocytes are twice as many as COs detected in *Mlh1* mutants (p=0.019, two-tailed *t* test). One explanation for the difference in the chiasmata numbers between these two mutants could be due to different strain background of these two lines (Koehler et al. 2002). The data would be more persuasive if the newly generated *Cntd1* mutant line were crossed into the same genetic background as *Mlh1* mutants. Another alternative explanation for these extra chiasmata appearing in *Cntd1* mutant could be that the other CO pathway, such as Class II CO pathway, is up-regulated in *Cntd1* mutants. Cross-regulation between different CO pathways has reported previously. The deletion of the major player of Class II CO pathway *Mus81* from mice does not cause any changes in chiasmata, but leads to an increase in MLH1-MLH3 foci on pachytene chromosomes, implying possible crosstalk between two major CO recombination pathways (Holloway et al. 2008). A number of proteins have been implicated as regulators between these two CO pathways. For

example, BLM was found to be able to physically interact with MLH1 and MUS81 i*n vitro* (Langland et al. 2001; Zhang et al. 2005). In mouse meiosis, the absence of *Blm* causes an increase of chiasmata numbers at diakinesis (Holloway et al. 2010). Given that the number of MLH1–MLH3 foci during pachynema is normal in *Blm* deficient mice (Holloway et al. 2010), the additional chiasmata or chiasmata-like structures may be derived from MLH1–MLH3 independent CO pathway, the Class II CO pathway, which suggests the role of *Blm* in regulating meiotic recombination across different CO pathways. More recently, the gene *Slx4* (or *Btbd12*) was also implicated as a possible mediator between the Class I and Class II pathways in the mouse (Holloway et al. 2011). In wild-type meiocytes, CNTD1 may act as an inhibitor for Class II CO formation by directly or indirectly interacting with Class II CO machinery. The loss of CNTD1 may result in the release of those proteins responsible for producing Class II COs, and then trigger the generation of more COs from this pathway.

In *Cntd1* mutant females, meiotic progression was also disrupted. Chromosome spreads made from germ cells from embryonic ovaries indicated that prophase I was disrupted in *Cntd1* females at a similar meiotic stage as *Cntd1* mutant males, and MLH1 foci were also missing from *Cntd1* mutant oocytes during pachynema. However, unlike *Cntd1* spermatocytes, none of which survived to complete meiosis, follicle development appeared normal in 4 week-old female mutants. When fertilized, some of these oocytes were able to reach 2-cell or even 4-cell stage, indicating the completion of meiosis in these oocytes. Interestingly, while the number of oocytes in 4 week-old mutant females is close to normal, there is a gradual loss of oocytes through adult life such that, by 8 weeks of age, the ovaries of *Cntd1* mutant females are essentially devoid of germ cells. This phenotype is distinct from *Mlh1*, *Mlh3, Msh4* and *Msh5* mutant females, and suggests a premature ovarian failure phenotype associated with residual chiasmata that exceed

some of those found in these other *zmm* mutants. Although all these CO-deficient mutants display infertility in females, ovaries from *Mlh1* and *Mlh3* mutants are histologically normal and contain follicles of all developmental stages (Baker et al. 1996; Edelmann et al. 1996; Lipkin et al. 2002), while oocyte development and ovarian structure are completely disrupted in *Msh4* and *Msh5* mutant females (de Vries et al. 1999; Kneitz et al. 2000). *Cntd1* mutant females appear to have an intermediate phenotype, which may reflect the difference in the requirement of these different genes for the completion of oogenesis. MSH4 and MSH5 may function at an earlier stage of gametogenesis compared to MLH1, MLH3 and CNTD1, and the absence of these two proteins quickly triggers apoptosis of the oocytes. While MLH1, MLH3 and CNTD1 may work at a similar time point during prophase I to process meiotic COs, CNTD1 could have some extra functions after prophase I, which may be related with other stages of meiosis or follicular development.

Collectively, our results provide the first detailed analysis of the function of CNTD1 during mammalian gametogenesis. Consistent with the finding in *C. elegans*, I showed that the deletion of *Cntd1* in mice caused severe defects in meiotic CO formation, which may underlie the sterility in both male and female mutants. No epididymal sperm were found in $Cntd1^{lacZ/lacZ}$ males, and mutant females underwent severe oocyte-depletion after puberty. Importantly, these data indicate a pivotal role for CNTD1 in regulating meiotic COs, possibly by helping select the sites of late recombination nodules through promoting or stabilizing other Class I CO-promoting proteins on meiotic chromosomes.

Clearly, the mechanism of CO regulation by CNTD1 is still unknown. As a cyclin-related protein, CNTD1 may partner with a cyclin-dependent kinase (CDK) to form a CNTD1/CDK complex, and this complex could bind to some downstream targets and regulate meiotic COs.

One candidate of the downstream target is MSH5, which has a cyclin B-binding domain in its C-terminal (personal communication, Cohen and Edelmann). Future studies will be necessary to confirm the interaction between CNTD1 and MSH5, and also identify more possible interacting partners of CNTD1. It is hoped that investigation of these interactors will help us dissect out the specific roles CNTD1 plays in meiosis, and hence shed more lights on the process of meiotic recombination in mammals.

6. References

Argueso JL, Wanat J, Gemici Z, Alani E. 2004. Competing crossover pathways act during meiosis in Saccharomyces cerevisiae. *Genetics* **168**(4): 1805-1816.

Baker SM, Plug AW, Prolla TA, Bronner CE, Harris AC, Yao X, Christie DM, Monell C, Arnheim N, Bradley A et al. 1996. Involvement of mouse Mlh1 in DNA mismatch repair and meiotic crossing over. *Nature Genetics* **13**(3): 336-342.

Borner GV, Kleckner N, Hunter N. 2004. Crossover/noncrossover differentiation, synaptonemal complex formation, and regulatory surveillance at the leptotene/zygotene transition of meiosis. *Cell* **117**(1): 29-45.

Cohen PE, Pollack SE, Pollard JW. 2006. Genetic analysis of chromosome pairing, recombination, and cell cycle control during first meiotic prophase in mammals. *Endocr Rev* **27**(4): 398-426.

Cole F, Kauppi L, Lange J, Roig I, Wang R, Keeney S, Jasin M. 2012. Homeostatic control of recombination is implemented progressively in mouse meiosis. *Nat Cell Biol* **14**(4): 424-430.

de los Santos T, Hunter N, Lee C, Larkin B, Loidl J, Hollingsworth NM. 2003. The Mus81/Mms4 endonuclease acts independently of double-Holliday junction resolution to promote a distinct subset of crossovers during meiosis in budding yeast. *Genetics* **164**(1): 81-94.

de Vries SS, Baart EB, Dekker M, Siezen A, de Rooij DG, de Boer P, te Riele H. 1999. Mouse MutS-like protein Msh5 is required for proper chromosome synapsis in male and female meiosis. *Genes Dev* **13**(5): 523-531.

Edelmann W, Cohen PE, Kane M, Lau K, Morrow B, Bennett S, Umar A, Kunkel T, Cattoretti G, Chaganti R et al. 1996. Meiotic pachytene arrest in MLH1-deficient mice. *Cell* **85**(7): 1125-1134.

Evans EP, Breckon G, Ford CE. 1964. An air-drying method for meiotic preparations from mammalian testes. *Cytogenet Cell Genet* **3**: 289-294.

Guillon H, Baudat F, Grey C, Liskay RM, de Massy B. 2005. Crossover and noncrossover pathways in mouse meiosis. *Mol Cell* **20**(4): 563-573.

Harding SD, Armit C, Armstrong J, Brennan J, Cheng Y, Haggarty B, Houghton D, Lloyd-MacGilp S, Pi X, Roochun Y et al. 2011. The GUDMAP database--an online resource for genitourinary research. *Development* **138**(13): 2845-2853.

Hillers KJ, Villeneuve AM. 2003. Chromosome-Wide Control of Meiotic Crossing over in C. elegans. *Curr Biol* **13**(18): 1641-1647.

Hodges CA, LeMaire-Adkins R, Hunt PA. 2001. Coordinating the segregation of sister chromatids during the first meiotic division: evidence for sexual dimorphism. *J Cell Sci* **114**(Pt 13): 2417-2426.

Holloway JK, Booth J, Edelmann W, McGowan CH, Cohen PE. 2008. MUS81 generates a subset of MLH1-MLH3-independent crossovers in mammalian meiosis. *PLoS Genet* **4**(9): e1000186.

Holloway JK, Mohan S, Balmus G, Sun X, Modzelewski A, Borst PL, Freire R, Weiss RS, Cohen PE. 2011. Mammalian BTBD12 (SLX4) protects against genomic instability during mammalian spermatogenesis. *PLoS Genet* **7**(6): e1002094.

Holloway JK, Morelli MA, Borst PL, Cohen PE. 2010. Mammalian BLM helicase is critical for integrating multiple pathways of meiotic recombination. *J Cell Biol* **188**(6): 779-789.

Hunter N, Kleckner N. 2001. The single-end invasion: an asymmetric intermediate at the double-strand break to double-holliday junction transition of meiotic recombination. *Cell* **106**(1): 59-70.

Jessop L, Lichten M. 2008. Mus81/Mms4 endonuclease and Sgs1 helicase collaborate to ensure proper recombination intermediate metabolism during meiosis. *Mol Cell* **31**(3): 313-323.

Jones GH, Franklin FC. 2006. Meiotic crossing-over: obligation and interference. *Cell* **126**(2): 246-248.

Kan R, Sun X, Kolas NK, Avdievich E, Kneitz B, Edelmann W, Cohen PE. 2008. Comparative analysis of meiotic progression in female mice bearing mutations in genes of the DNA mismatch repair pathway. *Biol Reprod* **78**(3): 462-471.

Keeney S, Giroux CN, Kleckner N. 1997. Meiosis-specific DNA double-strand breaks are catalyzed by Spo11, a member of a widely conserved protein family. *Cell* **88**: 375-384.

Kneitz B, Cohen PE, Avdievich E, Zhu L, Kane MF, Hou H, Jr., Kolodner RD, Kucherlapati R, Pollard JW, Edelmann W. 2000. MutS homolog 4 localization to meiotic chromosomes is required for chromosome pairing during meiosis in male and female mice. *Genes Dev* **14**(9): 1085-1097.

Koehler KE, Cherry JP, Lynn A, Hunt PA, Hassold TJ. 2002. Genetic control of mammalian meiotic recombination. I. Variation in exchange frequencies among males from inbred mouse strains. *Genetics* **162**(1): 297-306.

Kolas NK, Svetlanov A, Lenzi ML, Macaluso FP, Lipkin SM, Liskay RM, Greally J, Edelmann W, Cohen PE. 2005. Localization of MMR proteins on meiotic chromosomes in mice indicates distinct functions during prophase I. *J Cell Biol* **171**(3): 447-458.

Langland G, Kordich J, Creaney J, Goss KH, Lillard-Wetherell K, Bebenek K, Kunkel TA,

Groden J. 2001. The Bloom's syndrome protein (BLM) interacts with MLH1 but is not required for DNA mismatch repair. *J Biol Chem* **276**(32): 30031-30035.

Lenzi ML, Smith J, Snowden T, Kim M, Fishel R, Poulos BK, Cohen PE. 2005. Extreme heterogeneity in the molecular events leading to the establishment of chiasmata during meiosis i in human oocytes. *Am J Hum Genet* **76**(1): 112-127.

Lipkin SM, Moens PB, Wang V, Lenzi M, Shanmugarajah D, Gilgeous A, Thomas J, Cheng J, Touchman JW, Green ED et al. 2002. Meiotic arrest and aneuploidy in MLH3-deficient mice. *Nat Genet* **31**(4): 385-390.

Mahadevaiah SK, Turner JM, Baudat F, Rogakou EP, de Boer P, Blanco-Rodriguez J, Jasin M, Keeney S, Bonner WM, Burgoyne PS. 2001. Recombinational DNA double-strand breaks in mice precede synapsis. *Nat Genet* **27**(3): 271-276.

Marcon E, Moens P. 2003. MLH1p and MLH3p localize to precociously induced chiasmata of okadaic-acid-treated mouse spermatocytes. *Genetics* **165**(4): 2283-2287.

Martini E, Diaz RL, Hunter N, Keeney S. 2006. Crossover homeostasis in yeast meiosis. *Cell* **126**(2): 285-295.

Moens PB, Chen DJ, Shen Z, Kolas NK, Tarsounas M, Heng HH, Spyropoulos B. 1997. Rad51 immunocytology in rat and mouse spermatocytes and oocytes. *Chromosoma* **106**(4): 207-215.

Oh SD, Lao JP, Taylor AF, Smith GR, Hunter N. 2008. RecQ helicase, Sgs1, and XPF family endonuclease, Mus81-Mms4, resolve aberrant joint molecules during meiotic recombination. *Mol Cell* **31**(3): 324-336.

Peters AH, Plug AW, van Vugt MJ, de Boer P. 1997. A drying-down technique for the spreading of mammalian meiocytes from the male and female germline. *Chromosome Res* **5**(1): 66-

68.

Roy A, Kucukural A, Zhang Y. 2010. I-TASSER: a unified platform for automated protein structure and function prediction. *Nat Protoc* **5**(4): 725-738.

Sayle RA, Milnerwhite EJ. 1995. Rasmol - Biomolecular Graphics for All. *Trends in Biochemical Sciences* **20**(9): 374-376.

Svetlanov A, Baudat F, Cohen PE, de Massy B. 2008. Distinct Functions of MLH3 at Recombination Hot Spots in the Mouse. *Genetics* **178**(4): 1937-1945.

Uroz L, Rajmil O, Templado C. 2008. Premature separation of sister chromatids in human male meiosis. *Hum Reprod* **23**(4): 982-987.

Wang D, Enders GC. 1996. Expression of a specific mouse germ cell nuclear antigen (GCNA1) by early embryonic testicular teratoma cells in 129/Sv-Sl/+ mice. *Cancer Lett* **100**(1-2): 31-36.

Woods LM, Hodges CA, Baart E, Baker SM, Liskay RM, Hunt PA. 1999. Chromosomal influence on meiotic spindle assembly: abnormal meiosis I in female Mlh1 mutant mice. *Journal of Cell Biology* **145**(7): 1395-1406.

Yokoo R, Zawadzki KA, Nabeshima K, Drake M, Arur S, Villeneuve AM. 2012. COSA-1 Reveals Robust Homeostasis and Separable Licensing and Reinforcement Steps Governing Meiotic Crossovers. *Cell* **149**(1): 75-87.

Zalevsky J, MacQueen AJ, Duffy JB, Kemphues KJ, Villeneuve AM. 1999. Crossing over during Caenorhabditis elegans meiosis requires a conserved MutS-based pathway that is partially dispensable in budding yeast. *Genetics* **153**(3): 1271-1283.

Zhang R, Sengupta S, Yang Q, Linke SP, Yanaihara N, Bradsher J, Blais V, McGowan CH, Harris CC. 2005. BLM helicase facilitates Mus81 endonuclease activity in human cells.

Cancer Res **65**(7): 2526-2531.

Zhang Y. 2008. I-TASSER server for protein 3D structure prediction. *BMC Bioinformatics* **9**: 40.

CHAPTER 5

Discussion and Future directions

Since their discovery in *E. coli*, mismatch repair (MMR) proteins have been found to function in a variety of cellular activities, ranging from correcting endogenous DNA mismatches to facilitating the progression of meiosis. Meiosis is a specialized cell division responsible for producing haploid gametes from diploid precursor cells in sexually reproducing organisms. Early interests in mismatch repair proteins during meiotic events arise from studies in yeast during 1990s, in which mutations in specific MutS or MuL homolog proteins led to severe defects in meiotic recombination (Alani, Reenan et al. 1994; Ross-Macdonald and Roeder 1994; Hollingsworth, Ponte et al. 1995; Hunter and Borts 1997; Wang, Kleckner et al. 1999).

In yeast, and probably also in mice, it is believed that a single MutS heterodimer of MSH4-MSH5 together with a single MutL heterodimer of MLH1-MLH3 collaborate together to determine crossover (CO) sites on meiotic chromosomes. MSH4-MSH5 is thought to promote COs by stabilizing the formation of double Holliday Junction (dHJ) , and then recruiting MLH1-MLH3, which facilitates the resolution of this DNA intermediates by recruiting other downstream factors (Hoffmann and Borts 2004). However, it is still not clear how MLH1-MLH3 functions in dHJ resolution and which protein is the downstream resolvase responsible for the resolution. Hence, the second and third chapters of this thesis are aimed at answering to these questions by investigating two unique features of one MutL homolog mouse MLH3: one highly conserved endonuclease domain colocalized within the predicted MutL C-terminal dimerization domain, and one vertebrate- specific region within exon 2 of *Mlh3*.

During mammalian meiosis, the number of MSH4-MSH5 foci appearing on zygotene chromosomes significantly outnumbers the MLH1-MLH3 foci appearing in pachynema. In mice, more than one hundred MSH4-MSH5 foci can be detected on zygotene chromosomes per nucleus, but only a small subset of these (~23 foci per nucleus) are eventually processed and stabilized by MLH1-MLH3 to become Class I COs. Most MSH4-MSH5 foci are repaired through NCO, or other pathways, and it is presumed that some of these may be through MLH1-independent CO pathway (Cohen, Pollack et al. 2006; Cole, Kauppi et al. 2012). However, it is not known how MLH1-MLH3 selects Class I CO sites from the total pool of MSH4-MSH5 sites. Previous research in the Cohen lab has shown that MLH3 binds to meiotic chromosome during early pachynema before forming a heterodimer with MLH1 (Kolas, Svetlanov et al. 2005), which implies that MLH3 may play a pivotal role in deciding which MSH4-MSH5 sites to choose for COs, possibly with the help from other CO promoting proteins. Thus, in Chapter 4, mouse CNTD1, a candidate for promoting CO decision in mouse, was investigated.

In Chapter 2, in order to investigate the role of the conserved domain of MLH3 in mouse meiosis, I generated a transgenic mouse line *Mlh3*^{DN} containing a point mutation in the potential endonuclease domain. In line with the strict conservation of this domain across eukaryotes, I hypothesized that disruption of this domain would lead to the abolishment of normal meiotic progression *in vivo*. Chromosome spreading performed on *Mlh3*$^{DN\ neo/-}$ oocytes containing one copy of the null *Mlh3* allele and one copy of the point mutant allele showed that pairing, synapsis and early double strand break processing are normal in the mutant oocytes, but that the Class I CO pathway was impaired, illustrated by the significantly decreased MLH1/MLH3 foci. In the future, this transgenic mouse line will be an ideal system for investigating the *in vivo* function of

this endonuclease domain in mouse meiosis, and also for elucidating the relationship between endonuclease activity and dimerization function of this domain. Meiotic progression in the meiocytes from the mutants should be more carefully evaluated by counting the numbers of RAD51, MSH4/MSH5, and MLH1/MLH3 foci on chromosomes of different prophase I substages, which will provide more details on how initiation of double strand break repair and formation of early and late recombination nodules may differ in *Mlh3*^{DN} mutants compared with wild-type littermates. It is expected that if the endonuclease domain is important for the interaction of MLH3 with MSH4/MSH5 or MLH1, the MSH4/MSH5 foci during early pachynema and MLH1 foci during mid to late pachynema may be changed compared with wild-type level. Thus, I would predict that failure of the DN mutant to bind MSH4/MSH5 would result in loss of MLH3 and MLH1 association at double strand break repair sites, while failure of the DN mutant to bind MLH1 would result in accumulation of MLH3 on the chromosomes early in pachynema but a failure of MLH1 to localize to these sites in mid-pachynema.

To establish whether the DN point mutation disrupts the interaction between mouse MLH3^{DN} and other proteins, immunoprecipitation of MLH3^{DN} can also be used, followed by western blotting with antibodies against potential interacting proteins, such as MSH4 and MLH1 (Wang, Kleckner et al. 1999; Lipkin, Wang et al. 2000; Santucci-Darmanin, Neyton et al. 2002). Besides these known interacting proteins, the list of potential interactors of mouse MLH3 should be further expanded either by protein pull-down using anti-MLH3 antibodies, from which the associated proteins can be analyzed by mass spectrometry, or by two-hybrid experiment in either yeast or mammalian cells. The predicted dimerization domain containing the potential endonuclease domain can be used as the “bait” to identify as-yet-undetermined binding proteins. To know whether the DN mutation in the endonuclease domain abolishes such interactions, the

prey identified from the screen will be put back to the two-hybrid system, and will be tested for the interaction with the new bait, in which the endonuclease domain contains DN mutation. Additionally, the phenotype of this *Mlh3*^{DN} transgenic line, such as fertility and meiotic progression, should be compared with *Mlh3* full null line. RNA-seq experiments can be performed on purified germ cells of different prophase I stages from these two mutant strains, and compared with wild-type control. The changes in genome-wide expression level, especially those genes related with mismatch repair and meiosis, can be detected and analyzed, which will provide useful information on the downstream effectors of MLH3 and how the mutations in MLH3 affect mouse meiosis.

In Chapter 3, I focused on the large mammalian-specific region within exon 2, which results in a double-sized MLH3 protein compared with its yeast counterpart. We hypothesize that the unique region in exon 2 is important for the function of mouse MLH3 in maintaining genome integrity, and confers mammalian- specific functions to mouse MLH3. Yeast two-hybrid screening was performed to identify possible interacting partners of this region, and I also integrated an MSI reporter assay into spontaneously immortalized MEF cells. The MSI reporter assay will be a useful system for screening of key sub-motif within this unique region, and such studies are currently ongoing. As discussed in Chapter 3, this unique region could also be inserted into another MutL homolog protein, which does not contain it. For example, this unique region can be integrated into mouse PMS2. The fusion form of PMS2 and wild-type MLH1 can be expressed *in vitro*, and the formation of PMS2-MLH1 heterodimer can be examined. If the PMS2-MLH1 dimerization is not affected by the insertion, the mismatch repair activity of this heterodimer will be checked using biochemical method and compared with wild-type PMS2-MLH1, which may provide more insights into the function of this unique region. Another

interesting experiment would be to insert this region into yeast MLH3 protein and use this fusion protein to replace the wild-type mouse MLH3 either in a mammalian cell line or in a transgenic mouse. Different from mouse MLH3, yeast MLH3 was never found to be associated with satellite sequences at centromere (Choo 1997; Kolas, Svetlanov et al. 2005). It would be very interesting to see whether this insertion would confer the ability to bind to the satellite sequence in the centromere region (or other repeat sequences) of mouse chromosomes, or even to complement the *Mlh3* null allele.

In Chapter 4, I studied a potential CO promoting protein mouse, CNTD1. Studies of the *C. elegans* orthologue COSA-1 suggests that this protein is essential for designation and reinforcement of meiotic COs and functions in conjunction with other conserved CO-promoting proteins (Yokoo, Zawadzki et al. 2012). Additionally, mRNA expression data from mouse shows that *Cntd1* transcripts are highly enriched in testis and the expression of CNTD1 in mouse ovaries peaks from embryonic day 14 to embryonic day 18, which overlaps the period when prophase I happens in mouse ovaries (Harding, Armit et al. 2011). Given the evidence above, I hypothesized that CNTD1 might regulate meiotic CO sites through promoting or stabilizing other Class I CO-promoting proteins on meiotic chromosomes. This hypothesis is supported by our findings from the *Cntd1* mutant mice. It is shown that the deletion of *Cntd1* in mice causes severe defects in meiotic CO formation, which leads to sterility in both males and females. No epididymal sperm was found in *Cntd1* mutant males, and mutant females underwent severe oocyte-depletion after puberty. *Cntd1* mutant meiocytes display normal DSB formation, pairing, synapsis and the formation of early recombination nodules in both male and female mutants. However, Class I COs, indicated by MLH1/MLH3 foci, were dramatically reduced in mutants, coupled with significantly decreased chiasmata number at diakinesis and abnormal chromosome

Figure 5-1. A model for CO-regulation through CNTD1 in mouse meiosis.

A cartoon summary depicting step-wise specification and selection of CO sites is shown. In mouse, the recombination process is induced by double strand breaks in the beginning of prophase I. Early recombination events are marked by strand invasion proteins such RAD51 and DMC1. More than 200 RAD1 foci can be detected per nucleus at leptonema/zygonema, a subset of which (~ 150 foci per nucleus) are processed by MSH4 and MSH5. The number of MSH4-MSH5 foci keeps dropping to less than 100 foci by late zygonema (Cole, Kauppi et al. 2012). Only a small portion of these MSH4-MSH5 foci are stabilized by MLH1-MLH3 (~ 23 per nucleus). CNTD1 may help select proper MLH1/MLH3 sites for COs from MSH4/MSH5 sites through facilitating and stabilizing the binding of MLH1/MLH3 onto meiotic chromosomes.

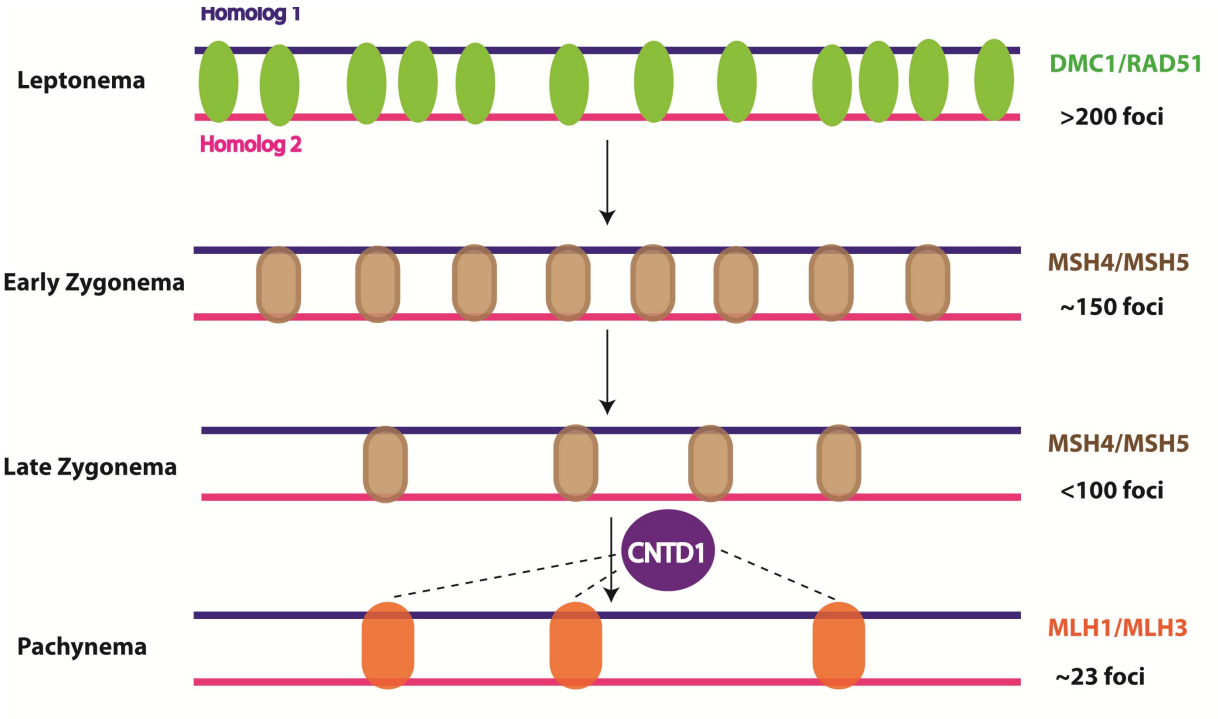

segregation during metaphase I. These results suggest a model for CNTD1 action during prophase I, as depicted in Figure 5-1. In this model, CNTD1 functions downstream of MSH4/MSH5, but in the same recombination pathway as MLH1 and MLH3. CNTD1 may help select proper MLH1/MLH3 sites for COs from MSH4/MSH5 sites through facilitating and stabilizing the binding of MLH1/MLH3 onto meiotic chromosomes. Alternatively, or in addition, CNTD1 may mediate interactions between cell cycle regulatory elements, such as cyclin-CDK complexes, and the recombination machinery.

There are still plenty of questions to be answered in the CNTD1 project. Due to the lack of a proper CNTD1 antibody that works on meiotic chromosome spreads, I failed to determine the prophase I substages when CNTD1 functions. There are two options to solve this problem. One is to purify germ cells of various stages and then perform western blotting on each sample. The second and also a more straightforward resolution is to develop an antibody for mouse CNTD1 that works on meiotic spreads. This antibody will also be useful to check the change of CNTD1 foci on chromosomes from other meiosis-defective mutants.

Additionally, the mechanism of CO regulation by CNTD1 is still not clear. It is important to identify interacting proteins of CNTD1 during meiosis. Either protein-pull down or two-hybrid experiments can be used for the screening. The proteins identified in these experiments should be checked on meiotic chromosome spreads using immunofluorescent staining and distribution of these proteins in *Cntd1* mutant and wild-type meiocytes should be examined and compared.

I have shown that CNTD1 functions mainly through the Class I CO pathway since CNTD1 protein level was not affected in the absence of MUS81, the key player of the Class II CO pathway. Nevertheless, it will still be important to check the status of Class II CO pathway in *Cntd1* mutants. Previous research in the Cohen lab has shown that the lack of MUS81 can lead to

an increase of MLH1-MLH3 foci on pachytene chromosomes, implying possible crosstalk between two major CO recombination pathways (Holloway, Booth et al. 2008). One future experiment will be to check the status of MUS81 during prophase I on chromosomes from CNTD1 mutants using immunofluorescent staining of meiotic chromosomes. *Cntd1* mouse line can also be crossed with *Mus81* mouse line to obtain *Cntd1* and *Mus81* double mutant mice. CO formation at diakinesis stage in these double mutants would be evaluated, and then compared with *Cntd1* and *Mus81* single mutant mouse to see whether there is any additive reduction in chiasmata numbers in the double mutant line.

Another interesting area to explore in the mouse *Cntd1* project is the oocyte-depletion phenotype observed in females. This phenotype is reminiscent of human premature ovarian syndrome (POF), an ovarian defect characterized by the premature depletion of ovarian follicles before the age of 40 years (Persani, Rossetti et al. 2010). POF can be secondary to autoimmune inflammatory disease, viral infection, environmental toxics, and radiation or chemotherapy, but in most cases, the etiology is genetic (Cordts, Christofolini et al. 2011). The genetic causes of POF often results from chromosomal abnormality, such as X chromosome (Sherman 2000), or mutations in single genes, and lead to follicle reduction and/or impaired follicular development. Mouse models have been used to study the genes associated with pathophysiological changes in POF. Most of these models are aimed at investigating factors involved in folliculogenesis after the formation of primordial follicles (See table 5-1).

It is believed that, in mammals, the number of oocytes within the ovaries is fixed for each female. The fertile lifespan of one female is dependent on the size of the oocyte pool at birth and the rapidity of the oocyte pool depletion. Thus, while defects in folliculogenesis could cause apoptosis or depletion of follicles/oocytes, impaired meiosis will result in unhealthy gametes,

which will also lead to depletion of oocyte in ovaries. Previous research using mutant mice defective for meiotic genes, such as *Msh4*, *Msh5*, *Mlh1*, *Mlh3*, *Dmc1*, and *Smc1β*, has shown that these mutants have similar phenotype to clinical observations found in human POF (Edelmann, Cohen et al. 1996; Pittman, Cobb et al. 1998; de Vries, Baart et al. 1999; Edelmann, Cohen et al. 1999; Kneitz, Cohen et al. 2000; Lipkin, Moens et al. 2002; Takabayashi, Yamauchi et al. 2009). However, it is of note that they are not the ideal models for human POF. In *Msh4, Msh5* and *Dmc1* mutant females, oocyte development and ovarian structure are completely disrupted at an early age (Pittman, Cobb et al. 1998; de Vries, Baart et al. 1999; Kneitz, Cohen et al. 2000), while ovaries from *Mlh1* and *Mlh3* mutants are histologically normal and contains follicles of all developmental stages (Baker, Plug et al. 1996; Edelmann, Cohen et al. 1996; Lipkin, Moens et al. 2002). Both phenotypes are different from what is observed in most human POF patients, who lose their oocytes in 20-30s. As discussed in Chapter 4, *Cntd1* mutant females appear to have an intermediate phenotype compared with the other meiotic deficient mutants (See Table 5-1), and more closed to human POF. Actually, the phenotype we observed in ovaries from *Cntd1* mutants is similar to *Smc1β* mutant females (Takabayashi, Yamauchi et al. 2009). However, although both mutant lines undergo decrease in the number of oocytes after 4 weeks of age, oocyte-depletion in *Cntd1* mutant line is more rapid compared with *Smc1β* mutants. While there are still developing follicles observed in *Smc1β* mutant ovaries at 8 weeks of age, ovaries from *Cntd1* mutants are almost depleted of oocytes at the same age.

One important future experiment would be to determine the specific stage when oocytes undergo depletion in ovaries of *Cntd1* mutants. Evaluation of serial sections of ovaries aged from late embryonic stage to 8 week-old will be necessary. Total follicle/oocyte numbers, ratios of follicles of different developmental stages (such as primordial follicles, primary follicles,

Table 6-1 Genes associated with human premature ovarian failure (POF).

	Gene name	Function of the gene	Ovarian phenotype of the knockout mice	Possible cause of POF	References
Bcl-2	B cell leukemia/ lymphoma 2	antiapoptotic	Fertile; Significantly decreased primordial follicles	Up-regulation of apoptosis in oocytes due to a lack of antiapoptotic factors	(Morita, Perez et al. 1999)
Gdf9	Growth differentiation factor 9	Growth factor synthesized by oocytes and modulating somatic cell functions in vivo	Sterile; primordial and primary follicles can be formed but not beyond the primary one-layer follicle stage	Defects in follicular development beyond primary follicle stage.	(Dong, Albertini et al. 1996)
Amh	Anti-Mullerian hormone	A member of the transforming growth factor-beta superfamily of growth and differentiation factors	Fertile; more primordial follicles are recruited in AMH null mice than in wild-type littermates.	NA	(Durlinger, Kramer et al. 1999)
Fshr	Follicle-stimulating receptor	Essential for folliculogenesis in the female	Sterile; thin uteri, smaller ovaries due to a block in folliculogenesis before antral follicle formation	Follicules cannot reach antral follicle stage.	(Dierich, Sairam et al. 1998)
Foxo3	Forkhead transcription factor	Transcription factor; functions at the earliest stages of follicular growth as a suppressor of follicular activation	Age-dependent decline in reproductive fitness and were sterile by 15 weeks of age; early depletion of functional ovarian follicle	Global activation of primordial follicles before the onset of sexual maturity, leading to the premature depletion of ovarian follicles	(Castrillon, Miao et al. 2003)
Foxl2	Forkhead domain/winged-helix transcription factor	One winged-helix/forkhead domain transcription factor	Sterile; granulosa cells do not complete the squamous to cuboidal transition leading to the absence of secondary follicles and oocyte atresia.	Primordial follicles are activated two weeks after birth in the absence of functional granulosa cells, which leads to oocyte atresia and progressive follicular depletion.	(Schmidt, Ovitt et al. 2004)
Nobox	Newborn ovary homeobox	Oocyte-specific homeobox gene	Sterile; atrophic ovaries that lacked oocytes at 6 weeks of age	Abolishing the transition from primordial to growing follicles in mice, which leads to postnatal oocyte loss.	(Rajkovic, Pangas et al. 2004)
Sohlh1	Spermatogenesis and oogenesis-specific basic helix-loop-helix-1	Transcriptional regulator in oocyte	Sterile; atrophic ovaries that lacked oocytes at 10 weeks of age	Defects in follicle development during the primordial-to-primary follicle transition.	(Pangas, Choi et al. 2006)
Pten	Phosphatase and tensin homologue deleted on chromosome 10	A negative regulator of phosphatidylinositol 3-kinase (PI3K), which is a lipid kinase important for cell proliferation, survival, migration, and metabolism	Subfertile, become infertile after ~3 months of age; early depletion of ovarian follicles	Primordial follicle pool becomes activated and then depleted in early adulthood	(Reddy, Liu et al. 2008)
Skp2	S-phase kinase-associated protein 2	an F-box protein that plays an important role in the progression of the S phase of the cell cycle by contributing to the ubiquitin-dependent degradation of p27	Subfertile, become infertile after ~8 months of age; reduced ovarian size at 2 month of age	Increase apoptosis in the ovary resulting from polyploidy of granulosa cells; significant decrease in the remaining pool of functional gametes shortly after sexual maturity	(Fotovati, Abu-Ali et al. 2011)

Table 6-1 Genes associated with human premature ovarian failure (POF) (Continued).

	Gene name	Function of the gene	Ovarian phenotype of the knockout mice	Possible causes of POF	References
Msh4	MutS homolog 4	meiotic recombination	Sterile; steady loss of germ cell quickly after birth, no primordial follicle formation	Loss of oocytes before dictyate arrest	(Kneitz, Cohen et al. 2000)
Msh5	MutS homolog 5	meiotic recombination	Sterile; rudimentary ovaries with no follicles and oocytes at 2~3 months of age	Loss of oocytes before dictyate arrest	(de Vries, Baart et al. 1999; Edelmann, Cohen et al. 1999)
Mlh1	MutL homolog 1	meiotic recombination	Sterile; normal follicular development, some oocytes can reach the 2-cell zygote stage after fertilization	NA	(Edelmann, Cohen et al. 1996)
Mlh3	MutL homolog 3	meiotic recombination	Sterile; normal follicular development, some oocytes can reach the 2-cell zygote stage after fertilization	NA	(Lipkin, Moens et al. 2002)
Dmc1	Dosage suppressor of mck1 homolog	Single strand exchange during DSB repair	Sterile; reduced ovarian size, no follicles in adults	Oocytes get arrested around the pachytene stage or earlier; subsequent death of oocytes results in complete depletion in the ovary by adulthood.	(Pittman, Cobb et al. 1998)
Smc1β	structural maintenance of chromosomes 1B	Sister chromatid cohesin	Sterile; normal follicular development at 4 weeks of age, but the number of follicles in mutant mice decreases from 4 to 8 weeks of age	Oocytes progress through meiosis I to dictyate arrest, but massive aneuploidy is found during the meiotic divisions	(Takabayashi, Yamauchi et al. 2009)

secondary follicles and antral follicles) should be counted for each age group and compared with wild-type and heterozygous littermates. The next question would be how oocyte-depletion happens in *Cntd1* mutants. The damage in oocytes cause by impaired meiosis and significantly reduced chiasmata in diakinesis could be a contributor, which may lead to release of apoptotic signal in the oocytes or to surrounding somatic cells. Meanwhile, besides regulating CO formation during meiosis, CNTD1 may also partner with other proteins and participate in processing the signals between oocytes and somatic cells during folliculogenesis. Deletion of CNTD1 may cause defects in somatic cell function in maturing follicles and leads to loss of follicles. To decide whether somatic cells or oocytes trigger the depletion, somatic cells and oocytes could be purified separately from the ovaries around the time of depletion and cell death via apoptosis could be checked by western blotting using apoptotic markers, such as cleaved Caspase-3 and PARP (Fotovati, Abu-Ali et al. 2011). Furthermore, changes in various signaling pathways related to oognesis and folliculogenesis before and after depletion can be detected by RNA-seq experiments, in which the transcriptome-wide expression profile in somatic cells and oocytes from mutant, heterozygous and wild-type mice can be analyzed and compared.

Closing comments

Given the results from these studies, I would like to propose a model for DSB repair through Class I CO pathway in mouse. In early zygonema, MSH4-MSH5 heterodimer binds to DNA intermediates loaded with RAD51/DMC1 with low degree of CO interference. When the cell enters late zygonema/early pachynema, the strength of interference increases and most of the MSH4-MSH5 foci get lost from the chromosomes, and DSBs in these sites need to be repaired

through NCO pathway or Class II CO pathway or MLH1-MUS81 independent pathway. The stabilization of MSH4-MSH5 foci on meiotic chromosome during this stage requires the presence of MLH3 and CNTD1, both of which may be confined by or directly contribute to CO interference. CNTD1 may pair with some cell cycle mediator to reinforce a subset of MSH4-MSH5 foci for MLH3 to bind. The interaction between CNTD1 and MLH3 could depend on the mammalian specific unique region of mouse MLH3, considering that both this unique region and the orthologue of CNTD1 are absent in yeast. MLH3 then interacts with MSH4-MSH5 to recruit MLH1 and other downstream effectors which may participate in maturing and resolving the CO. Such downstream effectors may include the Exonuclease, EXO1, and MLH3 itself, via its endonuclease domain.

Ultimately, the studies described in this thesis have furthered our knowledge about mouse meiosis through investigating one MutL homolog and its potential interacting protein. These results also leave us with a lot of open questions for future research, all of which will expand our understanding on mammalian meiosis.

References

Alani, E., R. A. Reenan, et al. (1994). "Interaction between mismatch repair and genetic recombination in Saccharomyces cerevisiae." Genetics **137**(1): 19-39.

Baker, S. M., A. W. Plug, et al. (1996). "Involvement of mouse Mlh1 in DNA mismatch repair and meiotic crossing over." Nature Genetics **13**(3): 336-342.

Castrillon, D. H., L. Miao, et al. (2003). "Suppression of ovarian follicle activation in mice by the transcription factor Foxo3a." Science **301**(5630): 215-218.

Choo, K. H. A. (1997). "The centromere." Oxford University Press, Oxford.

Cohen, P. E., S. E. Pollack, et al. (2006). "Genetic analysis of chromosome pairing, recombination, and cell cycle control during first meiotic prophase in mammals." Endocr Rev **27**(4): 398-426.

Cole, F., L. Kauppi, et al. (2012). "Homeostatic control of recombination is implemented progressively in mouse meiosis." Nat Cell Biol **14**(4): 424-430.

Cordts, E. B., D. M. Christofolini, et al. (2011). "Genetic aspects of premature ovarian failure: a literature review." Arch Gynecol Obstet **283**(3): 635-643.

de Vries, S. S., E. B. Baart, et al. (1999). "Mouse MutS-like protein Msh5 is required for proper chromosome synapsis in male and female meiosis." Genes Dev **13**(5): 523-531.

Dierich, A., M. R. Sairam, et al. (1998). "Impairing follicle-stimulating hormone (FSH) signaling in vivo: targeted disruption of the FSH receptor leads to aberrant gametogenesis and hormonal imbalance." Proc Natl Acad Sci U S A **95**(23): 13612-13617.

Dong, J., D. F. Albertini, et al. (1996). "Growth differentiation factor-9 is required during early ovarian folliculogenesis." Nature **383**(6600): 531-535.

Durlinger, A. L., P. Kramer, et al. (1999). "Control of primordial follicle recruitment by anti-Mullerian hormone in the mouse ovary." Endocrinology **140**(12): 5789-5796.

Edelmann, W., P. E. Cohen, et al. (1996). "Meiotic pachytene arrest in MLH1-deficient mice." Cell **85**(7): 1125-1134.

Edelmann, W., P. E. Cohen, et al. (1999). "Mammalian MutS homologue 5 is required for chromosome pairing in meiosis." Nature Genetics **21**(1): 123-127.

Fotovati, A., S. Abu-Ali, et al. (2011). "Impaired ovarian development and reduced fertility in female mice deficient in Skp2." J Anat **218**(6): 668-677.

Harding, S. D., C. Armit, et al. (2011). "The GUDMAP database--an online resource for genitourinary research." Development **138**(13): 2845-2853.

Hoffmann, E. R. and R. H. Borts (2004). "Meiotic recombination intermediates and mismatch repair proteins." Cytogenet Genome Res **107**(3-4): 232-248.

Hollingsworth, N. M., L. Ponte, et al. (1995). "MSH5, a novel MutS homolog, facilitates meiotic reciprocal recombination between homologs in Saccharomyces cerevisiae but not mismatch repair." Genes Dev **9**(14): 1728-1739.

Holloway, J. K., J. Booth, et al. (2008). "MUS81 generates a subset of MLH1-MLH3-independent crossovers in mammalian meiosis." PLoS Genet **4**(9): e1000186.

Hunter, N. and R. H. Borts (1997). "Mlh1 is unique among mismatch repair proteins in its ability to promote crossing-over during meiosis." Genes Dev **11**(12): 1573-1582.

Kneitz, B., P. E. Cohen, et al. (2000). "MutS homolog 4 localization to meiotic chromosomes is required for chromosome pairing during meiosis in male and female mice." Genes Dev **14**(9): 1085-1097.

Kneitz, B., P. E. Cohen, et al. (2000). "MutS homolog 4 localization to meiotic chromosomes is

required for chromosome pairing during meiosis in male and female mice." Genes Dev **14**(9): 1085-1097.

Kolas, N. K., A. Svetlanov, et al. (2005). "Localization of MMR proteins on meiotic chromosomes in mice indicates distinct functions during prophase I." J Cell Biol **171**(3): 447-458.

Lipkin, S. M., P. B. Moens, et al. (2002). "Meiotic arrest and aneuploidy in MLH3-deficient mice." Nat Genet **31**(4): 385-390.

Lipkin, S. M., V. Wang, et al. (2000). "MLH3: a DNA mismatch repair gene associated with mammalian microsatellite instability." Nat Genet **24**(1): 27-35.

Morita, Y., G. I. Perez, et al. (1999). "Targeted expression of Bcl-2 in mouse oocytes inhibits ovarian follicle atresia and prevents spontaneous and chemotherapy-induced oocyte apoptosis in vitro." Mol Endocrinol **13**(6): 841-850.

Pangas, S. A., Y. Choi, et al. (2006). "Oogenesis requires germ cell-specific transcriptional regulators Sohlh1 and Lhx8." Proc Natl Acad Sci U S A **103**(21): 8090-8095.

Persani, L., R. Rossetti, et al. (2010). "Genes involved in human premature ovarian failure." J Mol Endocrinol **45**(5): 257-279.

Pittman, D. L., J. Cobb, et al. (1998). "Meiotic prophase arrest with failure of chromosome synapsis in mice deficient for Dmc1, a germline-specific RecA homolog." Mol Cell **1**(5): 697-705.

Rajkovic, A., S. A. Pangas, et al. (2004). "NOBOX deficiency disrupts early folliculogenesis and oocyte-specific gene expression." Science **305**(5687): 1157-1159.

Reddy, P., L. Liu, et al. (2008). "Oocyte-specific deletion of Pten causes premature activation of the primordial follicle pool." Science **319**(5863): 611-613.

Ross-Macdonald, P. and G. S. Roeder (1994). "Mutation of a meiosis-specific MutS homolog decreases crossing over but not mismatch correction." Cell **79**(6): 1069-1080.

Santucci-Darmanin, S., S. Neyton, et al. (2002). "The DNA mismatch-repair MLH3 protein interacts with MSH4 in meiotic cells, supporting a role for this MutL homolog in mammalian meiotic recombination." Hum Mol Genet **11**(15): 1697-1706.

Schmidt, D., C. E. Ovitt, et al. (2004). "The murine winged-helix transcription factor Foxl2 is required for granulosa cell differentiation and ovary maintenance." Development **131**(4): 933-942.

Sherman, S. L. (2000). "Premature ovarian failure in the fragile X syndrome." Am J Med Genet **97**(3): 189-194.

Takabayashi, S., Y. Yamauchi, et al. (2009). "A spontaneous smc1b mutation causes cohesin protein dysfunction and sterility in mice." Exp Biol Med (Maywood) **234**(8): 994-1001.

Wang, T. F., N. Kleckner, et al. (1999). "Functional specificity of MutL homologs in yeast: evidence for three Mlh1-based heterocomplexes with distinct roles during meiosis in recombination and mismatch correction." Proc Natl Acad Sci U S A **96**(24): 13914-13919.

Yokoo, R., K. A. Zawadzki, et al. (2012). "COSA-1 Reveals Robust Homeostasis and Separable Licensing and Reinforcement Steps Governing Meiotic Crossovers." Cell **149**(1): 75-87.